Shrinkage behaviour of 3D printing concrete mixture

An experimental and numerical study

Richa Priyadarshi

TU Delft

Shrinkage behaviour of 3D printing concrete mixture

An experimental and numerical study

by

Richa Priyadarshi

in fulfilment of the requirements for the degree of
Master of Science
in Structural Engineering

at the Delft University of Technology,
to be defended publicly on Tuesday June 29, 2021 at 10:30 AM.

Student number:	4803558	
Project duration:	22 August, 2020 – 29 June, 2021	
Thesis committee:	Dr. ir. M. Luković,	Delft University of Technology, Chair
	Dr. ir. H. R. Schipper,	Delft University of Technology
	Prof. Dr. ir. M. A. N. Hendriks,	Delft University of Technology
	Dr. ir. B. Šavija,	Delft University of Technology
	Ir. M. J. A. M. Bruurs,	Witteveen+Bos

An electronic version of this thesis is available at http://repository.tudelft.nl/.

TU Delft

Witteveen + Bos

Acknowledgement

Back in 2017, I first read about the research of 3D printed concrete structures in The Netherlands. Since then the revolutionary technology attracted me and I tried to keep up-t0-date with the trend. Finally in my graduation thesis, I got to study the domain of 3D printing in-depth.

First of all, I would like to thank Marijn Bruurs and Hans Laagland for providing me the opportunity of working on such an innovative topic but also giving me the freedom in my research. Also, thank you Marijn for the detailed discussions and providing me the industrial examples of different project works. It helped me a lot in understanding the practical issues. I want to express my gratitude to my thesis committee for sharing their knowledge, providing guidance, and taking the time to discuss the progress of my research. I want to thank Branko Šavija for your elaborate feedback on my report and guiding me to select the appropriate experiments for my research. Thank you Mladena Luković for your timely suggestions to make my research work more stronger. Also I would like to thank Max Hendriks and Roel Schipper for your constructive feedback throughout my research. Being in the tough corona time where all the meeting were held online, you surely provided great support and timely guidance.
I want to thank my fellow Witteveen en Bos collegeaus for the discussions to improve my project.

A special thanks to Bruno Lobo and Nick Linssen . Bruno and Nick you were always ready to help me during the experiments in Delft, especially during these special times.
I also want to thank the people from MicroLab for supporting me during the execution of the experiments. Special thanks to Hua Dong for demonstrating the restrained ring test and always helping me during the experiment through your prompt email replies. Also, thanks to Maiko Van Leeuwan and Prof. Erik Schlangen for helping me arrange the experiments even at such a short notice.

Working through my thesis required more than just academic assistance, and I express a huge gratitude to everyone who has listened to and, at times, had to tolerate me over the last nine months. I cannot begin to express how grateful I am for their friendship, especially Ajinkya Doshi. Throughout my thesis not only you helped me with your simulation tips but more importantly always motivated me to keep going. Finally, I want to thank my family for their continuous support and love even from thousands of kilometers away.

I hope you will enjoy reading my work.

Richa Priyadarshi
Deventer, June 2021

Summary

Concrete is one of the most widely used construction materials across the world. Although, the traditional construction techniques are being improved for efficiency, cost and material optimization, there are disadvantages as well, such as the use of formwork, highly labour-intensive and limited architectural freedom for design and material savings. 3D printing of concrete structures is one of the emerging technologies promising the automation in construction industry. However, 3D printed concrete structures pose higher risks of shrinkage as compared to the conventional concrete structures due to their different construction techniques and material composition. Shrinkage can raise issues such as reduction in strength of the structures, poor durability and aesthetically unpleasant structures.

The research aims to study the shrinkage behaviour of the 3D printing concrete mixture in different restrained and curing conditions. Based on the experimental data, a finite element model has been developed to predict the shrinkage behaviour over time. The free shrinkage test was performed on cast samples and 3D printed samples of dimensions 160x40x40 mm^3. The specimens were kept in two curing conditions: covered with plastic sheet and (2) uncovered or exposed to environment from the time of casting. The shrinkage behaviour was studied for up to 60 days at relative humidity of 65% and temperature 20°C. A higher shrinkage values as compared to normal and high-performance concrete is observed in both 3D printed and cast samples. The 3D printed samples showed a higher shrinkage of 15-18% as compared to cast samples due to the 3D printing processes. Restrained ring test were performed for three curing conditions: (1) exposed to environment, (2) covered with plastic sheet and (3) sealed with waterproof tape. The sample exposed to drying cracked within 3 days followed by covered with plastic sheets in 4 days and the specimen in third condition cracked within 8 days. The experiment indicated that the autogenous shrinkage is so high in the concrete mixture to induce shrinkage cracking.

A finite element model has been developed to simulate the shrinkage behaviour of the concrete mixture based on the experiment results of the free shrinkage test of cast specimens. The capillary tension approach has been used as the theoretical framework. It uses the Kelvin-Laplace equation to calculate the capillary stresses and the Bentz deformation model to calculate the corresponding shrinkage strain. It is applicable for ambient relative humidity of more than 40%. The required input for the model are: degree of hydration over time, elastic modulus and distribution of relative humidity over time. The degree of hydration has been calculated using HYMOSTRUC software. The experimental results of the free shrinkage test for cast samples have been simulated in ANSYS. An inverse analysis has been used to obtain the material parameters required to model the moisture diffusion process. Transient heat equation has been used to model the diffusion process. Since the concrete mixture has a low water-cement ratio, the effect of autogenous shrinkage has been taken into account as well. The calibrated finite element model gave an error of 8-10% as compared to the experimental results. The moisture profile obtained from the model has been compared to an analytical model to validate the model. It shows good agreement, especially for upto 28 days.
Finally the developed finite element model has been applied on three case studies to assess the accuracy of the model. First, the restrained ring test has been simulated to validate the model based on the prediction of the cracking time. It showed that to accurately predict the shrinkage induced stresses, the creep and the relaxation phenomenon plays a crucial role as well. Second, the model has been used to simulate the shrinkage in a 3D printed flower pot restrained at varying time. Third, a parametric study has been designed using the developed model.

Overall the study concludes that the shrinkage in 3D printing concrete mixture is quite high as compared to the normal concrete even if conventionally cast. The 3D printing processes can increase the shrinkage further. The developed finite element model can be used as a tool to estimate the shrinkage strain.

Contents

1

Introduction

A paradigm shift in the construction industry has been induced by 3D concrete printing which promises better automation, faster, efficient and cost-effective construction of complex structures. 3D printing of concrete is an additive manufacturing technique of layer by layer extrusion of concrete to construct structures without using traditional formwork, potentially saving time, material and cost. Also, it provides the freedom of shapes in the structural design due to construction from the digital model without human interventions. Several new projects have been constructed over the past 10 years showing the potential of the large-scale application in the construction industry [1].

During many of these projects, shrinkage-induced cracking has been observed. One example of a 3D printed water reservoir possibly cracked due to plastic shrinkage is shown in figure 1.1. Shrinkage is the volumetric reduction in the concrete due to moisture loss either internally due to the cement hydration process or externally to the environment. If the structure is restrained, tensile stresses are produced due to shrinkage and can even lead to cracking if the tensile strength of the material is exceeded. Shrinkage induced cracks raise issues such as reduction in strength of the structures, poor durability, and aesthetically unpleasant structures. 3D printed structures are more prone to shrinkage due to factors such as immediate exposure to drying due to lack of formwork, low water-to-cement ratio, high cement content, and absence of coarse aggregates.

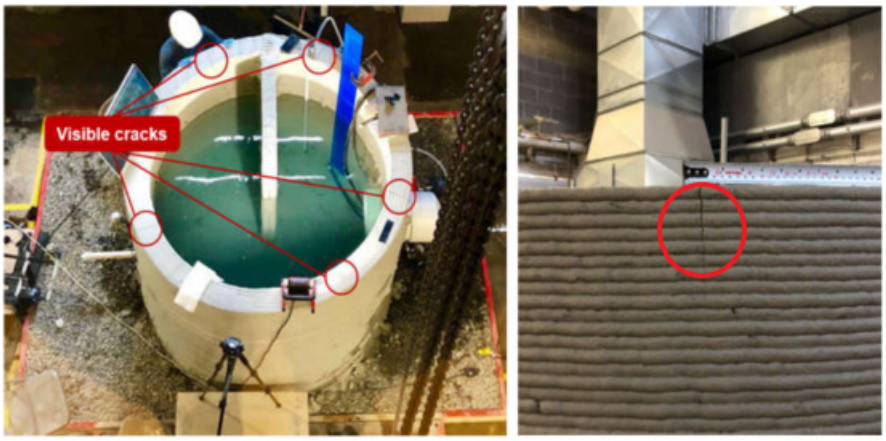

Figure 1.1: Shrinkage induced cracking in 3D printed water reservoir attributed to plastic shrinkage [2]

However, since the technology is relatively new, the risk of shrinkage in 3D-printed concrete structures is still being explored. Combrinck et al. [3] measured the plastic shrinkage in 3D printed concrete to be almost twice as compared to ordinary concrete and self-compacting concrete, which implies the necessity of research. Slavcheva et al. [4] reported the drying shrinkage of cement paste for 3D printed

concrete to be 1360 microstrains at a relative humidity of 50%, which is higher as than the total shrinkage of High-Performance concrete with a w/c ratio of 0.25 at around 500 microstrains [5]. Combrinck et al. [3] studied the crack propagation due to plastic shrinkage of 3D printed concrete. However, detailed research is required regarding the shrinkage behavior of 3D printed concrete mixture under different curing and restrained conditions to minimize the risk of cracking.

Various design guidelines such as ACI 209 [6], Eurocode 2 [7], CEB FIB Model Code 2010 [8], Japanese Standard Code [9], propose analytical models to predict the long term shrinkage behavior of normal concrete. The major parameters based on which shrinkage calculations are done are: ambient relative humidity, mechanical properties of concrete, average drying path length, etc. These analytical models are developed for the concrete mixtures with coarse aggregates, which have a restraining effect on shrinkage. Since 3D printing concrete mixtures do not contain coarse aggregates, the calculated value could be highly underestimated. Another limitation is that the analytical models assume a uniform section thickness. Huang et al. [10] used Finite Element Modelling to study the shrinkage behavior of hollow box girder sections with varying thickness. In reality, the cross-section can vary through the section, primarily when 3D printing technology is being used for more material and cost-optimized but complex cross-sections. For accurately predicting the shrinkage behavior of such structures, a vast amount of calculations are required on different geometries, which is computationally expensive.
To tackle the above-mentioned limitations of the analytical models, several researchers [10]–[12] have used Finite Element Modelling to simulate the moisture diffusion analyses in the concrete structures. A similar theoretical framework has been used in this study to develop a model for the prediction of shrinkage strain of 3D printing concrete mixture.

1.1. Problem statement

Shrinkage is an essential factor influencing the durability and mechanical properties of a concrete structure. 3D printed concrete structures pose higher risks of shrinkage as compared to conventional concrete structures due to their different construction techniques and material composition. This research investigates the shrinkage behavior of 3D printing concrete mix under different curing conditions to understand if the shrinkage is an issue for 3D printing concrete mixtures?

1.2. Aim of the thesis

The main objective of the research is to first understand the shrinkage behaviour of the 3D printing concrete mixture. Further, based on the experimental results, develop a numerical model that can predict the shrinkage strain of the structures constructed using the 3D printing concrete mixture. The specific sub-research questions to be answered in the research are:

- How is the free shrinkage behavior of cast and 3D printed samples? Two curing conditions are investigated: samples being covered and uncovered.
- How is the shrinkage strain development when restrained? Two curing conditions are investigated: samples being covered and uncovered.
- How can a finite element model be developed to predict the shrinkage behavior of 3D printed concrete structures with time under different environmental conditions based on the experimental results?

1.3. Scope of the thesis

Shrinkage is a complicated phenomenon dependent on material characteristics and environmental conditions. It develops for years in a concrete structure. It will be difficult to study the long-term shrinkage behavior of a newly developed material. Therefore the research is limited by certain assumptions as follows:

- The research is restricted to the shrinkage behavior of a specific concrete mixture. The mix composition remains the same throughout the research. Also, the shrinkage behavior of up to 60 days has been studied.

- The research focuses on the shrinkage due to moisture loss and cement hydration process only. Other forms of shrinkage such as contraction due to temperature or carbonation shrinkage are not investigated.
- The thesis is based on extrusion-based concrete printing only.
- The numerical model is developed based on the capillary tension approach of the shrinkage mechanism. Hence it is applicable for concrete structures above RH= 40%. Typically the relative humidity above 40% is present outdoors; for example, the average relative humidity of The Netherlands, is between 80%-83% depending on the region, in the period 1991-2020 by KNML (Koninklijk Nederlands Meteorologisch Instituut) [13].

1.4. Research Methodology and thesis outline

First, a background study will be presented in chapter 2 to understand the shrinkage phenomena in concrete, its driving mechanism, and the key parameters influencing it. The 3D printing process is then explained, focusing on the material properties and casting process, which influence its shrinkage behavior. Finally, two case studies of 3D-printed concrete structures cracked due to shrinkage will be reviewed. The key findings provide the understanding of the shrinkage phenomenon in the 3D printed structures.

The second part deals with experimental study. The shrinkage behavior in the two restrain conditions has been studied under two different environmental conditions: covered and uncovered. Free shrinkage test is performed for the unrestrained condition, and the ring test has been performed for restrained conditions. Further, the difference between the shrinkage behavior of 3D printed and cast specimens is investigated under free shrinkage. Chapter 3 describes the experimental setup, whereas chapter 4 provides the experimental results and the relevant deductions.

The third part focuses on developing a finite element model to simulate the shrinkage strain of the specimen based on the experimental results. Chapter 5 explains the theoretical framework for modelling the shrinkage phenomenon and the required input parameters. Chapter 6 discusses the development of the numerical model and its verification. This will provide the critical material parameters required for the numerical model to further predict the shrinkage behavior of other concrete structures under different environmental conditions. Further, chapter 7 describes three case studies to test the validity of the developed numerical model.

Finally, chapter 8 discusses the results and chapter 9 concludes the research and provides the practical implications and recommendations drawn from the study.

2

Background

The chapter aims to provide a deeper understanding of the shrinkage phenomenon in concrete. Then the possible reasons for shrinkage in 3D printing concrete mixtures have been reviewed. First, the shrinkage types in concrete, their influencing parameters, and the governing mechanism have been discussed. Then, the 3D printing process has been discussed, focusing on the significant characteristics from the shrinkage point of view. Finally, two case studies are reviewed from the literature to understand the shrinkage phenomenon.

2.1. Types of shrinkage

Shrinkage is a time-dependent phenomenon in a concrete structure that occurs due to a reduction in the volume of concrete over time, due to the movement or loss of water. It can occur due to internal reactions (autogenous and chemical shrinkage) or evaporation (drying or plastic shrinkage). When the concrete structure is restrained, it leads to the development of tensile stresses. If these stresses exceed the tensile strength of the concrete, it can result in cracking. These cracks are aesthetically unpleasing and can be a significant problem to the durability of the concrete structure.

Three types of shrinkage are mainly identified in the concrete due to internal or external moisture loss: plastic shrinkage, autogenous shrinkage, and drying shrinkage. The shrinkage strain is usually proportional to the amount of moisture loss [14]. Thus, the shrinkage phenomenon is described for different stages in terms of relative humidity. The internal relative humidity of the concrete is defined as the relative humidity of the gaseous phase in equilibrium with the interstitial liquid phase in the pore network of the concrete [15].

2.1.1. Initial saturation of concrete-Plastic shrinkage

When the concrete is mixed with water, it exhibits plastic behavior for the first 4 to 8 hours [3], depending on the mixture composition and the environmental conditions. Plastic shrinkage is caused due to the evaporation of free pore water from the exposed concrete surface if the rate of bleeding of water is less than the evaporation rate. The capillary water evaporates, resulting in shrinkage stresses in the concrete paste. Proper curing methods, the use of sunshades to limit the concrete surface temperatures, optimizing concrete placement at the coolest time of the day are common practices to reduce the plastic shrinkage by minimizing the rate of moisture loss.
In a freshly mixed concrete mixture, a layer of water covers the solid cementitious particles, forming a flowable cement paste. This provides fluidity to the mixture. During the time of casting, water fills the voids of the solid skeleton, and the cement particles are connected to each other through the layer of water as shown in figure 2.1(a). A continuous network of liquid exists, making the relative humidity close to 1 and the concrete is fully saturated. Since the concrete is in the liquid phase, there is no rigidity in the structure leading to high shrinkage strains but producing minor stresses.

Influencing factors
It is mainly dependent on the rate of evaporation, the surface area of the exposed surface, and the curing method. The rate of evaporation is determined by the relative humidity, concrete temperature, and wind speed. The higher the evaporation rate and the larger the exposed surface, the probability of plastic shrinkage increases, which may result in cracking.

2.1.2. Decrease in relative humidity due to self-desiccation

The absolute volume of cement and water is more than the formed final hydration products which have a higher density as compared to the original reactants, commonly termed as chemical shrinkage [16]. In the liquid stage, the internal shrinkage purely occurs due to the chemical shrinkage since the material lacks the resistance to the change in volume. Once the setting time of the concrete is reached, it indicates the formation of a rigid network of hydration form. After that, the internal porosity increases due to the volume change of hydration but does not lead to external shrinkage [17]. External volume changes are governed due to the continuous water consumption during the cement hydration process.

Autogenous shrinkage is defined as the unrestrained deformation of the concrete if retained sealed at a constant temperature [18]. The pore volume reduces at a lower rate as compared to the volume of water, leading to partially empty pores. As a consequence, there is a decrease in the internal relative humidity referred to as self-desiccation as shown in figure 2.1. Loss of capillary water induces tensile stresses and the surrounding matrix of hydration products is compressed.

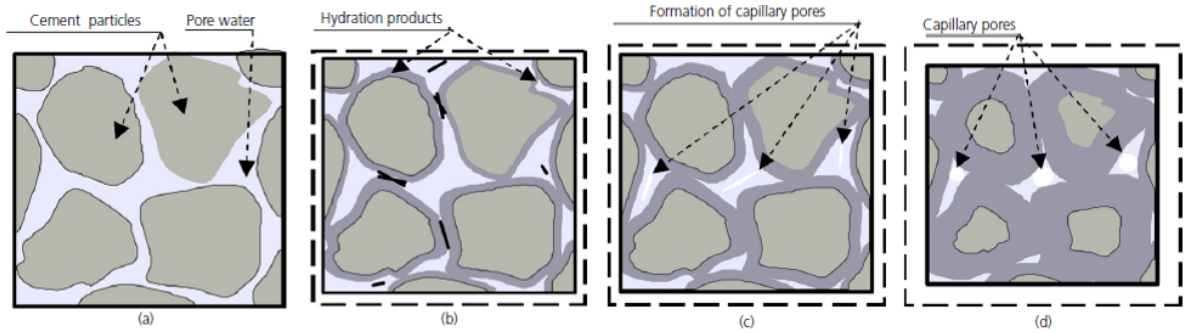

Figure 2.1: Depiction of the microstructure formation of the cement paste [11]: (a) Freshly mixed cement paste (b) Setting of paste (c) Initiation of formation of capillary pores (d) Drop in relative humidity

The autogenous shrinkage develops uniformly throughout the concrete structure. It is susceptible to cracking as it mainly develops at the early age of cement paste when the mechanical properties such as modulus of elasticity, fracture energy etc. are poorly developed. The cracking caused due to the autogenous shrinkage may result in reduced strength and durability issues. Several researchers [19]–[23] have investigated the change in relative humidity with time due to self-desiccation for concrete. However, none of the research is explicitly focused on concrete mixtures for 3D printing. Zhang et al. [22] studied the RH distribution on an OPC-based concrete specimen of 150x150x150 mm^3 with different w/c ratios in sealed condition. A similar experiment was conducted by Kim Lee et al. [19] for 100x100x100 mm^3 sealed and unsealed specimen. The results are shown in figure 2.2. The specimen N30 has a w/c ratio of 0.3 and has decreased RH of up to 85% on 28 days. The decrease in RH inside concrete decreases with w/c. Similar trends have been observed by Jiang et al. [20].

Influencing factors
Autogenous shrinkage is dependent on the material properties of concrete, such as degree of hydration of the binder, water-cement ratio, cement content, etc.

- **Water-cement ratio**- Since the mixtures with low w/c ratio or w/b ratio have less free capillary water and lower relative humidity, they exhibit higher autogenous shrinkage as shown in figure 2.2. According to Power's law, a minimum 0.45 w/c ratio is required for the concrete to reach complete hydration [24]. However, with concrete having a lower w/c ratio such as High Performance Concrete, autogenous shrinkage is a crucial issue.

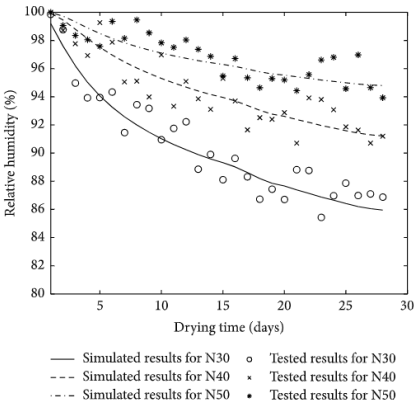

(a) Relative humidity due to self desiccation conducted by Zhang et al. [22] where N30, N40 and N50 has w/c= 0.3, 0.4 and 0.5

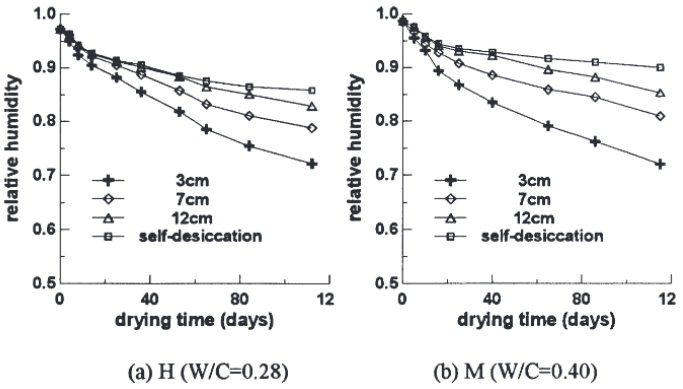

(b) Relative humidity due to autogenous and drying shrinkage conducted by Kim Lee et al. [19] for w/c= 0.28 and 0.4

Figure 2.2: Change in internal RH due to autogenous and drying shrinkage for different w/c ratio

- **Cement type and fineness**- Use of supplementary cementitious materials such as silica fume increases the autogenous shrinkage due to denser pore structures. As water is emptied from the lower pore radius, higher capillary forces are generated. Jennings et al. [25] concluded that the increased finess of cement decreased the RH at a higher rate, increasing the autogenous shrinkage. It can be attributed to an accelerated rate of the cement hydration process and the consequent water consumption.

- **Curing temperature**- Bentur et. al [26] showed experimentally that at higher curing temperature, the microstructure is coarser due to a higher rate of reaction. Bigger capillary pores result in lower capillary tension.

- **Effect of aggregates**- Autogenous shrinkage of mortar is lower than the cement paste of same water-cement ratio due to restraining effect of aggregates and lower cement content per unit volume [24].

2.1.3. Decrease in relative humidity causing drying shrinkage

When the concrete is exposed to a dry environment, it tends to reach a moisture equilibrium. As the cement paste dries, the relative humidity of the pores starts to decrease, and as a result, the radius of the meniscus decreases as well. The larger pores connected to the specimen surfaces are dried out first due to higher relative humidity differences. The loss of water does not cause significant volume change. Then the smaller pores connected to the empty pores lose water as the RH continues to decrease. The process is illustrated in figure 2.3 retrieved from the work of Liu et al. [27] where the drying process has been simulated based on 3D lattice approach.
Drying shrinkage starts at the end of the final setting of concrete, as soon as the concrete is exposed to drying, initially increases with time and gradually decreasing rate in years after setting. Kim Lee et al.[19] studied the decrease in RH and the corresponding drying shrinkage. The results are shown in figure 2.2(b) studied for 200x100x100 mm^3 specimen with w/c=0.28 and 0.4 kept at RH= 50% and T= 20°C. As the depth from the drying surface is increased, the RH is higher.

The key factors affecting drying shrinkage are:

- **Environmental conditions**- The drying process of the water is defined from the environmental conditions such as ambient relative humidity, temperature, and wind velocity. Due to higher RH differences inside the concrete and environment, diffusion will occur to maintain equilibrium.

- **Geometry of the structure**- The area exposed to the drying conditions controls the shrinkage as well. A smaller and slender member will dry more quickly than large, thick concrete for the same drying period. Also, the moisture gradient near the surface will be higher than the core of the member.

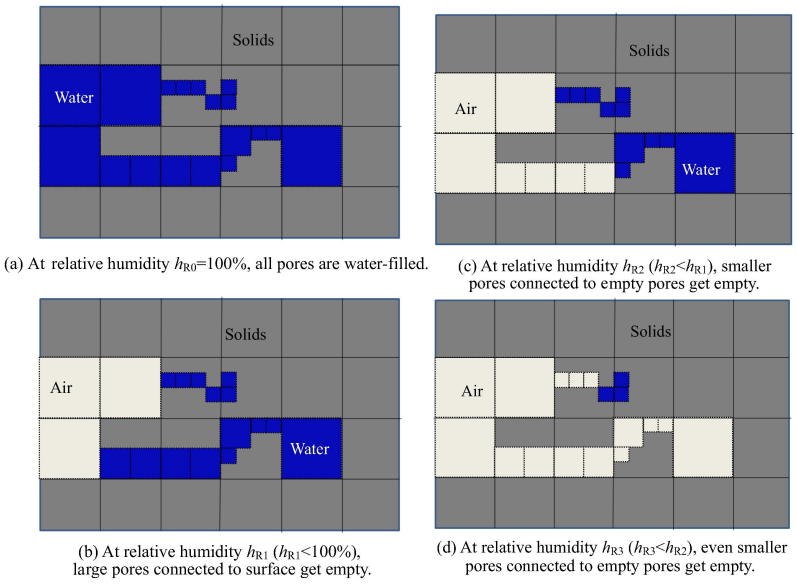

(a) At relative humidity h_{R0}=100%, all pores are water-filled.

(c) At relative humidity h_{R2} (h_{R2}<h_{R1}), smaller pores connected to empty pores get empty.

(b) At relative humidity h_{R1} (h_{R1}<100%), large pores connected to surface get empty.

(d) At relative humidity h_{R3} (h_{R3}<h_{R2}), even smaller pores connected to empty pores get empty.

Figure 2.3: Schematic figure of moisture loss in pores in two-dimension [27]

- **Curing conditions**- It controls not only the external environmental conditions but also defines the characteristic properties of the microstructure. Proper curing will prevent early age drying and also produce a dense concrete structure.
- **Effect of aggregates**- Similar to the autogenous shrinkage, the presence of aggregate will restrict the drying shrinkage deformation as well. Higher the aggregate/cement ratio, lower the shrinkage strain.

A summary of the types of shrinkage along with the duration of development, the governing parameters, and the significant effects can be seen in table 2.1.

Type of Shrinkage	**Duration of development**	**Key parameters**
Plastic Shrinkage	First few hours	Curing method, environmental conditions
Autogenous Shrinkage	Days-weeks	w/c ratio, cement type and fineness, presence of aggregates
Drying Shrinkage	Months-years	Environmental conditions such as RH, temperature, wind speed, the geometry of member, curing conditions, presence of aggregates

Table 2.1: Summary of the types of shrinkage and their duration of development and the influencing parameters

2.2. Driving mechanism of shrinkage

The self-desiccation due to the cement hydration process and the evaporation of water from the pores of concrete are the two primary mechanisms acting simultaneously, leading to a decrease in the relative humidity of the pores, causing shrinkage. The diffusion of water vapor through continuous vapor space becomes the dominant mechanism for moisture transfer in the concrete [28]. There is a decrease in pore water either due to the cement hydration or moisture diffusion. It causes the formation of the meniscus radius. Thus the relative humidity of the pores decreases as well. The higher the moisture loss, the greater the decrease in the humidity. The driving mechanism behind the autogenous and drying shrinkage has been researched for decades. A general agreement about the relationship between relative humidity and shrinkage has been established. Finally, three significant mechanisms are proposed by the researchers to study shrinkage: (1) Change in surface tension, (2) Disjoining pressure, and (3) Capillary Tension approach.

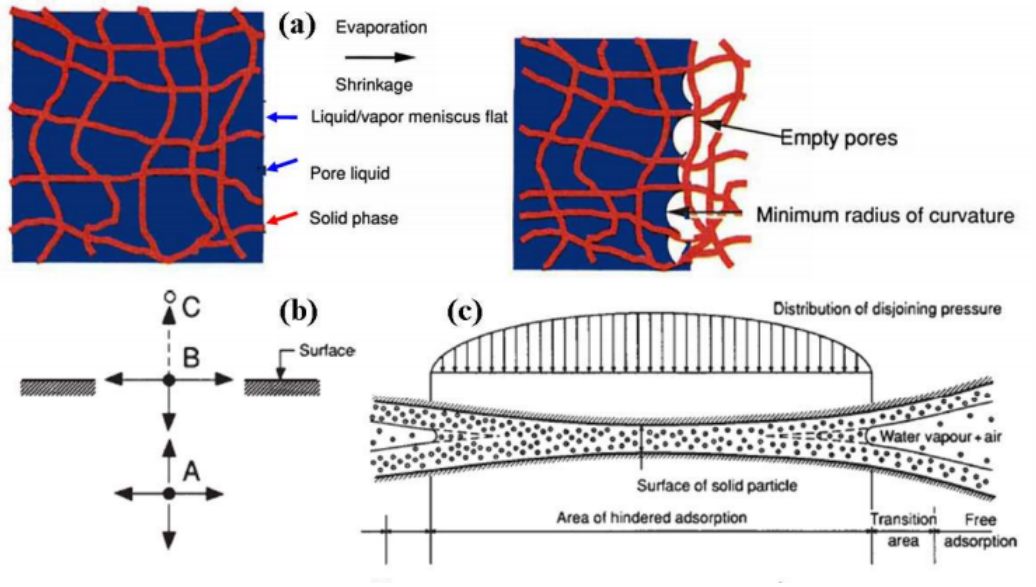

Figure 2.4: Illustration of different mechanisms of shrinkage in concrete, (a) Capillary tension approach due to meniscus formation, (b) Surface tension forces on moolecule A inside material in equilibrium with molecule B on surface exerting compressive stress on solid (c) Disjoining pressure in hindered adsorption area, retrieved from [29]

2.2.1. Surface tension of solid gel particles

Due to the asymmetrical attractive forces on atoms or molecules in the vicinity of the surface of solid a surface tension force is produced. When the relative humidity in the pores decreases, the thickness of the absorbed layer decreases as well. This increases the surface tension resulting in shrinkage. The surface tension approach has been used mainly to model autogenous shrinkage. It has been suggested that the mechanism is only valid in low RH regimes for up to RH= 40% to as low as RH= 20% [14].

2.2.2. Disjoining pressure

Due to the asymmetrical attractive forces on atoms or molecules in the vicinity of the surface of solid a surface tension force is produced. When the relative humidity in the pores decreases, the thickness of the absorbed layer decreases as well. This increases the surface tension resulting in shrinkage. The surface tension approach has been used mainly to model the autogenous shrinkage. It has been suggested that the mechanism is only valid in low RH regimes for up to RH= 40% to as low as RH= 20% [14].

2.2.3. Capillary tension Approach

In a porous medium such as the cementitious material, the vapor-liquid equilibrium is restored due to the formation of menisci in the pores. The difference between the gas pressure above the meniscus and the pressure inside the liquid is called capillary pressure. The emptying of pores causes tensile stresses in the capillary water (due to surface tension forces), which generated compressive forces in the surrounding solid resulting in elastic shrinkage strains. The mechanism is governing in relative humidity of above 40%.

A summary of the governing mechanism based on the relative humidity range is shown in table2.2. Typically the relative humidity above 40% is present outdoors; for example, the average relative humidity of The Netherlands, is between 80%-83% depending on the region, in the period 1991-2020 by KNML (Koninklijk Nederlands Meteorologisch Instituut [13]). The capillary tension approach has been used to model the autogenous and drying shrinkage mechanism in this research. Also, a majority of researchers consider capillary pressure as the principle shrinkage mechanism at high RH (greater than 40% to 50%), such as [21], [23].

Pore category	Size of Pore	RH at pore emptied	Shrinkage Mechanism
Capillary	75 nm	90%	Capillary tension
Large gel mesopores	2-5 nm	40%	Disjoining pressure
Small gel	1.2-2 nm	20%	Surface tension
Interlayer	75 nm	0%	Capillary tension

Table 2.2: Dominating shrinkage mechanism based on different characteristics of pore in cement paste [30]

Kelvin's Equation
The relative humidity in the pores can be expressed in terms of the radius of meniscus r, surface tension of water γ and the absolute temperature T based on Kelvin's Equation [31]: The pores are assumed to be spherical and partially filled with pore solution.

$$\text{RH} = exp\left(-\frac{2\gamma M}{\rho RT} \right) \tag{2.1}$$

where,
RH [-] is the relative humidity in the capillary pores,
M [kg/mol] is the molar weight of the water,
ρ [kg/m^3] is the density of water,
R [J/mol-K] is the ideal gas constant,
T [K] is the absolute temperature and
γ [N/m] is the surface tension of the pore solution.

In the above equation, the contact angle of 0°(complete wetting) at the vapor interface is assumed. For a curing temperature of 20°C, $M = 0.01802$ kg/mol, $\rho = 1000$ kg/m^3, the relation between the humidity inside the pores H and the radius of the capillary pores, r is shown in figure 2.5. As the relative humidity inside the concrete decreases from 100% to 40%, the equivalent radius of the capillary pores of the cement paste from which water is emptied changes from approximately 106.6 nm to 1.17 nm, respectively. As smaller and smaller pores are emptied in the concrete either due to self-desiccation or external drying, the higher the decrease in relative humidity.

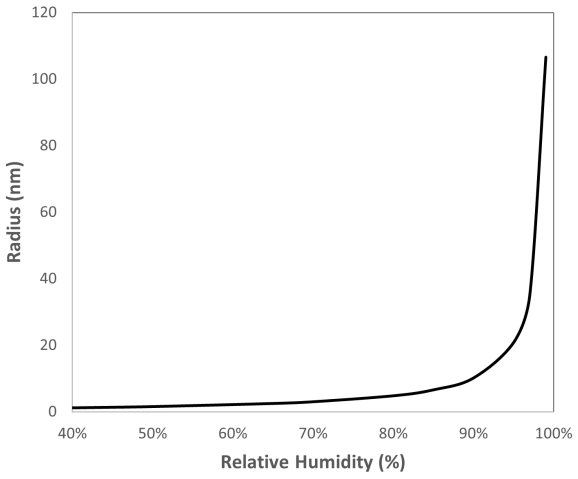

Figure 2.5: Relation between relative humidity of capillary pores and radius of meniscus of liquid/vapor interface at T= 20°C calculated using the Kelvin's Law

Laplace's Equation
The stresses produced in the pore liquid in terms of the radius of meniscus can be expressed based on Laplace's equation [14]:

$$\sigma_{\text{cap}} = \frac{2\gamma}{r} \tag{2.2}$$

where,
σ_{cap} [MPa] is the capillary tension,
γ [N/m] is the surface tension of the liquid,
r [m] is the radius of the menisci curvature

The relation between the relative humidity and the capillary tension produced within the pore liquid at a curing temperature of T= 20°C has been shown in 2.6 calculated by combining Kelvin and Laplace equation. For example, when a pore of 50 nm empties, the internal humidity in the pore decreases to about 98%, and correspondingly, capillary stress of 3 MPa is produced. As the water is removed from the smaller pores (r decreases), the capillary tension generated is higher.

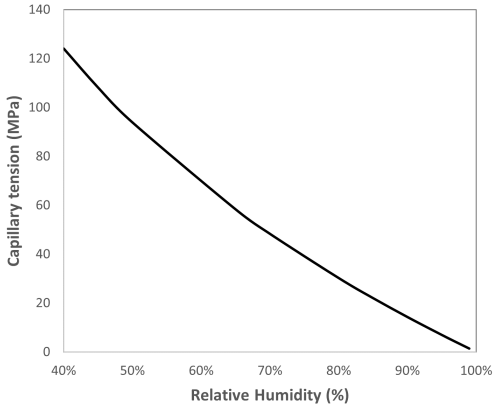

Figure 2.6: Relation of relative humidity and capillary tension calculated using the Kelvin-Laplace equation for T= 20°C

Bentz Deformation Model

The produced capillary stresses due to the loss of water from the capillary pores cause deformation of the porous concrete or mortar. Bentz et al. [32] proposed a model to calculate the deformation of the cement paste due to the capillary stresses approximating the cement paste to be an elastic material. The linear deformation due to the shrinkage can be calculated as follows:

$$\varepsilon = \frac{S_w \sigma_c}{3}\left(\frac{1}{K_p} - \frac{1}{K_s}\right) \tag{2.3}$$

where,
ε is the linear strain or shrinkage,
S_w is the degree of saturation (with a value between 0 and 1),
σ_c [MPa] is the capillary tension calculated from equation 2.2,
K_p [MPa] is the bulk modulus of the porous material, which is cement paste and
K_s [MPa] is the bulk modulus of the solid framework within the porous material, which is concrete/mortar.

The equation is only valid for a fully saturated linear elastic material [23]. However, since the hydrating cement paste is partially saturated, it is approximated by taking the degree of saturation into account. Further, the degree of saturation and capillary stresses are strongly dependent on the pore size distribution of the hardening cementitious material. A concrete having fine pores either produces higher capillary stresses at a given saturation or maintains a higher saturation at a given equilibrium. In both cases, the concrete with finer pores would show more shrinkage [33].

The capillary tension approach has been used in numerical modeling by various researchers [21] to model the total shrinkage mechanism (combination of autogenous and drying shrinkage). This research uses the same approach to model the diffusion process using Finite Element Modelling, explained in detail in Chapter 5 of the report.

2.2.4. Stresses generated due to the shrinkage strains

Mainly two types of stresses will be generated due to shrinkage: stresses due to restrained linear shrinkage and warping stresses due to differential drying shrinkage in the element. When the stress in the cross-section exceeds the tensile strength of the concrete, the element will crack.

Due to autogenous shrinkage or self-desiccation, the stresses cause a uniform reduction of internal relative humidity through the entire concrete thickness [34]. As a result, the strain distribution across the cross-section due to autogenous shrinkage will be uniform. On the other hand, the drying shrinkage produces differential shrinkage distribution across the cross-section generating non-uniform stresses. The shrinkage strain is assumed to be proportional to the relative humidity distribution, h(z) in the cross-section. The strain profile of a plain concrete slab has been shown in figure 2.7. Since the loss of moisture from the surface is higher than the core cross-section, the top will shrink more than the bottom, resulting in warping stresses, and the element will lift upwards.

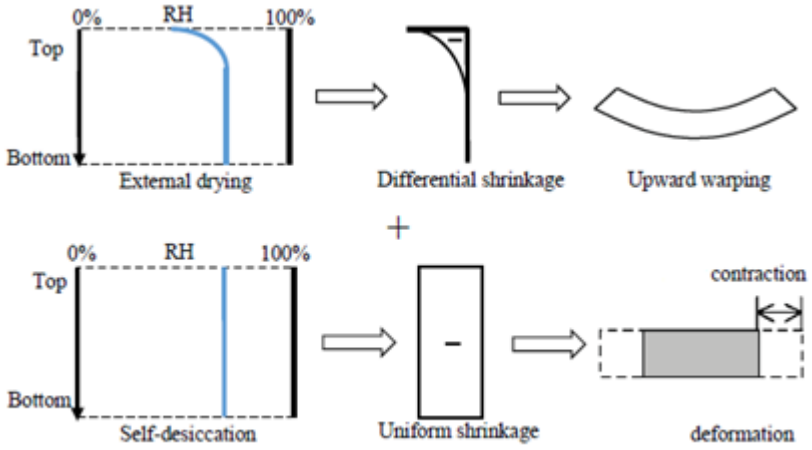

Figure 2.7: Illustration of the deformation due to external drying and self-desiccation [34]

2.3. 3D printed concrete

2.3.1. 3D printing process

The 3D printing process has various potential benefits, such as reducing construction time, cost, architectural freedom, and quality improvement of the construction. The printing facility uses a six-degree robotic arm mounted on a 10 meters rail. The print area that can be utilized is 11 x 3.5 x 3.5 m^3 (LxBxH). First, the dry mixture stored in a silo is mixed with water. Then it is pumped through a 30 m long hose connected to the printer head. The design of the structure to be 3D printed is provided to the robot arm through a digitally designed tool path of the multiple layers.

Since a 3D printed structure lacks formwork, it has different requirements as compared to conventional concrete mixtures. The material should be able to maintain the shape after deposition along with the initial strength to carry its own weight. A balance is required between the viscosity so that the material is fluid enough to pass through the system but once printed stiff enough to carry the subsequent layers. Numerous research [35]–[38] has been done on the mechanical and rheological requirements of 3D printed structures. However, since the research focuses on shrinkage behaviour, the key features related to shrinkage have been discussed here.

2.3.2. Casting process

Interlayer adhesion

Since in 3D printing technology, the structure is printed layer by layer, the interlayer adhesion becomes a crucial factor compared to cast-in-situ structures resulting in anisotropic behavior. Moreover, if the printing time interval is too high, then the initial layers can also restrain the freshly printed subsequent layers inducing shrinkage cracking. Nerella et al. [39] studied the microstructure of OPC-based 3D

printed structure. A higher amount of large pores at the interface and in the core and higher porosity as the possible mechanisms for the weak interface were observed. For delay in printing time of 0 min, 10 min, and 60 min of 4-layered concrete structure, Van Der Putten et al. [40] concluded that the chloride ingress in 3D printed specimen is higher as compared to molded specimens indicating increased porosity induced by the printing process. An increased time gap increases the porosity at the interface and consequently the chloride ingress rate of the printed elements.

Figure 2.8: Signs of water-intake at the layer interface probably attributed to high interlayer porosity [39]

Curing conditions
Plastic shrinkage and drying shrinkage are strongly dependent on environmental conditions such as relative humidity, temperature, and wind speed. Since 3D printed structures lack formwork, they are immediately exposed to the environment directly after printing, risking higher evaporation. However, since the structures are printed indoors, the environmental conditions are more controlled. Le. et al. [41] investigated the influence of curing conditions on the printed concrete sample (cured in water, damp hessian and T= 20°and RH= 60%) on drying shrinkage. The highest shrinkage was obtained for a fully exposed specimen having a drying shrinkage of 597 microstrains within 30 days. Similarly, Zhang et al. [42] found the drying shrinkage of 3DCP cured in 20 °C and RH= 50% to be 840 microstrains after 70 days.

2.3.3. Review of the material composition

In order to ensure an optimal deposition process, cement mixtures suitable for 3D printing are required to have the appropriate rheological and composition properties such as extrusion through the nozzle with ease, shape retention after deposition, proper adhesion between the printed layers, which makes the mix composition of 3D printing concrete mixtures different from traditional ones. As discussed in the previous section, the shrinkage is strongly dependent on the concrete's material composition, which may lead to the high susceptibility of 3DCP towards it. The main characteristics of the material composition of 3DCP in terms of binder, water-cement ratio, aggregates, and admixture are discussed as follows:

Binder
Most of the mixtures of 3DCP use CEM I Portland Cement as the highest portion of the binder content. Other supplementary cementitious materials such as fly ash, silica fume, and limestone fillers replace up to 40% of the cement. Fly ash is added to improve the flowability due to the ball bearing effect [43]. Silica fume has the advantage of accelerating the cement hydration due to large surface area and filling fine gaps in the cementitious matrix. The cement content in 3DCP is typically high in the range of 500-600 kg/m^3. It adds to the adiabatic heat released leading to thermal shrinkage [44]. Due to the silica fume, the microstructure is denser and smaller pore resulting in more shrinkage.

Water-binder ratio
The flowability and the mechanical properties of the hardened materials are affected by the w/c ratio of the concrete. Lower the w/c ratio, higher mechanical strength, and lower flowability are obtained. However, to main appropriate workability, minimum water content is required. Also, for a 3D concrete mixture, along with flowability for proper extrusion, the structure must be buildable and should have initial strength to hold the self-weight and subsequent layers. Since 3D printing mixtures have different binders as discussed previously, it is better to use the term water-to-binder ratio instead of w/c ratio. Typically the w/b ratio in 3DCP is in the range of 0.2-0.4 [45]. Wang [46] documented the w/b ratio

used for 3D printing mixtures in the literature. It was found that w/b ratios of 0.3-0.4 are most frequently used followed by 0.2-0.3 in mix proportions for 3D printable concrete. In concrete with a w/c ratio less than 0.4, the internal moisture is not sufficient to fully hydrate the cement particles, increasing the probability of autogenous shrinkage in 3DCP [24]. Typically superplasticizers are added to increase the workability while keeping the w/c ratio low. Kruger et al. [37] observed that taking superplasticizer outside the boundary of 1% per binder weight made the mixture too wet and caused deformation and inability to print.

Aggregates
The fine aggregate or sand with a 2 mm maximum particle size [4] is a typical choice for the 3D printable blends due to the limitation of nozzle size, pumpability, and proper extrusion of the concrete. Passing coarse aggregates through the pump and narrow nozzle is highly challenging. Furthermore, layers with coarse aggregates could not maintain the printed layers' original form [47]. Also, it is difficult for the layers to retain the original shapes with coarse aggregates in the printed layers. However, aggregates restrain the shrinkage and provide stiffness to the concrete. Due to the absence of the coarse aggregate, higher shrinkage is expected in 3DCP than normal concrete.

Admixtures
Admixtures are used to control the rheological properties and might not influence the shrinkage behaviour as such. 3DCP has various admixtures such as viscosity modifying agents (VMAs), superplasticizers, accelerators and retarders [46]. VMAs are used to maintain and stabilize the dimensions of the printed specimen. Superplasticizers are added to enhance the flowability during the extrusion. Accelerators are used to control the setting behaviour to improve the buildability of the structure. Due to the fast rate of cement hydration, it may decrease the extrudability, especially for long printing time. Retarder are used to keep a sufficient open time and allow a continuous printing flow by delaying the setting time.

Fibers
Fibers are widely used in 3D printed concrete structures to provide reinforcement, improve flexural strength, and control plastic shrinkage. Potential options for the fiber reinforcement being used in 3DCP are fibers of polypropylene, glass, carbon, steel, and basalt fibers. Panda et al. [38] showed that as the weight percentage of glass fibers was increased from 0.25% to 1%, the flexural strength of the printed samples was increased.

2.4. Case study of shrinkage cracks in 3DCP

2.4.1. 3D printed wall restrained by lintel beam

Hoffmann et al. [48] designed a 3D printed wall with timber lintels on the top based on the printing processes, the influence of mechanical and rheological properties of 3D printed fresh concrete. The wall dimensions are: length= 800 mm, width= 65 mm, and height is 280 mm. The lintel is designed as an LVL beam with crossband veneers having dimensions of length= 400 mm, b= 60 mm, and h= 50 mm. The 3D concrete mix has a w/c ratio of 0.23. The binder is mainly composed of 70% CEM I 52.5R Portland cement, 20% fly ash, and 10% silica fumes. The 28-day strength of the concrete mix is 113.7 MPa.
The right and left side wall sections are printed at the same time. After that, the lintel is installed over the opening. Finally, the top beam is printed on the lintel and the wall sections. The 3D printed wall can be seen in figure 2.9a. After one day of completion of the printed structure, cracks were observed in the uppermost layers having a crack width of 0.8 mm, as shown in figure 2.9b. The relative humidity at which the structure is kept is RH= 60 %. According to the authors, the main reason for the cracking is due to the high shrinkage of the 3D-printed concrete. The following three factors are suggested in the research responsible for the cracking: (i) restrained shrinkage due to the rigid lintel beam. (ii) friction between the surface of the lintel beam and concrete structure and (iii) the left and right side wall sections are printed simultaneously, and the shrinkage deformation is uniform towards the cross-section core. The shrinkage of the overlying layers is constrained by the dead weight of these wall sections. The mentioned reasons are more related to the material characteristics indicating that the shrinkage of the concrete mixture is high to cause cracking when restrained by the lintel beam. The mitigation measures to minimize the shrinkage suggested in the research are by internal or external curing.

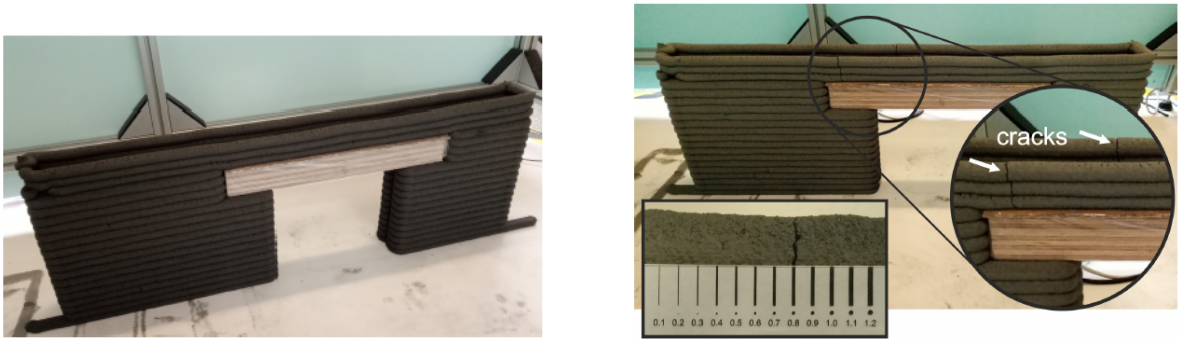

(a) 3D printed wall (b) Cracks due to shrinkage after one day of placement

Figure 2.9: Shrinkage cracks in 3D printed wall, retrieved from [48]

2.4.2. Flower Pot, Print Factory

Two experiments were performed on the printed elements to study the influence of pouring wet sand inside the element on the time of cracking. The flower pots are shaped in a zig-zag pattern as shown in figure 2.10. Each element has a height of 450 mm, an average thickness of 55 mm, and a perimeter of 10140.8 mm In the first element, the wet sand was poured inside the element after one day of printing. The first two cracks were observed after five days of printing. A third crack was observed after six days of printing. In the second element, the wet sand was poured after 14 days of printing. The first two cracks were observed after 26 days of printing and a third crack after 31 days of printing. The sand was kept wet every alternate day. The cracking pattern of element 1 and 2 is shown in figure 2.10.

The possible causes of cracking can be autogenous and drying shrinkage induced in the element. The stresses generated due to shrinkage: stresses due to restrained linear shrinkage and warping stresses due to differential drying shrinkage if exceeded the tensile strength could lead to cracking.

(a) Element 1 (b) Element 2

Figure 2.10: Crack pattern in (a) Element 1 (b) Element 2

An analytical calculation based on Eurocode 2 and JSCE [9] was performed to calculate the shrinkage strains shown in Appendix A. Several assumptions such as rapid hardening cement (Class R), lower w/c ratio, lower time until curing, etc. have been made so that the behavior is similar to the 3D printed concrete mixture. Calculations of Eurocode 2 show a total shrinkage of 450 microstrains (drying shrinkage= 416 microstrains and autogenous shrinkage= 34 microstrains) at 28 days. Whereas JSCE shows a total shrinkage of 788 microstrains (drying shrinkage= 586 microstrains and autogenous shrinkage= 202 microstrains) at 28 days. JSCE includes the autogenous shrinkage in the calculation and has shown better agreement for concrete having low w/c ratio [17].
In this case, based on Eurocode 2 it was estimated that element 1 should crack within 10 days but in

reality, it cracked within 5 days. For element 2, the calculated shrinkage stresses were not sufficient to cause cracking. Calculations according to JSCE gave closer results estimating cracking within 4 days and 33 days for elements 1 and 2 respectively. It implies that Eurocode 2 highly underestimates the calculated shrinkage strains since it is developed for concrete having coarse aggregates. Also, both autogenous and drying shrinkage are crucial for 3D printed concrete.

2.5. Summary

The chapter summarizes the literature review of the shrinkage process in concrete, the 3D printing process, the key characteristics in terms of the casting process, and the material composition, making 3DCP more susceptible to shrinkage. The most important findings of the chapter are listed below:

- Shrinkage in the concrete structure is a volumetric reduction caused by the moisture loss to the environment or cement hydration process which causes a decrease in relative humidity in the pores. As the capillary pores empty, they generate tensile forces due to surface tension. To maintain equilibrium the surrounding matrix shrinks due to the generated compressive forces.
- The autogenous shrinkage occurs due to reduction in relative humidity because of the self-desiccation process in the concrete. It produces uniform strains across the cross-section. Low w/c ratio, high cement content, absence of coarse aggregates, dense microstructure are the factors that make 3D printing concrete susceptible to autogenous shrinkage.
- Drying shrinkage occurs due to the moisture loss to the environment. It can produce differential stresses in the structure. It mainly depends on the environmental conditions such as temperature, relative humidity, wind speed; the geometry of the member, and the curing condition. Since 3D printed structures lack formwork they have immediate exposure to the environment after printing, they are more prone to drying shrinkage.
- The driving mechanism of the autogenous and drying shrinkage can be modeled based on the capillary tension approach if the relative humidity of the structure is more than 40%.

3

Experimental Setup

The chapter describes the experiments performed to study the shrinkage behavior of the concrete mix for cast and 3D printed concrete in unrestrained and restrained conditions. The material properties, experimental setup, and measurement are explained in detail.

3.1. Introduction

The shrinkage-induced cracking depends on multiple factors such as the degree of restraint, stress relaxation, time of restraint, moisture gradient, etc. These factors also affect the occurrence of cracking. In this chapter, the shrinkage behavior of the material is studied in the two extreme restrained conditions: free (degree of restraint= 0) and fully restrained condition (degree of restraint= 1). Free shrinkage test has been conducted for the cast sample and 3D printed samples to study the difference in the shrinkage behavior. The curing conditions also play an essential role in the drying shrinkage, so the test is conducted under the two environmental conditions of covered and exposed. In one case, the samples are completely exposed to the environment after de-molding to capture the field condition if the 3D printing technology is used outdoors. Typically, when a structure is 3D printed in the factory, it is covered in plastic for the first few days for curing. For the restrained condition, the ring test has been performed until cracking is observed under three environmental conditions: covered in plastic, sealed with tape, and completely exposed.

3.2. Material properties

The concrete used for the research is a commercial product. The exact material composition of the mix is not known since it is a commercial product. The mix is comprised of the following raw materials:

- Ordinary Portland Cement, OPC (CEM I 52.5R)
- Limestone filler
- River sand (maximum particle size of 1 mm)
- Additives such as rheology modifiers and superplasticizers

The concrete mixture is a ready-mix concrete mixture comprising dry raw materials and the user is expected to add the water according to the requirement. The exact water-cement ratio is not known; however, it is between 0.25-0.4. The mechanical properties of the concrete mixture are shown in table 3.1.

Properties	**Values**
Compressive Strength (28 days)	56±5.5 MPa
Flexural strength (28 days)	10.1 ±1.4 MPa
Elastic Modulus (28 days)	30 GPa
Shrinkage (91 days)	1±0.03 mm/m

Table 3.1: Mechanical properties of the concrete mixture

3.3. Free shrinkage test

Free or unrestrained shrinkage tests are used to evaluate the shrinkage potential of the concrete. Since the specimen is in unrestrained condition, it can freely change in length in the specified temperature and relative humidity conditions. A free shrinkage test is performed to study the shrinkage behavior of cast and 3D printed specimens under covered and uncovered conditions. Plastic has been used for the covered specimen; however, using waterproof tape to seal the specimen can improve the autogenous shrinkage measurements as the water loss to the environment can be minimized. Nevertheless, using tape in practical situations for long curing time on-site is unrealistic and the plastic sheet is the feasible solution for external curing.

3.3.1. Preparation of samples

Six prisms were cast and six prisms were 3D printed to compare the shrinkage behavior for the 3D printed and cast samples. The concrete mix was taken from the same batch of cement production to ensure homogeneity in the material. The cast samples were molded within an hour difference of printed samples. The cast samples were prepared in the laboratory, whereas the 3D printed samples were printed in the print factory, making the preparation process of both different.

Cast samples

Six prisms of dimensions 40x40x160 mm ^{3} were cast in the molds using the concrete mix as described above. The concrete mix was prepared in a Hobart mixer using 10.75% water by weight of the concrete mixture. Immediately after the casting, three prisms were covered tightly with plastic to ensure no water loss. The rest of the three prisms were exposed to the environment. Although the surfaces covered with mold were not exposed to the environment in the first 24 hours. After 24 hours, all the prisms were de-molded. The three specimens in covered plastic conditions were sealed tightly again, and the other three specimens were completely exposed. All the six specimens were kept in a climate chamber of RH= 65% and temperature, T= 20°C.

3D printed samples

Since it is difficult to 3D print such a small specimen of 160x40x40 mm ^{3} due to the printer's size limitations, it was decided to 3D print a larger structure and cut out the specimen from it. Generally, the diamond saw is used to cut the hardened concrete but to cool down the heated saw during cutting, water is applied. Since it is a shrinkage experiment, supplying external water may deviate from the actual shrinkage behavior of the material. It was decided to cut out the specimens by gently pushing the moulds while in the fresh state. The moulds were 3D printed for the specimen of size 160x40x40 mm ^{3} in PLA (Polylactic Acid) material as shown in figure 3.1.

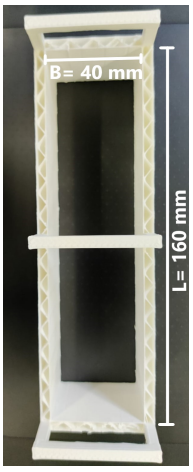

(a) Mould of specimen- top view

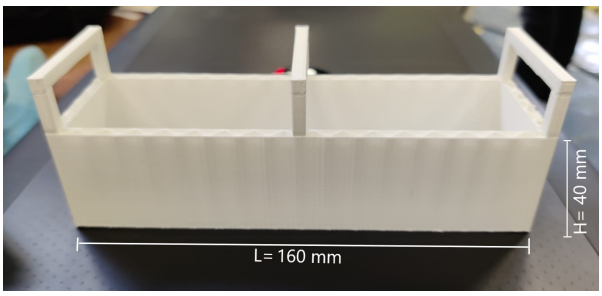

(b) Mould of specimen- side view

Figure 3.1: Mould of specimen for 3D printed prisms

The mould was gently pushed into the 3D printed structure ensuring the layers are not distorted. A

1600 x 100 x 40 mm^3 (LxBxH) rectangular frame was 3D printed at the 3D-print factory. Four layers of 10 mm height were printed as shown in figure 3.2. The print speed was 215 mm/min and the width of the nozzle width was 70 mm.

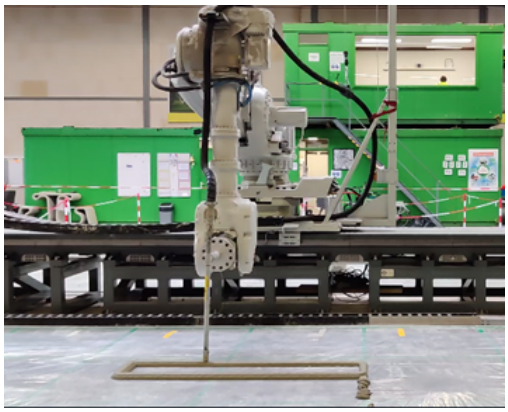

Figure 3.2: 3D printing of the rectangular frame

After printing, the prism was cut out of the structure by gently pressing the mould. Due to pressing, there was a slight bulge in the specimen in the direction of height. However, since the linear measurement of shrinkage is done in the length direction, not much influence is expected. After the prisms were cut out, three specimens were covered tightly with plastic sheets, whereas three specimens were left exposed to the environmental condition. The specimen in covered and uncovered conditions after moulding is shown in figure 3.3.

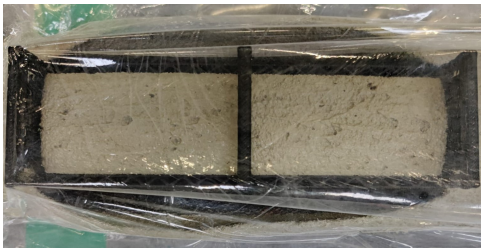

(a) Specimen covered with plastic sheet

(b) Specimen exposed to environment

Figure 3.3: Specimen for free shrinkage test in (a) covered condition (b) uncovered condition before de-moulding

3.3.2. Measurement of the shrinkage and mass loss

The change in length of the specimens in the direction of the length (L= 160 mm) and the mass loss of each specimen have been measured on 1, 3, 7, 14, 21, 28, 35, 49 and 60 days after the casting. The lengths of all the specimens at different days were measured using a digital length comparator. The measurement procedure for 3D printed and cast samples was the same. The length of the specimen at t=1 day, from de-moulding, has been taken as the original length. The linear shrinkage has been calculated as:

$$\varepsilon_L = \frac{L_t - L_i}{L_i} \tag{3.1}$$

where,
L_t is the length at t day, and
L_i is the initial length, taken as 160 mm.

Additionally, the mass loss is measured over time for all the specimen at the same day as well. This ensures the sealing condition of the covered specimen is proper as the moisture loss to the environment will lead to the mass loss of the specimen.

3.4. Restrained shrinkage test

A great majority of the concrete structures in the construction industry are restrained with varying degrees of restraint. Some examples of the restrained concrete structures are subgrade restraining the slabs-on-grade, bridge decks restrained by abutments, girders or beams, composite slabs restrained by the steel supporting girders. The free shrinkage test tells about the development of change in length. However, it may not always be sufficient for predicting the potential of cracking, which is influenced by complex interactions of strength gain, stiffness development, creep, shrinkage and the degree of restraint [49]. When the deformation of the structure is completely prevented it is considered to be 100% restrained with a degree of restrain of 1. When the structure is free to deform it is considered to have free shrinkage with 0% degree of restraint.
To study the early-age cracking several tests have been developed such as the cracking frame and temperature-stress testing machines, concentric ring tests.

3.5. Ring test

The ring test is a setup of two concentric steel rings in which the shrinkage cracking potential of cementitious mixtures (paste, mortar, or concrete) can be assessed. It is performed by casting the cementitious mixtures between two steel rings. Two strain gauges are attached at diametrically opposite ends at the mid-height on the surface of the inner steel ring. They are then connected to a data acquisition system that records the circumferential strain of the inner steel ring continuously. Over time, the concrete shrinks due to loss of moisture internally or externally but is restrained by the inner steel ring. This generates compressive stresses in steel ring and tensile stresses in the concrete. The development of compressive stresses in the steel ring is reflected as the strain recorded by the gauges. Once the maximum circumferential tensile stresses in the concrete exceed the tensile strength, cracking occurs. The tensile stress in the concrete around the crack is subsequently released, and the compressive stresses imposed on the steel ring by the concrete ring diminish, resulting in a sudden decline in the compressive stresses in the steel ring. It is reflected by a sudden drop in the measured strain. Further investigation of cracking can tell about the location of the crack, crack width, etc. An important point for the ring test is to perform it at a constant temperature as the steel can expand or contract if the temperature changes leading to a change in the degree of restrain.

The analytical solution of the ring test for calculating the generated shrinkage stresses is presented by Hossain et al. [49]. The calculations are done based on mould geometry, shrinkage strains, and mechanical properties of the concrete mix.

3.5.1. Preparation of specimen

The fresh mortar was prepared by mixing the ready-mix concrete mixture in a Hobart mixer, a single shaft pan mixer. Approximately 5 kg of the ready-mix concrete mix was required for one ring specimen in which 10.75% by weight of water was taken. First, the dry materials of the concrete mixture were mixed with water at low speed (25 RPM) for 1 minute and then at high speed (45 RPM) for two more minutes. Then the walls were scrapped and the mixture was mixed manually to ensure there is no residue at the bottom of the mixer. Finally, the mixture was mixed for two more minutes at high speed. The concrete mixture was poured between the two concentric rings. The inner radius and the outer radius of the inner steel ring are 75 mm and 87.5 mm, respectively. The outer radius of the cement paste ring is 125 mm. The exact dimensions can be seen in figure 3.5
The ring test setup was prepared by placing a thin foam between the outer ring and specimen for easy de-moulding. The inner ring was coated with vaseline to minimize the friction between the specimen and the inner ring. The lower surface was covered with plastic film to minimize friction as well. The fresh mortar was poured between the two rings. It was compacted well by hand in a layer-by-layer manner to avoid air voids. The top layer was leveled by a scrapper for a uniform surface. The samples were kept in a climate-controlled chamber at a temperature of 20 °C±0.2 °C and a humidity of 55%. The outer ring was de-molded after 24 hours of casting. One of the samples was exposed to drying from all sides, two specimens were completely sealed with plastic and one of them was tightly sealed with waterproof tape and covered with plastic as shown in figure 3.4.

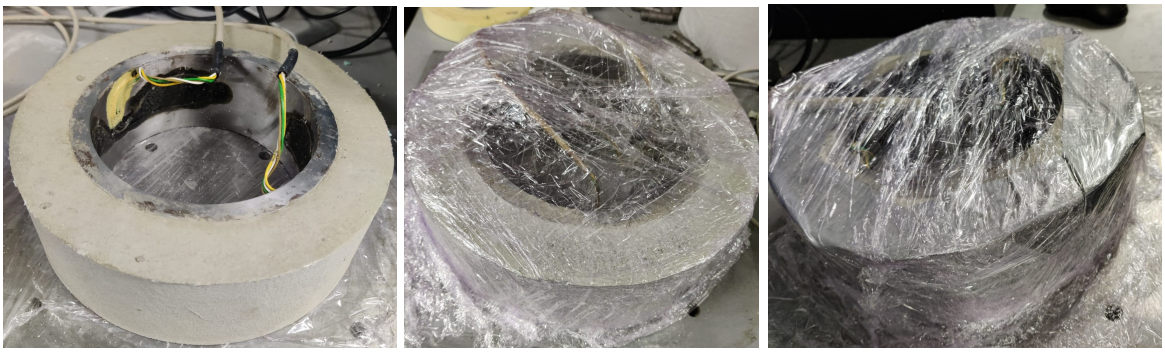

(a) (b) (c)

Figure 3.4: Experimental setup of the ring test of specimen (a) exposed to drying, (b) covered with plastic sheet and (c) sealed with waterproof tape and plastic sheet

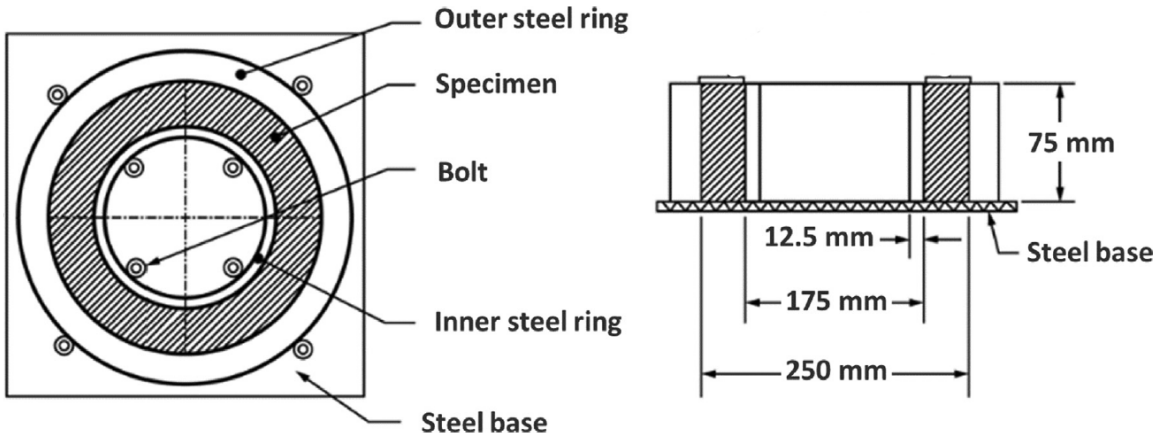

Figure 3.5: Configuration of the ring test (left) top view (right) side view retrived from [50]

The inner ring was equipped with two strain gauges at diametrically opposite directions to measure the steel ring's strain. The strain was recorded every 10 minutes. The recording started from approximately 20 minutes after water was mixed in the mortar mix preparation, up to the time of cracking. The residual stresses generated due to the strain can be analytically calculated by the following based on [49]:

$$\sigma_{\text{max}} = -\varepsilon_{\text{steel}}.E_{\text{steel}}.\left(\frac{R_{OI}^2 - R_{II}^2}{2R_{OI}^2}\right)\left(\frac{R_{OP}^2 + R_{OI}^2}{R_{OP}^2 - R_{OI}^2}\right) \tag{3.2}$$

where,
$\varepsilon_{\text{steel}}$ is the recorded strain of the inner steel ring
E_{steel} is the elastic modulus of steel
R_{II} is the inner radius of the inner steel ring
R_{OI} is the outer radius of the inner steel ring
R_{OP} is the outer radius of the concrete paste

The timely measurement of the weight of the specimen can ensure that the sealed specimen has minimum moisture loss to the environment. However, due to the setup configuration of the strain gauge connections, it is not possible to weigh the specimen time-to-time. Also, any disturbance to the specimen can cause an error in the strain gauge readings.

3.6. Summary

The chapter describes the experimental setup used to study the shrinkage behavior of the material. The key points are:

- In this research, free shrinkage and restrained shrinkage tests have been conducted to study the shrinkage behavior of the material under different curing conditions.
- Six cast and six 3D printed samples are prepared to investigate the shrinkage behavior. Out of these, three of each are covered in plastic and three in exposed condition at RH= 65% and T= 20°C. Uniaxial change in length has been used to measure the shrinkage strain time-to-time after de-moulding. Also, the weight loss has been measured for each specimen.
- Ring test has been performed over four specimens with one in exposed condition, two sealed under the plastic sheet and one sealed with waterproof tape under a plastic sheet. The strain of the inner steel ring has been recorded every 10 minutes till the time of cracking.

4

Experimental results

In this chapter, the experimental results of the free shrinkage test and the restrained ring test conducted under different environmental conditions for the concrete mix are discussed.

4.1. Free shrinkage test

The free shrinkage behaviour of six cast and six 3D printed samples have been investigated in the unrestrained condition on 1, 3, 7, 21, 28, 35, 49 and 60 days.

4.1.1. Cast sample

Out of the six cast samples, three are covered in plastic sheet (named as CC-S1, CC-S2 and CC-S3) whereas the remaining three are uncovered, exposed to the environmental condition (named as CUC-S1, CUC-S2 and CUC-S3). The specimen-wise shrinkage behaviour of the covered cast specimen is shown in figure 4.1(a) and the uncovered cast specimen in figure 4.1(b). The average shrinkage value of cast specimen in covered and uncovered condition at 60 days is 716 microstrains and 860 microstrains respectively. The specimen CUC-S2 shows a discrepancy in the behaviour as compared to the other two specimens (CUC-S1 and CUC-S3). Hence, the average shrinkage of the cast specimen in the uncovered condition is taken as 860 ±13.25 microstrains at 60 days considering the average of CUC-S1 and CUC-S3. A sharp increase in the rate of increase of the shrinkage in the first 28 days is observed especially in the uncovered samples after which the increase is only 2-4%.

Similar results are obtained by other researchers as well. Le. et al. [41] investigated the influence of curing conditions on the printed concrete sample (cured in water, damp hessian and T= 20°and RH= 60%) on drying shrinkage. The highest shrinkage was obtained for a fully exposed specimen having a drying shrinkage of 597 microstrains within 30 days. Similarly, Zhang et al. [42] found the drying shrinkage of 3DCP cured in 20 °C and RH= 50% to be 840 microstrains after 70 days.

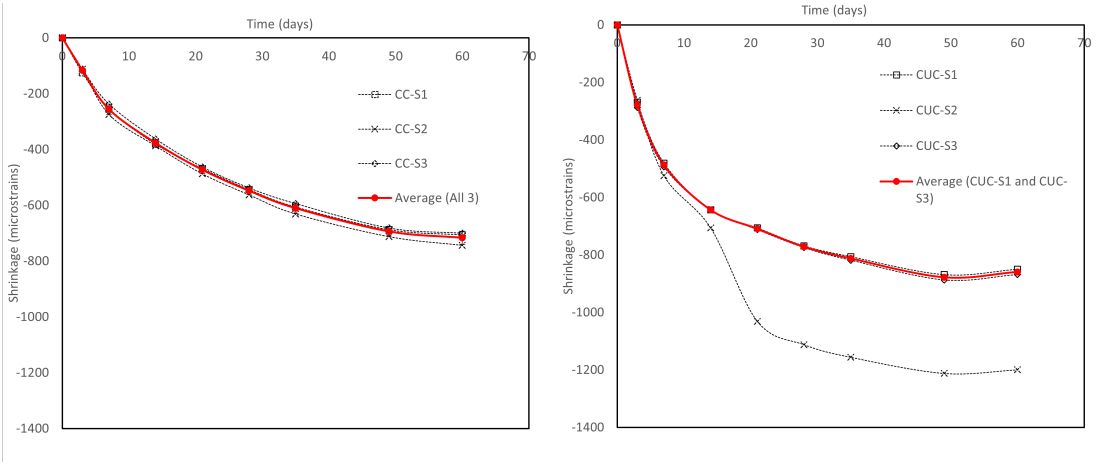

Figure 4.1: Specimen-wise shrinkage behaviour of cast samples in (a) covered condition (b) uncovered condition. CC= Cast in covered condition, CUC= Cast uncovered condition. Note that the average value is calculated out of three specimens shown in red

4.1.2. 3D printed sample

Out of the six 3D printed specimens, three are covered in plastic sheet (named as 3DC-S1, 3DC-S2 and 3DC-S3) whereas the remaining three are uncovered, exposed to the environmental condition (named as 3DC-S1, 3DC-S2 and 3DC-S3). The specimen-wise shrinkage behaviour of the covered 3D printed specimen is shown in 4.2(a) and the uncovered cast specimen in 4.2(b). The average shrinkage value of 3D printed samples in covered and uncovered condition at 60 days is 856 microstrains and 1100 microstrains respectively.

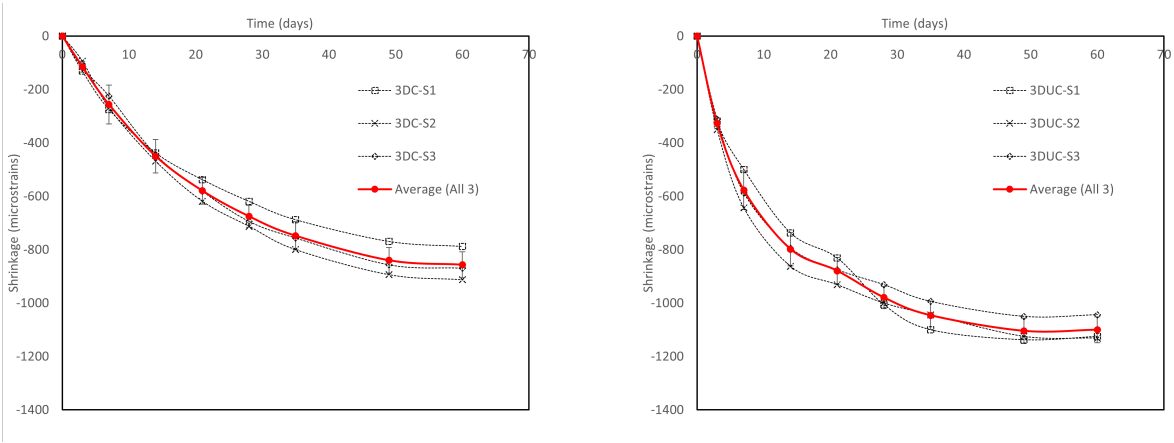

Figure 4.2: Specimen-wise shrinkage behaviour of 3D printed samples in (a) covered condition (b) uncovered condition. 3DC= 3D printed in covered condition, 3DUC= 3D printed in uncovered condition. Note that the average value is calculated out of three specimens shown in red

4.1.3. Comparison between Cast and 3D printed sample

The comparison of the shrinkage behaviour of the cast and 3D printed specimens in covered and uncovered specimens is shown in figure 4.3 using the average values as shown in figures 4.1 and 4.2. The 3D printed specimen shows a higher shrinkage as compared to the cast sample in both covered and uncovered condition. In uncovered situation, the shrinkage of 3D printed specimen is higher by 15.52%, 21.17% and 21.88% at 7, 28 and 60 day respectively as compared to cast specimen. Whereas in covered condition, the shrinkage of 3D printed specimen is higher by 0.01%, 18.83% and 16.3% at 7, 28 and 60 day respectively as compared to cast specimen. The shrinkage of cast samples in covered condition is the lowest as it is majorly autogenous shrinkage. Followed by the 3D printed samples in covered condition, however at 60 days the shrinkage is comparable to the cast specimen in uncovered

condition. The specimens in uncovered condition have a higher shrinkage caused by the moisture loss both to the autogenous and drying shrinkage.

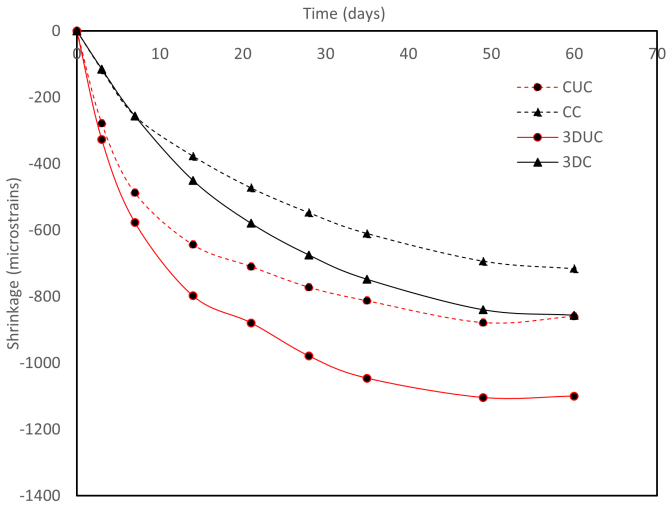

Figure 4.3: Comparison of shrinkage behaviour the cast and 3D printed specimens over time. Solid lines indicate 3D printed and dashed lines as cast samples. Red indicates uncovered samples and black indicates covered samples.

The higher shrinkage in 3D printed specimens can be attributed to the following reasons:

- Higher porosity at the inter-layer
  It is suspected that the 3D printed samples have a higher porosity as compared to the cast samples. When the shrinkage and mass loss curves are compared, even though the mass loss in 3D printed and cast sample is same, there is a higher shrinkage observed in the 3D printed sample. This implies that when there is moisture loss from capillary pores of lower radius, higher shrinkage stresses are produced (Equation 2.2) but the mass loss is not substantial. Also, a higher rate of mass-loss is observed in 3D printed sample as compared to cast samples in the first 7 days. Initial mass-loss attributes to the loss of free evaporable water. Kruger et al. [51] observed a higher porosity (7.9%) in 3D printed specimens as compared to the cast samples (6.8%), at a 15 microns CT scanning resolution.

- Increase in temperature of concrete due to friction and machinery heat while extrusion-
  The friction in the hose and the pump leads to an increase in the temperature during the print. The 3D printing machinery also gets heated up especially for a relatively long printing time. Wolfs [44] observed the temperature of extruded material immediately after the extrusion to be high as 35°C within 30 minutes of the start of printing as compared to the ambient temperature of 20°C. This may lead to higher plastic shrinkage due to faster moisture loss at higher temperatures. However, the results that the shrinkage in 3D printed and cast samples were found to be similar in the first 3 days. So the initial placement temperature might not have a strong influence on the recorded shrinkage.

- Lack of compaction-
  An in-situ concrete structure is cast in formwork and the entrapped air is removed by proper vibration. Whereas in the case of a 3D printed concrete structure, the concrete is directly pumped under pressure to the nozzle and extruded to print the structure. It may potentially lead to disparities between intralayer void sizes and shapes in the structure. Sanjayan et al. [52] observed a higher surface moisture content at zero minute delay time as compared to 20 minute delay time. The possible reason could be the extrusion of fresh mixture under high pressure that can lead to pressurized bleeding. It may result to the formation of a lubrication layer under high pressure of extrusion. Evaporation of this free water can lead to higher plastic shrinkage. In this case, the

shrinkage is recorded from one day after de-molding so it might be possible that the effect is not recorded.

4.1.4. Mass Loss

The average mass loss was measured as well over time for all the specimens as shown in figure 4.4. It was calculated as the difference in the mass of the specimen as compared to its initial mass. For the cast sample in uncovered condition (named CUC) the average mass loss is 0.83% at 60 days. For the 3D printed sample in covered condition (named 3DUC) the recorded average mass loss 0.87% at 60 days.
For the cast sample in covered condition (named CC) the average mass loss is 0.41% at 60 days. For the 3D printed sample in covered condition (named 3DC) the recorded average mass loss is 0.42% at 60 days. A similar trend in the average mass loss is observed in the samples having the same curing condition. This is expected as the samples in uncovered condition have moisture loss to the environment. The difference in the average mass loss between the 3D printed and cast samples is not significant for both covered and uncovered condition. Only a difference of 1-3% higher mass loss in 3D printed sample is observed as compared to cast sample.

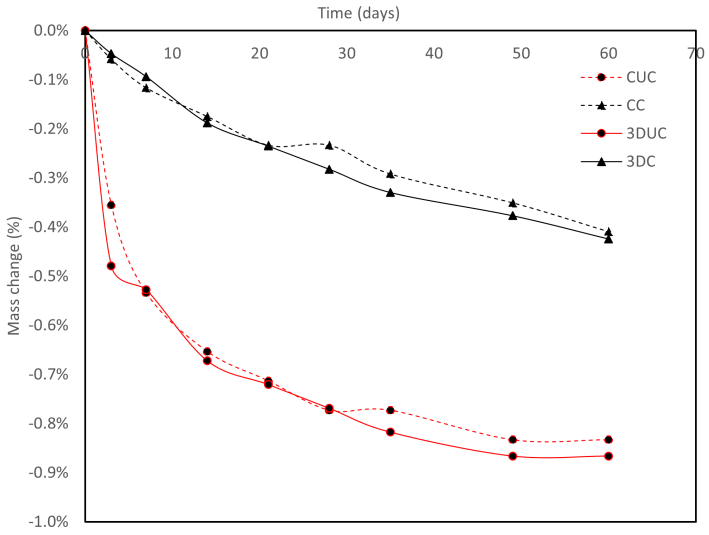

Figure 4.4: Mass loss of the cast and 3D printed specimens over time. Solid lines indicate 3D printed and dashed lines as cast samples. Red indicates uncovered samples and black indicates covered samples.

The weight of the specimen decreases over time due to the loss of water. The higher the mass loss of the specimen, the higher the drying shrinkage. Ideally, the weight loss should be negligible in the case of covered specimen. However, in this study, the specimen covered in plastic sheet showed a mass loss upto 0.42% at 60 days, implying moisture loss to the environment. So the recorded shrinkage values for specimen in covered condition cannot be attributed only to the autogenous shrinkage. The possible reason of the observed mass loss in the covered specimen is that the plastic sheet is not sufficient to prevent the moisture loss. Similar results can be seen in the restrained ring test (discussed in next section) as well for the specimens covered in a plastic sheet as compared to one covered with waterproof tape and plastic sheet. It is recommended to use waterproof tape if the autogenous shrinkage has to be measured. However, from practical point of view, a large 3D printed concrete structure has to be covered by plastic sheet to minimize drying shrinkage which is similar to the conducted experiment.

4.2. Restrained Ring test

4.2.1. Strain measurement

The radial strains of the steel ring measured by the strain gauges for the different specimens are shown in figure 4.5(a). The individual strains recorded by the two strain gauges applied diametrically opposite

on the specimen can be seen in Appendix B. The corresponding residual stresses based on the equation 3.2 have been calculated as shown in figure 4.5(b). The specimen in exposed condition (named SE) cracked after 2.8 days, covered in plastic sheet only (named SP-1 and SP-2) cracked after 3.7 days and 4.2 days respectively and covered with tape and plastic sheet (S-TP) cracked after 8 days. The rate of strain development is highest in specimen SE due to higher drying shrinkage due to moisture loss to the environment from the time of casting. Similarly, the rate of strain development is lowest in the specimen S-TP as mainly the shrinkage is due to the self-desiccation process. Also, in specimen S-TP a peak at about day 7 can be seen which starts to decrease but does not cause a sudden drop. Finally, the cracking occurred around day 8 implying that there was a microcracking at day 7 but did not lead to cracking of the specimen.

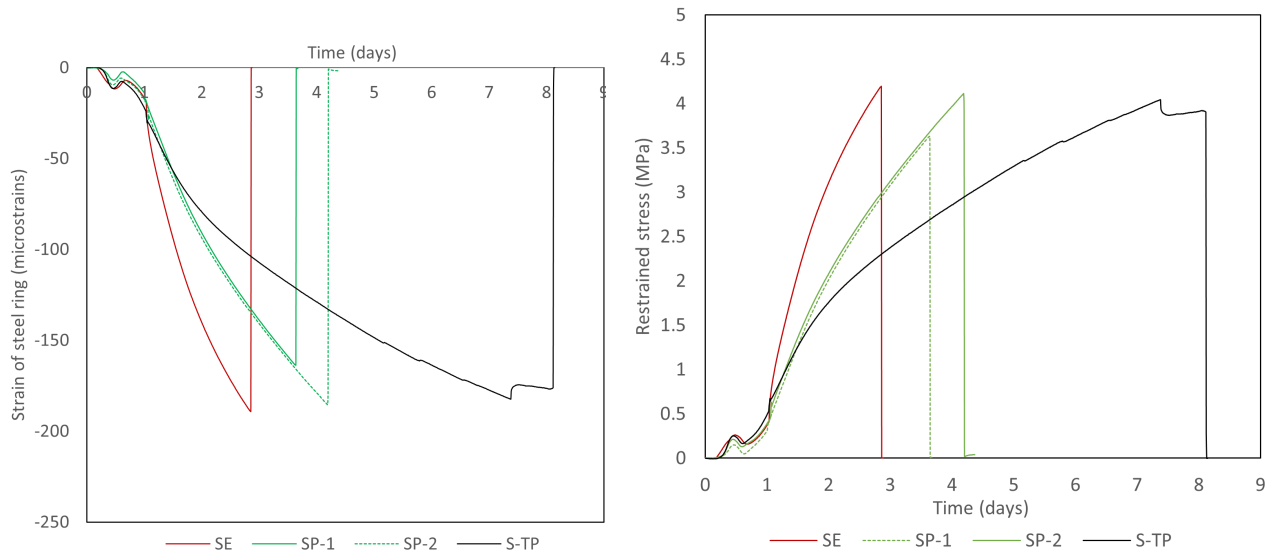

Figure 4.5: (a) Recorded steel ring strain for each specimen (b) Residual stress for each specimen calculated using equation3.2. Here SE= specimen exposed to drying, SP= specimen covered with plastic sheet and S-TP= specimen covered with tape and plastic sheet.

.

All the specimens cracked at a similar maximum residual stress of 4 MPa. It was expected that since the specimen sealed with waterproof tape cracked at 8 days, the tensile strength should be higher than 3 days. Thus the residual stresses at the time of cracking should be higher. The possible reason could be due to the difference in the produced stresses due to autogenous and drying shrinkage. Due to external drying, the outer surface shrinks more as compared to the inner circumferential surface, producing a stress gradient starting at the outer surface and gradually decreases towards the inside surface. Consequently, a flexural mode of failure is resembled [53]. The flexural strength of the concrete is higher than the tensile strength since it is a brittle material. In the case of autogenous shrinkage, the stress distribution is uniform across the cross-section. In this case, when the tangential stresses of the inner ring exceed the tensile strength, cracking occurs. Also, the environmental condition will influence the development of elastic modulus and tensile strength.

A slower development of self-induced stresses allows the relaxation to reduce the stresses in the specimen. As a result, reducing the rate of autogenous deformations can help to reduce the risk of cracking. One of the main conclusions from the test is that even in completely sealed condition with tape, the autogenous shrinkage is high enough to cause shrinkage-induced cracking if restrained immediately after casting.

4.2.2. Crack width

The average crack width of the different specimens after cracking is shown in figure 4.6. All the specimen have a single crack running from top to the bottom face of the ring and almost constant over the height of the specimen. The specimen in exposed condition has the highest average crack width of 0.9

mm, followed by the specimen covered in plastic having 0.8 mm of average crack width. The specimen covered in tape and plastic has the lowest average crack width of 0.1 mm.

(a) Average crack width= 0.9 mm (b) Average crack width= 0.8 mm (c) Average crack width= 0.1 mm

Figure 4.6: Average crack width of the specimen in (a) Exposed (SE) (b) Covered with plastic (SP-2) and (c) Covered with tape and plastic (S-TP)

4.3. Summary

The chapter describes the experimental results of the free shrinkage test and the restrained ring test. The key findings are:

- The average shrinkage value for the cast samples obtained at 60 days are 715 microstrains and 860 microstrains respectively in covered and uncovered conditions. Whereas the average shrinkage value for the 3D printed samples obtained at 60 days are 856 microstrains and 1100 microstrains. The rate of shrinkage is higher in the first 28 days for the uncovered samples.
- A difference of 1-3% was observed in the average mass loss of samples in the same environmental conditions. The average mass loss for uncovered and covered specimen is 0.83% and 0.42% at 60 days respectively.
- The 3D printed samples showed a higher shrinkage of 15-20% as compared to the cast sample. Combining the result of shrinkage and mass loss, it is suspected that the 3D printed samples have more capillary pores.
- The restrained ring test showed that the specimen in exposed condition cracked within 2.8 days whereas one covered in plastic sheet after 4 days and covered in waterproof tape and plastic sheet cracked after 8 days of casting. It indicates that the autogenous shrinkage in the concrete mixture is high to cause early age shrinkage-induced cracking.

5

Theoretical framework

A finite element model has been developed to simulate the free shrinkage behaviour of the cast sample in covered and uncovered conditions. This chapter discusses the theory to calculate shrinkage strains using the relative humidity distribution with Kelvin-Laplace Equation. The FEM simulation provides calibrated input parameters to calculate the RH distribution inside the specimen. Later the RH distribution obtained from the model has been used to calculate the shrinkage strain of the experimental results using the Bentz deformation model. The main parameters to calculate the shrinkage strain have been discussed along with the sensitivity analysis of the parameters.

5.1. Background

Initially, when water is added to the concrete mix, the pores between the solid cement particles are filled with water. A skeleton structure is formed after the setting of fresh concrete. Due to the cement hydration process, capillary pores are formed and to compensate for the volume decrease, corresponding menisci are formed. To reach equilibrium, the initial relative humidity of 100% in vapour saturated stage gradually decreases.

5.1.1. Kelvin-Laplace Equation

Due to drying, the pores inside the micro-structure lose water, thus inducing capillary pressure. First, the water is lost from larger pores and then from smaller pores. The capillary pressure can be calculated using the Kelvin Equation which is based on the relative humidity. Since the RH inside the pores is changing with time due to drying and autogenous shrinkage, the capillary pressure is a function of time as well. The Laplace equation evaluates the capillary pressure using the radius of the pore at the water-gas interface affecting the drying. It assumes an idealized spherical pore structure and gives the capillary pore pressure $\sigma_{\text{cap}}(t)$ as-

$$\sigma_{\text{cap}}(t) = -\frac{\rho RT}{M} \ln(\text{RH}(t)) \tag{5.1}$$

where,
RH is the internal relative humidity, ratio of pressure of water vapor over the saturated water pressure
ρ is the density of water, taken as 1000 kg/m^3
R is the universal gas constant, taken as 8.314 J/mol-K
T is the temperature, taken as 293.15 K for 20°C
M is the molecular weight of water, taken as 0.018 kg/mol

The value of the molecular weight has been taken from similar studies valid for temperature range [23], [54]. The present experiments were performed at 20°C (293.15 K) under climate chamber so the temperature can be taken as a constant.

5.1.2. RH distribution

To calculate the capillary pressure due to moisture loss, the main input for the Kelvin-Laplace equation is the distribution of relative humidity over time as seen in equation 5.1. As discussed in chapter 2, the capillary pores RH decreases due to the self-desiccation and moisture loss to the environment. Kim et al.[19] modelled the relative humidity distribution in the early age concrete considering the effect of self-desiccation phenomena and the drying process. The modelling of autogenous shrinkage is crucial especially for concrete with a low w/c ratio at early ages.

$$\frac{\partial h(x,y,z,t)}{\partial t} = \frac{\partial}{\partial x}\left[D(h)\frac{\partial h}{\partial x}\right] + \frac{\partial}{\partial y}\left[D(h)\frac{\partial h}{\partial y}\right] + \frac{\partial}{\partial z}\left[D(h)\frac{\partial h}{\partial z}\right] - \frac{\partial h_a}{\partial t} \tag{5.2}$$

where,
h is the pore relative humidity,
$D(h)$ is the moisture diffusion coefficient assumed to be isotopic,
$\frac{\partial h_a}{\partial t}$ is rate of pore RH due to self-desiccation process.

Usually, for concrete having high w/c ratio (typically more than 0.4), the reduction of pore RH due to the self-desiccation process is negligible[24]. Since the concrete mixtures for 3D printing have low w/c ratio, both the reduction in RH due to the autogenous and drying should be modelled.

Diffusion process

The rate of moisture diffusion in concrete is directly proportional to the w/c ratio [19]. It implies that the moisture diffusion in concrete with low w/c ratio will be slower due to denser microstructure. Also, the decrease in relative humidity at the drying surface is higher than the inside of concrete, especially during the early stage of drying.

As seen in equation 5.2, the pore RH due to moisture loss is dependent on the moisture diffusion coefficient of the concrete. Ideally, the data required to calibrate the diffusion coefficient for the particular concrete mixture should be the evolution of RH in the pores over time, the RH distribution profiles across the cross-section for various environmental conditions and member sizes, ambient humidity conditions and exposure time to the drying atmosphere. However, due to the lack of the data and experiment at such large scale, the parameters in the equations are judiciously assumed and are empirically calibrated.

CEB FIP Model Code 1990 [32] proposes a non-linear moisture diffusion coefficient dependent on the pore RH under isothermal conditions as:

$$D(h) = D_1\left(\alpha + \frac{1-\alpha}{1+\left[\frac{1-h}{1-h_c}\right]^n}\right) \tag{5.3}$$

where,
D_1 is the maximum rate of diffusion at h=100%,
$\alpha = D_0/D_1$,
D_0 is the minimum rate of diffusion at h= 0%,
h_c is the pore RH at D(h)= 0.5D_1 and
n is a material parameter determining the steepness of the rate of permeability

- D_1- It determines the permeability at the saturation (h=100%) and is dependent on the distribution of pore size. The two main influencing factors are the w/c ratio and the hydration degree. [55].
- h_c- The transitional humidity indicates the value of RH as the center of the steepness of the permeability decrease. A concrete having high w/c ratio constitutes more number of large pores resulting in the decrease of permeability at a higher RH.
- α- It indicates the maximum relative decrease of permeability as the humidity decreases.

- n- This parameter determines the steepness of the permeability decrease with the humidity. Typically it is taken in the range of 1 to 15. The lower the value, smoother the permeability decrease.

The recommended value suggested by CEB-FIB are α = 0.05, h_c= 0.8 and n = 15. The values of the input parameters used by various researchers to model RH pores in concrete for different w/c ratio is shown in table 5.1.

Compressive strength [MPa]	w/b	D_1 (m^2/s)	n	h_c	α	Source
35.3	0.43	3.67×10^{-10}	15	0.8	0.05	[56]
35.3	0.43	2.78×10^{-10}	15	0.8	0.05	[56]
42.5 MPa	0.3		1	0.793	0.018	[22]
42.5 MPa	0.4	1.62×10^{-10}	1.5	0.792	0.022	
42.5 MPa	0.5	2.13×10^{-10}	2	0.795	0.04	
76	0.28	3.11×10^{-10}	15	0.8	0.05	[19]
53	0.4	3.5×10^{-10}	15	0.8	0.05	
22	0.68	7.278×10^{-10}	15	0.8	0.05	

Table 5.1: Input parameters of the non-linear diffusion coefficient in the literature

Self-desiccation Process

The decrease in pore relative humidity due to self-desiccation process is crucial for low w/c ratio. Kim et al [19], Jiang et al. [20], Zhang et al. [11] determined the RH distribution experimentally by measuring the RH over time using digital sensors in sealed specimen. Rahimi-Aghdam et al. [55] proposed an analytical hydration model to predict the relative humidity due to self-desiccation. The model, which is derived empirically, showed good match with the RH distribution experimentally obtained by Kim Lee et al. [19] and Jiang et al. [20] for low w/c ratio concrete as discussed by Rahimi et al.[55]. The model is described below as:

$$\begin{gathered} h_s = h_s^f \left(\frac{\alpha - \alpha_{\text{set}}}{\alpha_u - \alpha_{\text{set}}} \right)^{n_{wc}} \\ n_{wc} = 25(wc - 0.1); \\ h_s^f = 0.5(w/c)^{-0.26} - 0.53; \\ \alpha_{set} = 0.05 + 0.2(w/c - 0.3) \end{gathered} \tag{5.4}$$

where,
h_f is the RH at ultimate degree of hydration, suggested value is 0.75,
α_{set} is the degree of hydration at the setting time.

The empirical relations are calibrated for concrete without admixtures, at room temperature.
As explained in chapter 4, in this research, the attempt to measure the autogenous shrinkage was made by measuring the shrinkage of covered specimen. It did not produce the expected results. The mass loss observed was quite high. So in this research, the proposed analytical model [55] was used to calculate the decrease in RH due to self-desiccation process.

Surface factor

The exchange of the moisture from the surface to the environment is expressed as [10]:

$$J_w = \eta(h - h_{\text{env}}) \tag{5.5}$$

where,
J_w is the moisture flux across the surface (kg/m^{2}s),
η is the surface emissivity (kg/m^{2}s),
h_{env} is the ambient RH.
h is the pore RH.

Different values of surface emissivity are recommended in the literature. Bažant et al. [57] suggested 85×10^{-6} kg/m^{2}s for indoors and 350×10^{-6} kg/m^{2}s for outdoors. Ali et al. [58] suggested 6×10^{-6} kg/m^{2}s for indoors and 9×10^{-6} kg/m^{2}s for outdoors.

Another form of expressing the moisture loss at the surface commonly used in the literature [10] is $D(h)\left(\frac{\partial H}{\partial n}\right)|s = f(h_s - h_{en})$ where f is the surface factor. Huang et al. [10] calibrated the value of f as 3.5 $\times 10^{-9}$ - 6 $\times 10^{-9}$ m/s for concrete mixture with compressive strength of 54.5 MPa. West and Holmes [59] suggested a value of 10^{-8} - 10^{-7} m/s.
Since the parameter surface emissivity (η) or surface factor (f) increases the complexity by adding an additional factor for calibration, one method suggested by Zhao et al.[22] is to take the RH at the surface to be constant. The experiment performed by Li [60] showed that the moisture gradient at the interface of drying surface and the environment diminish gradually. Henceforth, it is suggested to use a constant relative humidity while modelling the moisture exchange at drying surface instead of the convective condition [60]. An alternative proposed by Bažant and Najjar [57] is to consider an additional equivalent thickness of 0.75 mm, a fictitious layer to the concrete whose surface RH equals to the ambient RH condition.
In this research, to reduce the complexity, the relative humidity at the drying surface is modelled as constant and equal to the ambient RH.

5.1.3. Bentz Deformation Model

Once the relative humidity distribution over the time is known, the capillary pressure can be determined from the Kelvin-Laplace equation (equation 5.1. Bentz et al. [32] expressed the deformation of the cement paste due to the pore pressure as follows:

$$\varepsilon_{Lin} = \frac{S_w(t)\sigma_{\text{cap}}(t)}{3}\left(\frac{1}{K_P(t)} - \frac{1}{K_S}\right) \tag{5.6}$$

where,
ε_{Lin} is the linear elastic strain (m/m),
S_W is the water saturation factor,
σ_{cap} is the capillary stress (MPa),
K_p is the bulk modulus of porous structure, which is cement paste (MPa),
K_S is the bulk modulus of solid cementitious component (MPa)

The equation is only valid for a fully saturated linear elastic material. To approximate it at partial saturation which is the case of cement paste, the saturation factor is taken. To take creep into account, the equation can be further modified as [21]:

$$\varepsilon(t,\tau) = \varepsilon(\tau) + \varepsilon(t,\tau)$$
$$\varepsilon_{el}(\tau) = \frac{S_w(\tau)\sigma_{cap}(\tau)}{3}\left(\frac{1}{K_P(t)} - \frac{1}{K_S}\right)$$
$$\varepsilon_{cr}(t,\tau) = \varepsilon_{el}(\tau)\phi(t,\tau)$$

where,
ε(t,τ) is the total deformation at time τ_n,
ε_{el} is the elastic deformation at time τ_n and
$\varepsilon_{cr}(t_n,\tau_n)$ is the time-dependent deformation at time τ_n determined by the creep coefficient.

Since the creep of 3D concrete is not studied in detail, in this study, the effective elastic of modulus is taken while calculating the shrinkage strain given in equation 5.6. Lura [23] and Song et. al [54] suggest a factor of 3 for high strength concrete.

Calculation of degree of saturation
The degree of saturation is the ratio of the evaporable water content, V_{ew} in the hardening paste to the total porosity of the cement paste during hydration, V_p expressed as:

$$S_w = \frac{V_e w}{V_p} = \frac{V_{iw} - V_{new}}{V_{iw} - V_{new} + V_{cs}} \tag{5.7}$$

where,
V_{iw} is the initial water content,
V_{new} is the non-evaporable water content and
V_{cs} is the volume of chemical shrinkage.

The development of degree of saturation can be experimentally calculated by obtaining the initial water content, volume of non-evaporable water and chemical shrinkage using equation 5.7. The volume of non-evaporable water is obtained by taking the difference in the mass of cement mix undergoing hydration at 105 °C and 950°C. One of the methods to obtain chemical shrinkage experimentally is to measure the volume decrease of paste by immersing it into a flask in a temperature bath. More details of these experiments can be studied in Tianshi Lu [21].

In this study, the development of saturation of degree has been calculated numerically using the software HYMOSTRUC. In numerous studies, HYMOSTRUC has shown good agreement with the experimental values [21]. It uses Power's volumetric model for Portland cement paste. However, 3D printing concrete mixture has different admixtures such as superplasticizer, thixotropic chemicals which can result in variation. The Power's model expresses the degree of saturation as:

$$S_w = \frac{V_e w(\alpha)}{V_p(\alpha)} = \frac{p - 0.72.(1-p).\alpha}{p - 0.52.(1-p).\alpha} p = \frac{w/c}{w/c + (\rho_w/\rho_c)} \tag{5.8}$$

where,
p is the initial porosity,
α is the degree of hydration,
ρ_w is the density of water,
ρ_c is the density of cement and
w/c is water to cement ratio.

The ultimate degree of cement hydration as a function of the w/c ratio for normal Portland cement concrete as proposed by Mills [61] is given by:

$$\alpha_u = \frac{1.031 w/c}{0.194 + w/c} \tag{5.9}$$

The development of degree of hydration can be calculated experimentally by obtaining the heat of hydration by performing isothermal calorimeter test.

Degree of hydration
Due to lack of experimental results of the degree of hydration of the particular concrete mixture, the values are obtained from HYMOSTRUC software by simulating the chemical reaction of the cement paste having a w/c= 0.3 under sealed hydration condition. The simulations are performed for Portland cement; although in reality, the concrete mixture has various chemical admixtures such as superplasticisers, thixotropic admixtures etc.impacting the degree of hydration. The result is shown in figure 5.1. The ultimate degree of hydration according to equation 5.9 for w/c= 0.3 will be 0.63 which is reached at 28 days.Further, the development of degree of saturation based on the Power's Model according to equation 5.8 has been calculated using the obtained degree of hydration.

Bulk Modulus of porous and solid material
The bulk modulus of the cement paste, K_p is calculated by:

$$K_p = \frac{E_p(t)}{3(1 - 2\nu_p)} \tag{5.10}$$

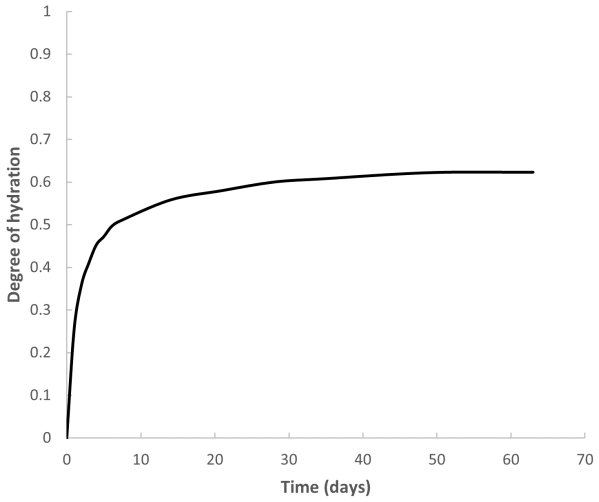

Figure 5.1: Evolution of Degree of Hydration calculated from HYMOSTRUC under sealed hydration

Here, E_p is the elastic modulus of the paste and ν_p is the Poisson's ratio.
The secant Elastic Modulus according to NEN-EN 12390-13:2012 on the concrete mixture reported the E-Modulus as 30 GPa at 28 days. Due to lack of values at discrete time points, the elastic modulus has been calculated according to Eurocode 2 assuming C30/37 concrete mixture which has a E-Modulus of 30 GPa at 28 days. The graph of the development of E-Modulus over time upto 91 days is shown in figure 5.2. The poisson's ratio, ν_p is taken as 0.2 as suggested by Wolfs et al. [44] for the concrete mixture. The bulk modulus of the solid material, K_s is taken as 44 GPa as suggested by Lura et al. [23].

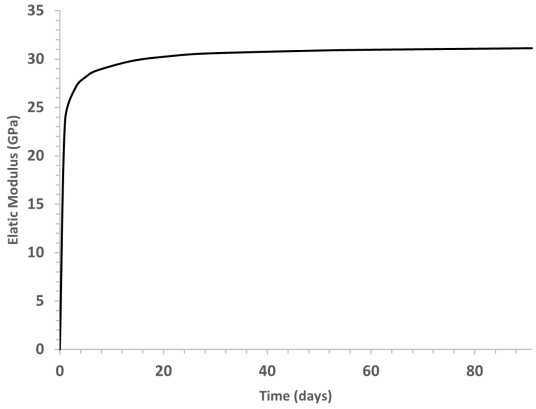

Figure 5.2: Development of Elastic Modulus over time calculated according to Eurocode 2

5.2. Calculation of Shrinkage strain

Combining the Kelvin-Laplace equation (equation 5.1) and the Bent'z deformation model (equation 5.6), the shrinkage strain to be calculated in terms of the RH distribution over time and other parameters can be written as:

$$\varepsilon_{Lin}(t) = -\ln \mathrm{RH}(t).S_w(t).\left(\frac{\rho RT}{3M}\right).\left(\frac{1}{K_p(t)} - \frac{1}{K_s}\right) \tag{5.11}$$

Figure 5.3 shows the summary of the calculation of shrinkage strain based on different parameters as shown in equation 5.11. The linear shrinkage strain obtained experimentally from the free shrinkage test as explained in section 3.3 is compared to the calculated values. The values of the parameters are discussed in detail in the previous section.

The relative humidity distribution with time for the cast specimen are used for the input in FEM Model as the shrinkage behaviour of 3D printed specimen is less reliable due to inadequate research on the impact of 3D printing process on the micro-structure of samples. The detail of the finite element model development is discussed in the next chapter (Chapter 6).

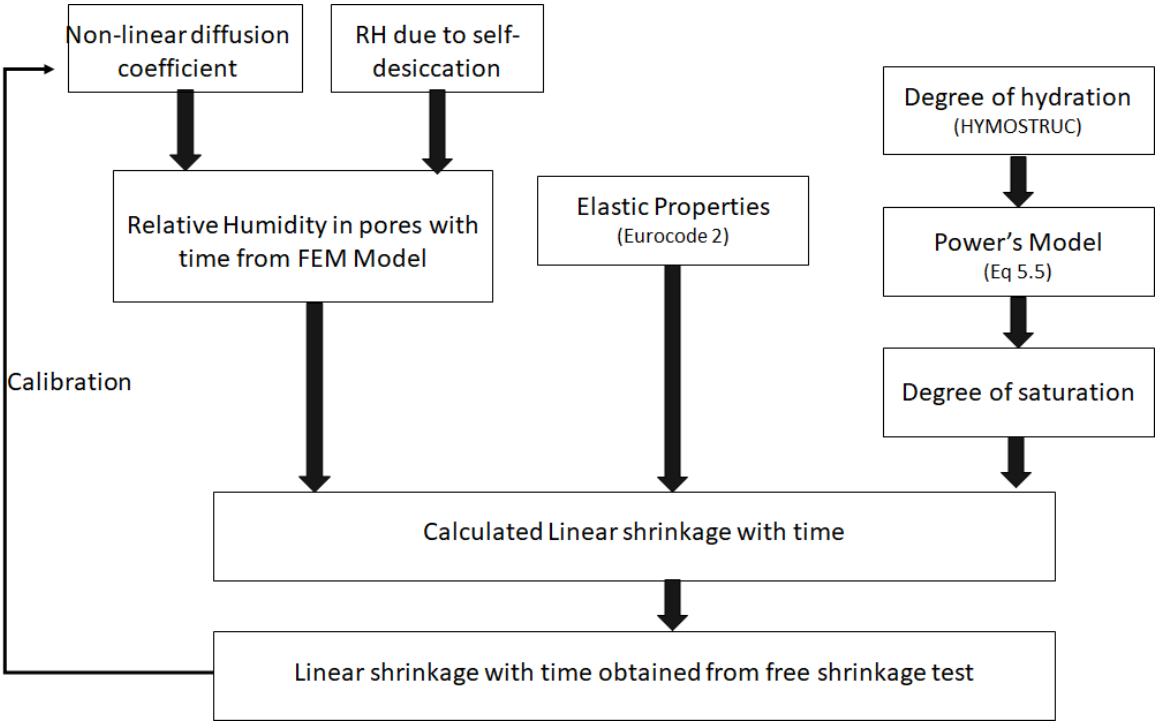

Figure 5.3: Flow diagram explaining the input parameters for calculation of development of relative humidity with time

5.2.1. Sensitivity analysis of the input parameters

The relative humidity distribution over time is calculated using the inverse analysis of the obtained experimental results. It is important to examine the impact of the assumptions to ensure that the error in the calibrated values are limited. The main assumptions during the calculations of the relative humidity are: (1) Calculated degree of saturation, (2) Elastic Modulus of the paste obtained from Eurocode 2, (3) Bulk Modulus of the solid and (4) Reduction factor to incorporate the creep effect. Each parameter is changed upto 30% to investigate the impact of the variation of the parameter on the calculated shrinkage over time. Note that the degree of saturation has varied to maximum 10% since the value cannot be more than 100%.

The sensitivity analysis shows that the influence of the parameters increases over time but remains under the maximum value of 10% at 28 days. The reduction factor of creep has the highest influence. It is recommended to have a thorough study of creep on 3D printed concrete and incorporate the value. The variation in the bulk modulus of the paste showed variation about 1%.

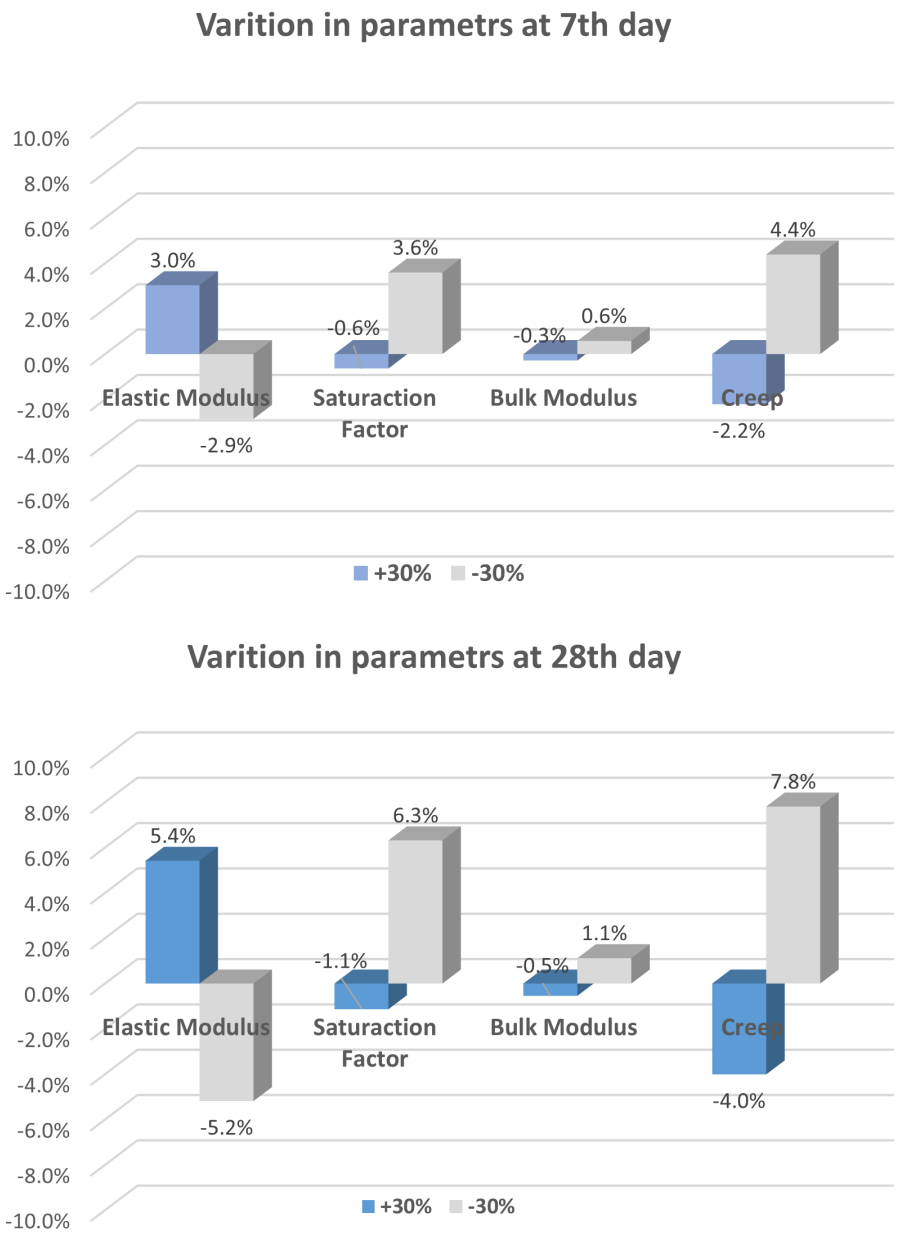

Figure 5.4: Variation of parameters by ±30 at (a) 7 days (b) 28 days

5.3. Summary

The chapter describes the main input parameters for calculating the shrinkage strain. First the relative humidity distribution is calculated from the numerical analysis, for which the main input parameter is diffusion coefficient. Then the relative humidity distribution is used to evaluate the capillary stresses based on Kelvin-Laplace Equation. Finally the Bentz deformation model is used to calculate the shrinkage strain over time. The input parameters are: degree of saturation, elastic modulus, creep factor and bulk modulus of the solid. Sensitivity analysis shows that by varying the parameters by ±30%, the creep factor and elastic modulus have the highest influence on the calculated shrinkage strain for the same RH values.

6

Model development

This chapter presents the details of the inverse analysis performed to obtain the main parameters of the relative humidity of capillary pores. The model is calibrated for the experimental results of the free shrinkage test. The results of shrinkage strain in covered and uncovered conditions are discussed. Also, a comparison of the moisture profile of the analytical and numerical model has been done for validation.

6.1. Background

The relative humidity distribution using FEM simulation has been modelled in various research. Peng et al. [56] used ANSYS to model diffusion whereas Jafarifar et al. [62] used ABAQUS software, Holmes et al. [59] used DIANA to simulate the RH distribution in a floor slab. In this study, the finite element model is developed in ANSYS 2020 R2. Symmetry conditions have been used to simulate the specimen of 160x40x40 mm^3.

The transient heat module has been used due to the analogy between the governing equation of heat transfer and moisture diffusion by simple substitution of the parameters. The analogy between the transient heat module in ANSYS and the relative humidity distribution in concrete is shown in table 6.1 in terms of governing equation, initial condition and boundary conditions. The RH is analogous to temperature, moisture diffusion coefficient to thermal conductivity and reduction of RH due to self-desiccation is described as a volumetric heat sink or internal heat generation. The extra multipliers such as density and specific heat capacity required in heat transfer analysis but not in moisture diffusion have been taken as unity [62]. For the covered specimen, the RH reduces only due to the internal cement hydration process. The governing equation and the boundary condition are:

$$\frac{\partial T}{\partial t} = -\frac{Q}{\rho c} \tag{6.1}$$

$$\text{Boundary condition: } -k\frac{\partial T}{\partial x}|_{x=0} = 0 \tag{6.2}$$

	Moisture Diffusion	Transient heat analysis
Governing equation:	$\frac{\partial h(x,t)}{\partial t} = \frac{\partial}{\partial x}\left(D(h)\frac{\partial h}{\partial x}\right) - \frac{\partial h_a}{\partial t}$ where, D(h) is the diffusion coefficient, h is the humidity inside concrete, h_a is humidity due to self-desiccation process	$\rho c\frac{\partial T(x,t)}{\partial t} = \frac{\partial}{\partial x}\left(k(T)\frac{\partial T}{\partial x}\right) + q_e$ ρ is the density, c is the specific heat capacity, k is the heat conductivity and q_e is the external heat flux source/sink
Initial Conditions:	$h(x,t_0) = h_0$ where h_0 is the initial humidity in the concrete at t=0	$T(x,t_0) = T_0$ where T_0 is the initial temperature at t=0
Boundary conditions:	$h_s = h_{en}$ where h_e is the ambient humidity conditions	$T_b = T_{en}$ where T_e is the ambient temperature and T_b is the boundary temperature

Table 6.1: Analogy between moisture diffusion and transient heat analysis

6.2. Initial and boundary conditions

The main input parameters required for the heat transient analysis in ANSYS are heat conductivity, specific heat capacity, density, film coefficient, initial and ambient temperature. Since the FEM simulation is done from the time of casting, the initial saturation inside the concrete is taken as RH= 100%. A constant ambient relative humidity of 65% is taken, the same as the ambient RH during the free shrinkage test.
The heat transfer from the surface to the environment has been modelled as an essential boundary condition as discussed in the previous chapter (Section 5.1.2).

6.3. Input parameters

The inverse analysis showed that the input parameters to calculate the diffusion coefficient namely, $D_0 = 2.48 \times 10^{-11}$ m^2/s, $\alpha = 0.005$, $n = 15$, $h_c = 0.86$ showed good agreement with the experimental results as discussed in the next section. The corresponding non-linear diffusion coefficient dependent on the relative humidity is shown in figure 6.1, calculated according to equation 5.3. The influence of these input parameters on the relative humidity distribution can be seen in Appendix C.

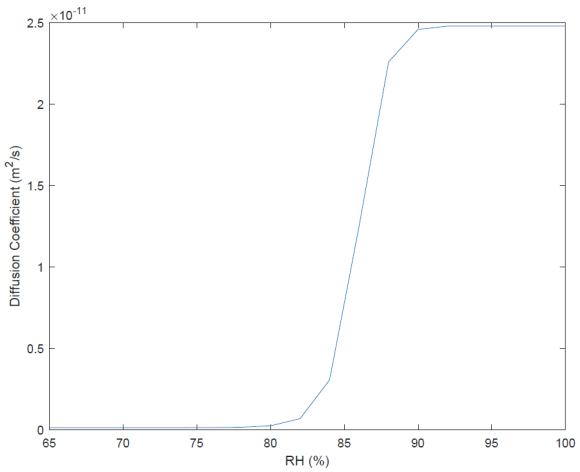

Figure 6.1: Dependency of diffusion coefficient on Relative Humidity for the concrete

The specific heat capacity and density have been taken as unity so that the diffusion coefficient can be equivalent to the parameters of heat diffusion as $D = \frac{K}{\rho c}$. In the heat analysis, the diffusion substance is the heat and not the temperature itself. The factor ρc is needed for converting the temperature to the heat per unit volume. In the case of diffusion, the concentration is by definition the amount of diffusion per unit volume and the conversion factor is not required, making $\rho c = 1$ [63].

6.4. Details of FEM elements

The specimen has been modelled as a three-dimensional FEM model in ANSYS with the diffusive parameters described in the previous section. The model is comprised of the solid element for moisture diffusion, SOLID90 HEX20.
SOLID90 element is a 3D 20-noded thermal solid conduction element in ANSYS having temperature as the degree of freedom. The reduction in the RH due to self-desiccation is modelled as the internal heat generation as a volumetric heat sink in the solid element.
A mesh size of 0.0025 m has been used. The mesh sensitivity analysis of the selected mesh size is discussed in section 6.5.3. Since the diffusion coefficient is dependent on the relative humidity, it is a non-linear analysis.

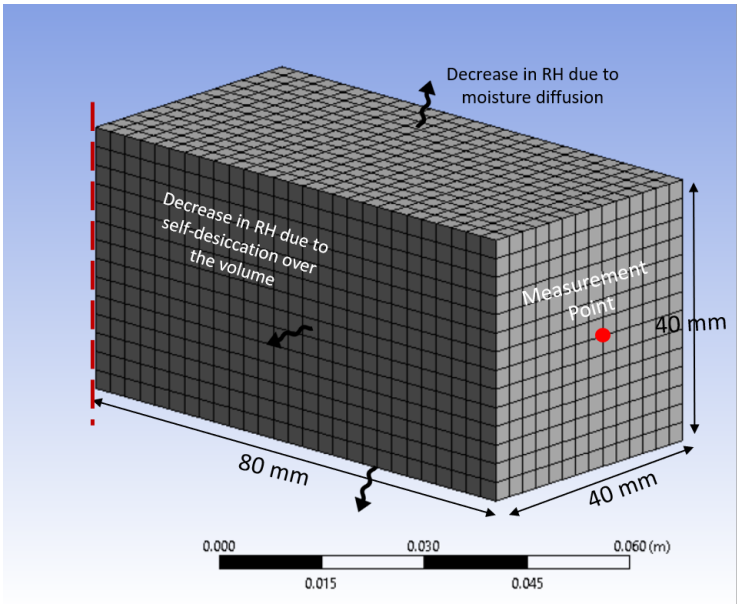

Figure 6.2: Finite Element Model of free shrinkage prisms. The dotted line indicates the plane of symmetry

6.5. Results of FEM Model

6.5.1. Covered specimen

For the sealed specimen, the convection from the surface is suppressed and only the internal heat generation is taken into account. Internal heat generation indicates heat loss as a volumetric sink source which leads to a uniform reduction of temperature in the model which is similar to a uniform reduction of RH due to self-desiccation. Only the experimental values for up to 14 days have been used to compare the obtained shrinkage strain values due to autogenous shrinkage. The simulation has been done only up to 14 days since a higher mass loss of the specimen was observed at a later stage as explained in Chapter 4. The change in RH over the cross-section at day 14 is shown in figure 6.3. The autogenous shrinkage produces a uniform strain throughout the cross-section of the structure which is also obtained in the numerical model.

The shrinkage strain obtained from the experiment of cast sample in covered condition up to 14 days and FEM simulation is compared in figure 6.4(a). The difference between the shrinkage strain obtained from experiment and the FEM analysis is -11.6%, 6.3% and 5.1% at 3, 7 and 14 days respectively, which seems reasonable. The value of reduction in RH due to self-desiccation process upto 60 days from FEM simulation is shown in figure 6.4(b). At day 60 the RH due to the self-desiccation process is

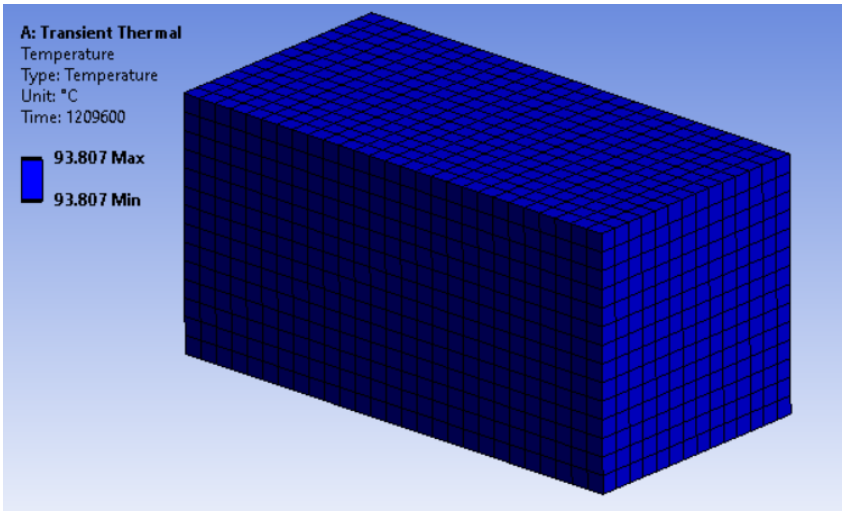

Figure 6.3: RH distribution at 14 days for covered specimen

obtained as 89.73%. Kim Lee et al. [19] reported RH in sealed specimen as approximately 88% at day 60 for concrete having w/c= 0.28.

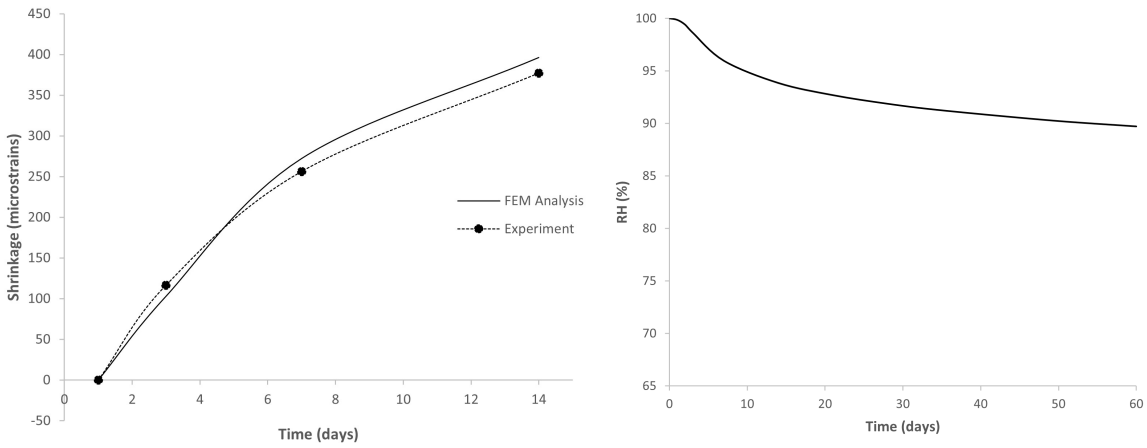

Figure 6.4: (a)Comparison of shrinkage strain of free shrinkage test in covered condition and FEM Analysis (b)Predicted value of shrinkage strain upto 60 days from FEM Analysis

6.5.2. Uncovered specimen

As discussed, for the uncovered specimen the relative humidity inside the pores decreases due to moisture diffusion process and the cement hydration process. The moisture diffusion coefficient is calibrated using inverse analysis to simulate the moisture diffusion inside the concrete. The parameters on which diffusion coefficient is dependent are namely, D_0, α, n, h_c as discussed earlier. As compared to the experimental value, the calibrated model has an error of -10% at day 7, 0.3% at day 14 and 7-8% from 21 day onward, which seems reasonable.
The evolution of the shrinkage over time and across the cross-section of the specimen is shown in figure 6.5. The RH decreases over time due to the self-desiccation and moisture loss to the environment. The internal RH significantly varies across the depth to the exposed surface. The maximum RH is always found at the center of the specimen. The maximum RH found at the center node is 93.52%, 87% and 84.17% at 7, 28 and 60 days respectively.

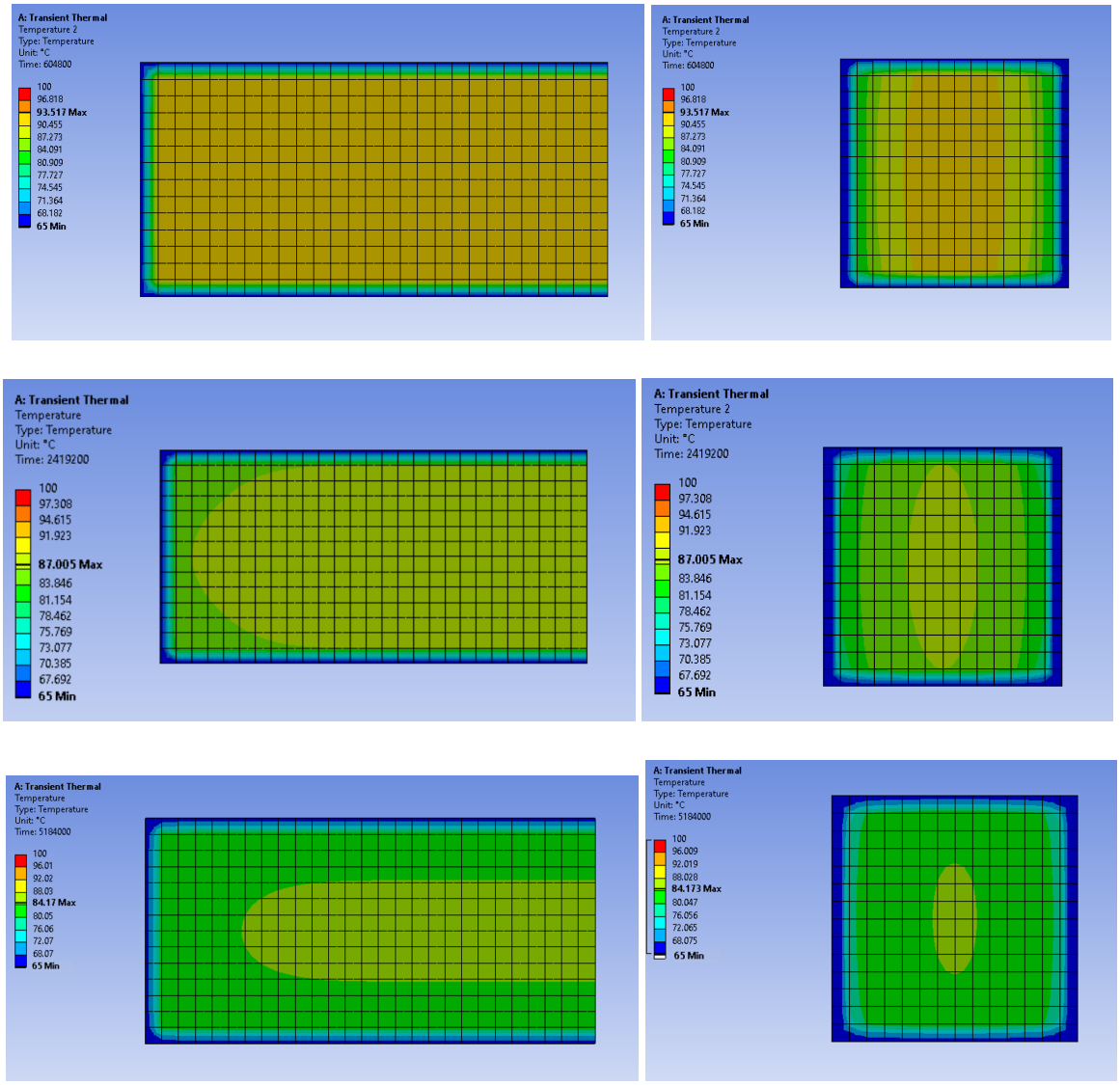

Figure 6.5: Evolution of Relative Humidity across cross-section of the specimen at (a)7 day (b) 28 day (c) 60 day

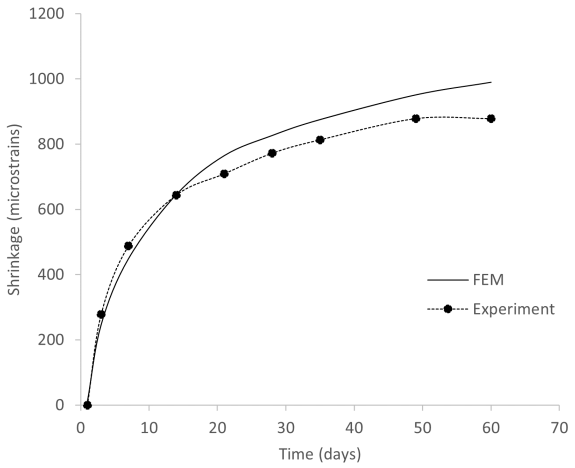

Figure 6.6: Comparison of experimental and results from FEM simulation

6.5.3. Mesh sensitivity analysis

Since the material has a low diffusivity, a small mesh size is likely to be expected for a reliable result. The outcome should reflect the structural response and should not depend on the size of the selected mesh. The optimum mesh size is a balance of the accuracy and processing power. The optimum mesh size is selected when more densification of the mesh does not noticeably affect the results of the numerical model.

For the development of the model, coarser to finer mesh sizes have been simulated to choose the correct mesh size. The results of the analysis for t = 28 days for a mesh size of 0.005 m and 0.001 m has been shown for the cross-section (0.04 x 0.04 m^2) at the center node in a two-dimensional model. The results of intermediate mesh sizes (0.01 m, 0.0025 and 0.0001 m) can be seen in Appendix D.

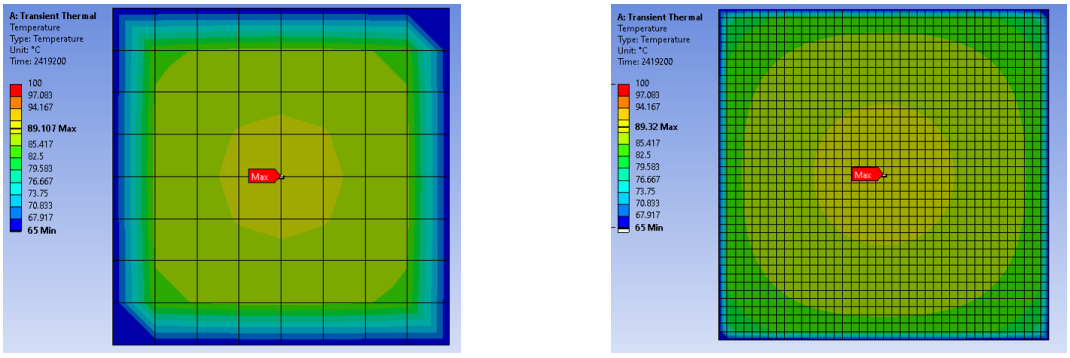

(a) (b)

Figure 6.7: RH distribution across the cross-section at t= 28 days for mesh size (a) 0.005 m (b) 0.001 m, X=0 is the center node and L is at the surface node

To further investigate the influence of the mesh sizes on the RH distribution across the cross-section, the relative humidity of all the nodes lying in the region ($X \geq 0$; $0 \leq Y \leq 0.02$ m; $Z = 0$) has been plotted for the same drying period for a half-plane in figure 6.8. X=0 has been taken at the center of the cross-section and the region lies between $-L \leq X \leq L$. Changing from a coarse (0.01 m) to fine mesh size (0.0005 m), show that the mesh size has a notable influence on the calculated relative humidity of the nodes near the surfaces. As the mesh size is reduced from 0.0025 m to 0.0005 m, results start to converge. Also, the output is almost the same for the nodes at the center (X = 0) in case of all the mesh sizes. The difference can be seen in figure 6.7 as well where the contours are not as smooth in appearance for the nodes near the surface of the coarse mesh. It indicates a lack in the number of integration points. The relative humidity is overestimated significantly for nodes near the exposed surface in coarse mesh. Henceforth, it is important to take a mesh size at least 0.0025 m to minimize the error in the relative humidity.

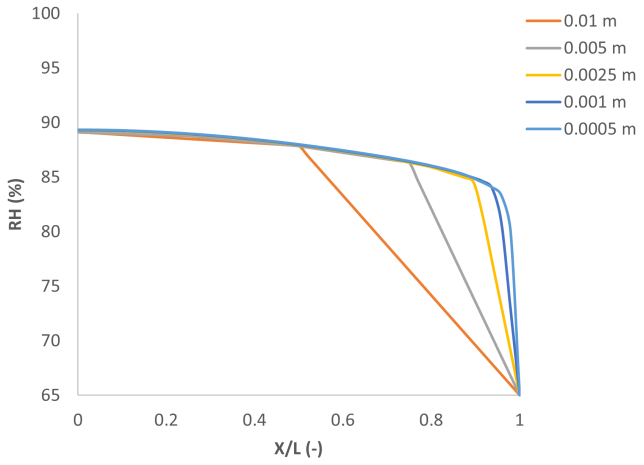

Figure 6.8: Comparison of moisture profiles for different mesh sizes

6.6. Verification of moisture profile

The diffusion model is verified using the analytical model suggested by Li et al.[64]. The approach has been used by Moon et al.[65], [66] and Li et al. [64] concluding it to be reasonable to describe the moisture gradient due to the drying inside the mortar.

The moisture profile along the cross-section for a linear half-plane can be calculated as[64]:

$$H(x,t) = H_a + (H_0 - H_a)erf\left[\frac{L-x}{2\sqrt{Dt}}\right] \tag{6.3}$$

where,
$H(x,t)$ is the internal relative humidity at a depth x from the drying surface,
H_a is the internal humidity of a completely sealed specimen, taken as 100% neglecting the autogenous shrinkage,
H_0 is the relative humidity of the environment,
D [m^2/s] is the constant moisture diffusion coefficient and
erf is the Gaussian error function
The main assumptions of the analytical model to calculate the relative humidity distribution across the cross-section of the specimen are: (1) constant diffusion coefficient and (2) assuming internal RH when sealed (H_a) as 100% , neglecting the effect of the autogenous shrinkage. Although a nonlinear diffusion coefficient has been used in the numerical model for higher accuracy, using a linear coefficient in the case of analytical model offers an enormous computational benefits with no loss in the generalities [65]. The nonlinear diffusion coefficient is dependent on the humidity itself (equation 5.2) making it difficult to solve analytically.

To verify the moisture profile of the numerical model with the analytical model, a drying prism of dimensions ($2L$ x $2L$) out of the specimen is considered since the analytical model is defined for a theoretical linear half-plane. In this case, the dimensions of the considered slice is (40 mm x 40 mm ^{2}) placed at the center of the specimen (Z = 0) The model lies between -L≤ X,Y ≤ L. A prism slice at the center is considered so that the end effects due to the moisture diffusion from the surfaces do not have a significant effect on the moisture movement in the interior of the concrete. It will result in the moisture movement perpendicular to the longitudinal axis so that the moisture profile of the cross-section can be calculated [64].

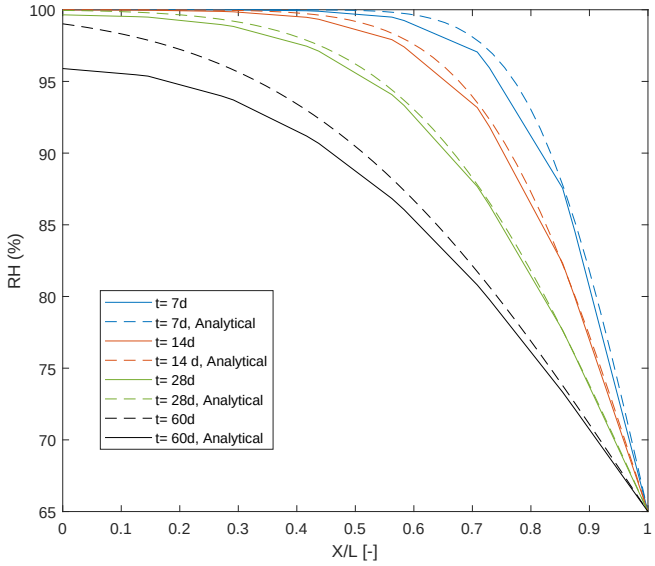

Figure 6.9: Comparison of analytical and numerical model at t= 7, 14, 28 and 60 days, X=0 is the center node and L is at the surface node

In the numerical analysis, a non-linear diffusion coefficient and the effect of the autogenous shrinkage have been taken into account. To compare with the analytical model, only the relative humidity distribution due to the drying shrinkage has been considered. The moisture profile in the specimen is plotted as the relative humidity of all the nodes lying in the region ($X \geq 0$; $0 \leq Y \leq L$; $Z = 0$) for the same drying period. The relative humidity using the analytical model for a constant diffusion coefficient (taken as the average value $D = 8 \times 10^{-12}$ m^2/s) has been plotted as well for comparison at t= 7, 14, 28 and 60 days in figure 6.9.
The moisture profile in figure 6.9 clearly shows relative humidity at the center of the specimen is the highest and the RH at the surface is equal to the ambient RH. The analytical model shows good agreement, especially up to 28 days. On a longer time frame, the numerical solution differs from the analytical results. A similar trend was also observed by Li et al.[64].

6.7. Summary

The key points discussed in the chapter are:

- Transient heat analysis can be used to predict the RH distribution due to self-desiccation and moisture diffusion process due to analogy in their governing equation and boundary conditions. The main input parameters are the diffusion coefficient and the reduction in RH due to self-desiccation.
- The relative humidity distribution of the specimen is simulated in ANSYS for covered and uncovered conditions. The experimental results of the free shrinkage test have been used to calibrate the input parameters of the non-linear diffusion coefficient. The simulated values have an error of -10% at day 7, 0.3% at day 14 and 7-8% from 21 days onward, which seems reasonable.
- Mesh sensitivity analysis showed that at least a mesh size of 0.0025 m should be taken to a reliable output independent of the mesh size.
- The moisture profile from the numerical model was compared to the analytical model. The main assumptions for the comparison were: (1) Effect of autogenous shrinkage was neglected, (2) a constant diffusion coefficient. The numerical analysis showed good agreement with the analytical model, especially for up to 28 days.

7

Case study

The developed finite element model has been used to predict the shrinkage strain and the corresponding induced stresses in three case studies: (1) restrained ring test performed during the experiments, (2) Flower pot experiment and (3) Parametric study on different boundary conditions.

7.1. Restrained ring test

To validate the numerical model, the shrinkage behaviour of the restrained ring test (as discussed in Chapter 3 and 4) has been simulated. The numerical model has been validated by comparing the time of occurrence of cracks in the experiment and that calculated from the model. The shrinkage strain is first calculated by transient thermal analysis. Then the strain is converted to the fictitious temperature drop equivalent to the calculated strain so that it can be applied in the static structural model for analyzing the stress development.
In the experiment, the ring specimens were tested in three curing conditions: exposed from the time of casting, covered with plastic sheet and covered with waterproof tape and plastic sheet. The specimen covered with plastic sheet is suspected to have moisture loss to the environment. Since the environmental condition is unclear in this case, only the two scenarios: (1) completely exposed, having both drying and autogenous shrinkage and (2) covered with waterproof tape and plastic sheet, having only autogenous shrinkage have been simulated.

7.1.1. Thermal model- RH distribution

The outer diameter of the concrete ring is 250 mm, inner diameter is 175 mm and the height is 75 mm as shown in figure 3.5. The specimens were kept at RH=55% and T= 20°C. The developed finite element model is used to predict the shrinkage strain for the element using transient thermal module of ANSYS. In the thermal analysis, 20-noded three-dimensional solid elements (SOLID90) having temperature as degree of freedom at each node were used to simulate the shrinkage behaviour of the specimen. The calibrated input parameters obtained for the particular concrete mixture were used for the model (Chapter 6). One-fourth of the ring has been modelled due to limitations on the number of nodes of the software license and faster computation time. The relative humidity of the exposed surfaces were set as RH= 55%.

The calculated shrinkage strain for the completely exposed sample having both drying and autogenous shrinkage and the specimen completely sealed having only autogenous shrinkage is shown in the figure 7.2. The strain has been calculated at the surface of inner ring since the strain gauges were attached at the mid-height of the inner steel ring.

7.1.2. Calculation of shrinkage stresses

The calculated shrinkage strain has been now applied to the mechanical model to analyze the shrinkage-induced stresses. It should be noted that the ANSYS does not explicitly enable shrinkage to be entered as a load or a material characteristic. As a result, a fictitious temperature loading can be used as an alternative method. The calculated shrinkage strain as shown in figure7.2 has been converted to the

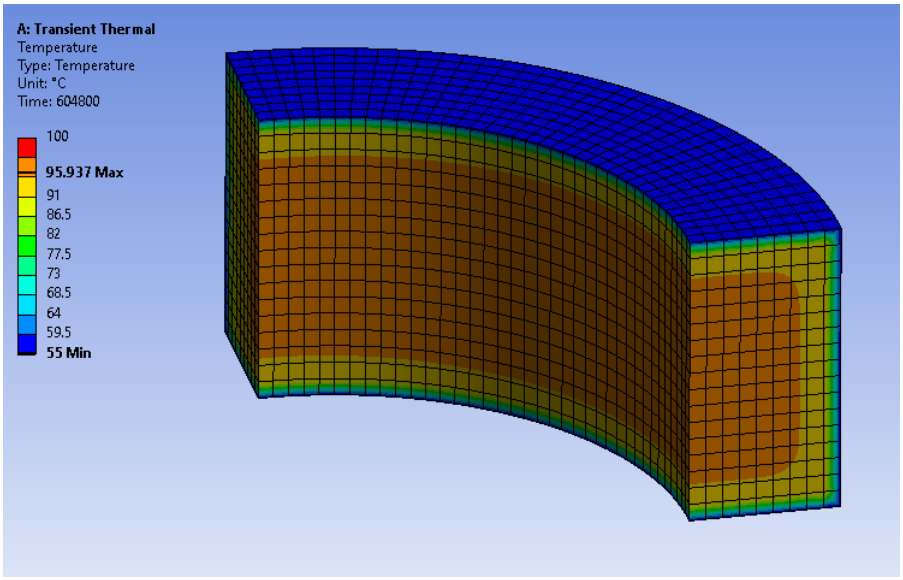

Figure 7.1: Calculated relative humidity distribution for exposed specimen at t=7 days. One-fourth of the ring specimen has been modelled.

equivalent temperature strain and applied to the model according to the equation:

$$\Delta T = \frac{\varepsilon_{Lin}}{\alpha} \tag{7.1}$$

where Δ T is the equivalent temperature, ε_{Lin} is the calculated shrinkage strain from FEM and α is the coefficient of thermal expansion taken as 10×10^{-6} per °C [67].

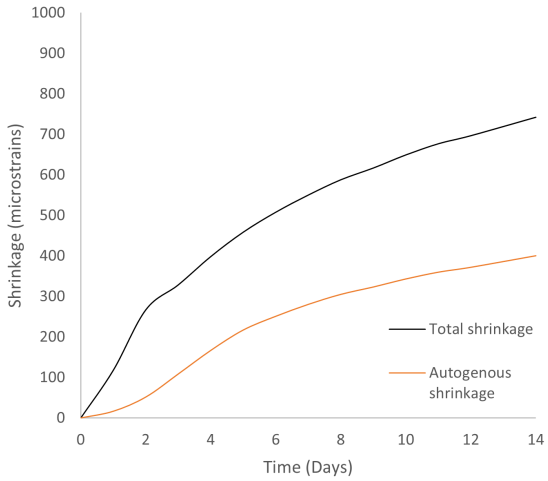

Figure 7.2: Calculated shrinkage strain of specimen in completely exposed condition (both drying and autogenous shrinkage) and sealed condition (autogenous shrinkage only) for nodes at the inner surface

The elastic modulus dependent on time is considered as hardening concrete is analysed. It is calculated by assuming C30/37 as discussed in Section 5.1.3 and Poisson's ratio is taken 0.2. Concrete has been modelled as a linear elastic and homogeneous material. No microcracking effect is considered in the analysis. During the preparation of the ring test, the surface of the steel rings is properly lubricated to prevent friction between the steel ring and concrete specimen. Accordingly, a friction-less surface can be assumed, implying no shear and tensile stresses transfer at the interface [65]. The effect of age-dependent creep has been taken by considering an effective elastic modulus. Analytically, the

following equation can be used to calculate the shrinkage of the concrete structure [68]:

$$\sigma = \frac{\varepsilon(t)E(t)}{1+\phi(t)} \times \text{DOR} \tag{7.2}$$

σ [MPa] is the shrinkage-induced stresses
E [MPa] is the elastic modulus of concrete
ε is the shrinkage strain
ϕ is the creep factor
DOR is the degree of restraint

For this case, the degree of restraint has been considered to be 1 as the concrete specimen is restrained by the steel ring. The creep factor has been calculated from the Eurocode 2 for the RH= 55% and time of loading, t_0= 0 days. Alternatively, Moon et al.[65] suggested to take effective elastic modulus as 60% of the elastic modulus to incorporate the creep effects for the ring test. Both the cases have been considered to investigate the influence of effective modulus on the estimated shrinkage stresses.

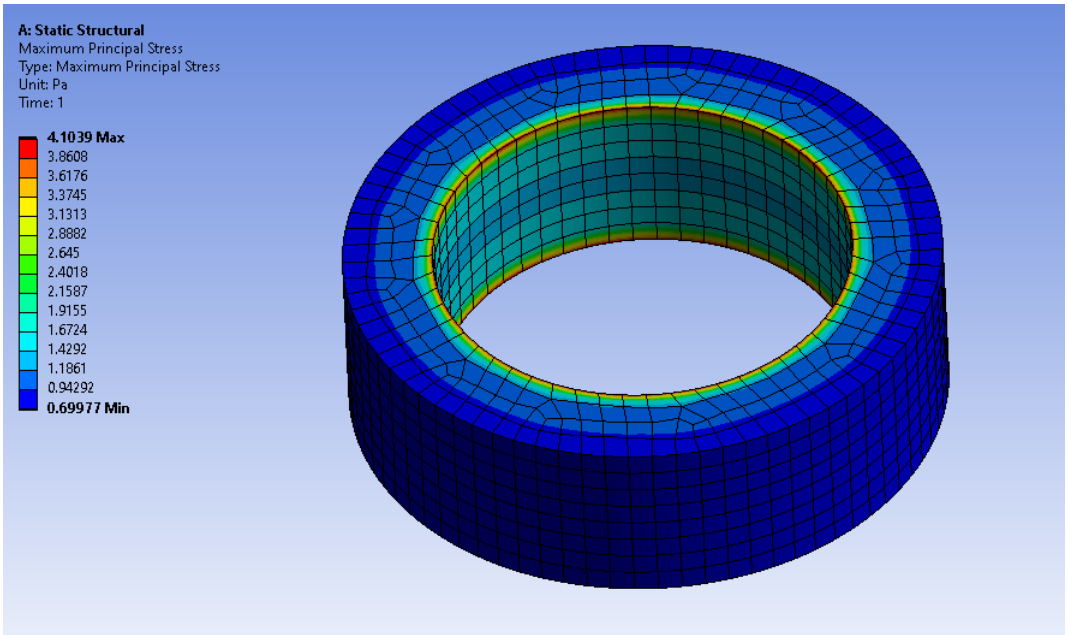

Figure 7.3: Stress at t= 3 days for the exposed specimen from FEM. The effective elastic modulus is calculated according to Eurocode 2

7.1.3. Results

The result of the shrinkage-induced stresses calculated from the finite element model has been shown in figure 7.4 for the two curing conditions. The maximum shrinkage stress of the structure is found at the inner surface as shown in the figure 7.3. It is expected as the concrete ring is restrained from inside.

In the experiment, the ring exposed to drying cracked within 2.8 days whereas the ring sealed with waterproof tape cracked within 8 days. In the numerical analysis, for the specimen exposed to drying (Figure 7.4 (a)) is estimated to crack at 1.5 days for effective modulus taken as 60% and at 1.8 days for creep factor calculated according to Eurocode 2. For the sealed specimen (Figure 7.4 (b)) the numerical analysis estimates the cracking at 7.5 days if Elastic modulus is taken as 60% and no cracking if calculated according to Eurocode 2. In terms of the stresses, the numerical simulation shows the cracking at 3.6 MPa for exposed specimen and 4.7 MPa for the sealed specimen as compared to the maximum residual stress of 4 MPa obtained in the experiment.

The case study shows that the extent of relaxation considered for the calculation of shrinkage-induced stresses has a significant influence on the time of cracking. In the case of sealed specimen, Eurocode 2 overestimates the relaxation whereas taking elastic modulus as 60% gives more accurate results.

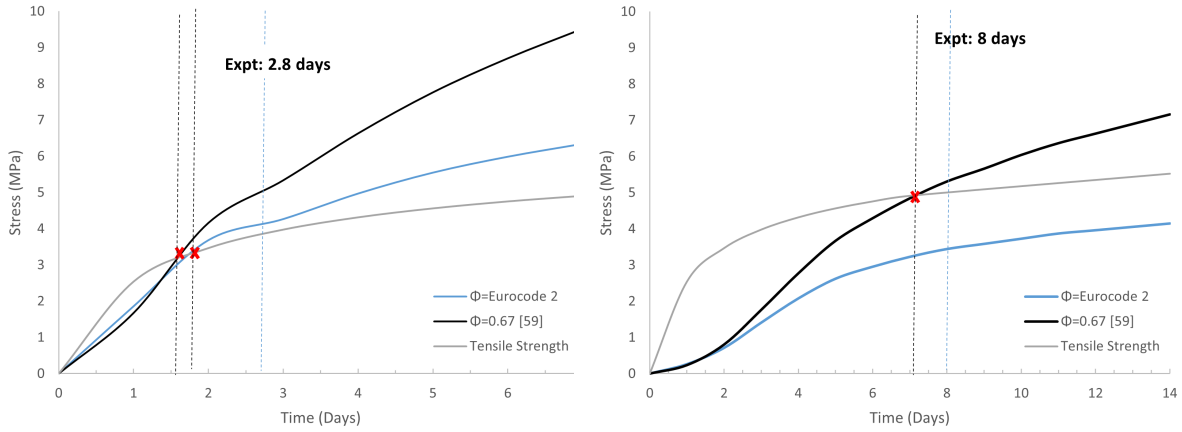

(a) Calculated stress vs time, exposed to drying

(b) Calculated stress vs time, sealed specimen

Figure 7.4: The calculated shrinkage stresses according to FEM simulation by taking different effective modulus (black= calculated according to Eurocode 2, blue= according to [65], a 60% effective modulus. Dotted line indicates the time of cracking when stresses exceeds the tensile strength

7.2. Flower Pot

The analytical calculations of the case study of the flower pot is already discussed in section (2.4.2). Two flower pots having a zig-zag pattern as shown in fig. 2.10 were 3D printed and restrained by pouring wet sand at different times. A numerical analysis has been performed using the developed FEM model to predict the shrinkage behaviour.

7.2.1. Details of the experiment

Each element has a height of 450 mm, average thickness of 55 mm and perimeter of 10140.8 mm. In the first element, the wet sand was poured inside the element after one day of printing. The detailed timeline are shown in table 7.1 .

Activity	Element 1	Element 2
Time of pouring sand	1 day after printing	14 days after printing
Occurrence of first 2 cracks	5 days after pouring sand	12 days after pouring sand
Occurrence of third crack	6 days after pouring sand	18 days after pouring sand

Table 7.1: Time of the occurrence of the cracks in the two elements

As discussed in the previous section, the numerical analysis is performed in two stages, thermal and structural analyses.

7.2.2. Simulation for shrinkage strain

The developed numerical model is used to predict the shrinkage strain for the element using transient thermal module of ANSYS. Similar to the restrained ring test, three-dimensional 20-node element has been used to first calculate the RH distribution over time which is then used as an input for the structural analysis. The ambient RH conditions are kept as RH= 65% at the exposed surfaces and T= 20 °C is assumed. The calibrated input parameters obtained for the particular concrete mixture were used for the model (Chapter 6). The main assumptions of the model are:

- Isotropic, homogeneous and linear elastic behavior of the concrete has been considered. 3D printed structure in reality is orthotropic material depending on the interval of printing.
- Only the influence of shrinkage strains has been considered. Other strains due to creep, adiabatic heat development etc. have not been taken into account.
- The relative humidity of the ambient environment has been considered as constant which might be variable in actual experimental conditions.

- The element is assumed to be monolithic. There might be imperfection due to 3D printing process, decreasing the stiffness of the structure. Also, the layer-wise printing should have a negligible difference in the stiffness of two layers as the time interval between printing of two layers is 0 minutes.

- The shrinkage strain calculated from the relative humidity distribution has been increased by a factor of 15% up to day 7 and after that by 20% to incorporate the effect of 3D printing process. Higher shrinkage was observed in 3D printed samples as compared to cast samples in the experiment (Chapter 4).

The distribution of the relative humidity across the cross-section (transverse direction) finite element model at is shown in figure 7.5 at t= 28 days.

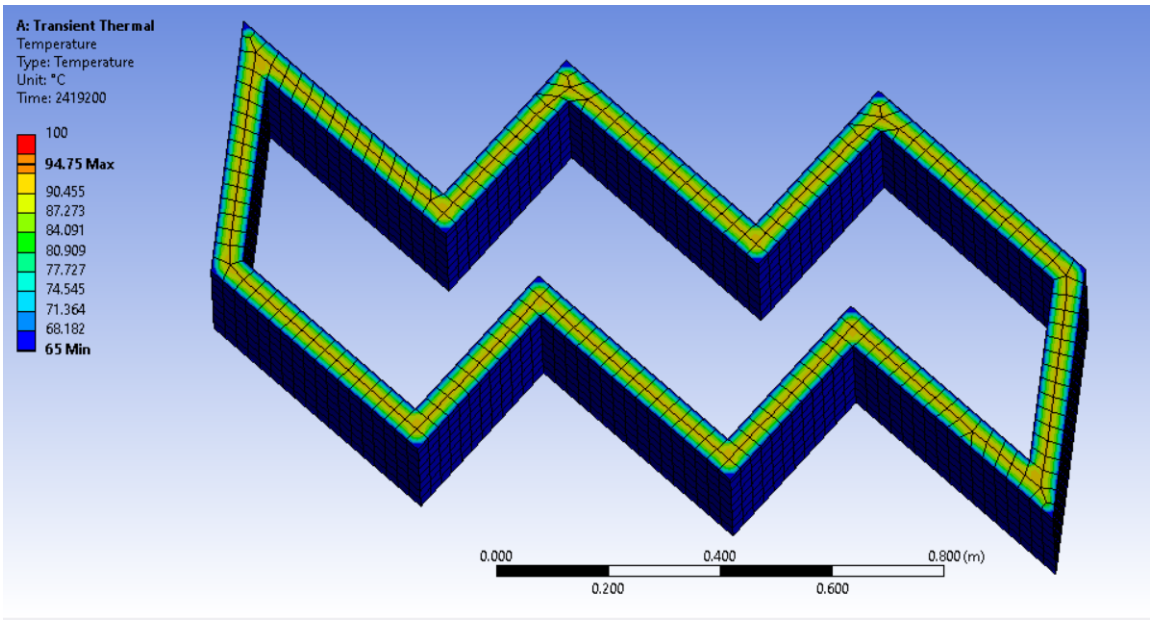

Figure 7.5: Temperature distribution (analogous to RH) at day 28 across the cross-section

Using the relative humidity distribution obtained from the thermal analysis has been used to calculate the shrinkage strain over time based on the capillary tension approach. The predicted value of the shrinkage strain over time for the nodes at the inner surface is shown in fig.7.6 for up to 50 days.

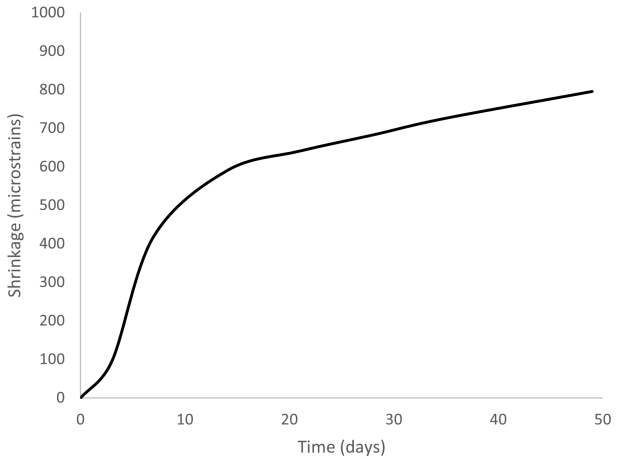

Figure 7.6: Calculated strain over time from FEM simulation for the nodes at the inner surface up to 50 days

7.2.3. Shrinkage stresses analysis

In this case, the boundary conditions or the environmental conditions of the element are unclear. The sand inside the element will restrain the elements axial. Although the sand was kept wet every alternate day, it might be possible that it leads to a difference in RH condition inside and outside surface of the elements as well producing warping stress.
In this study, the elements are assumed to be axial restrained due to the sand. The structural analysis for the shrinkage-induced stresses has been studied using the calculated shrinkage strain from thermal analysis.

Details of FEM model

A linear structural analysis has been performed in ANSYS 2020 R2 using the static structural module to calculate the shrinkage stresses of the model. The model comprises of 5024 elements and 30134 nodes in total. For the structural analysis, the model uses SOLID186 elements which are 3D 20-nodes solid elements. The concrete has been modelled as a linear material having the mechanical properties: age-dependent elastic modulus (figure 5.2), Poisson's ratio is taken as a constant of 0.2. The effective elastic modulus has been taken to incorporate the relaxation factor after 1 day of loading, calculated according to Eurocode 2. The inner surfaces of the structure has been modelled as fixed support to restrain it axially as shown in figure 7.7.

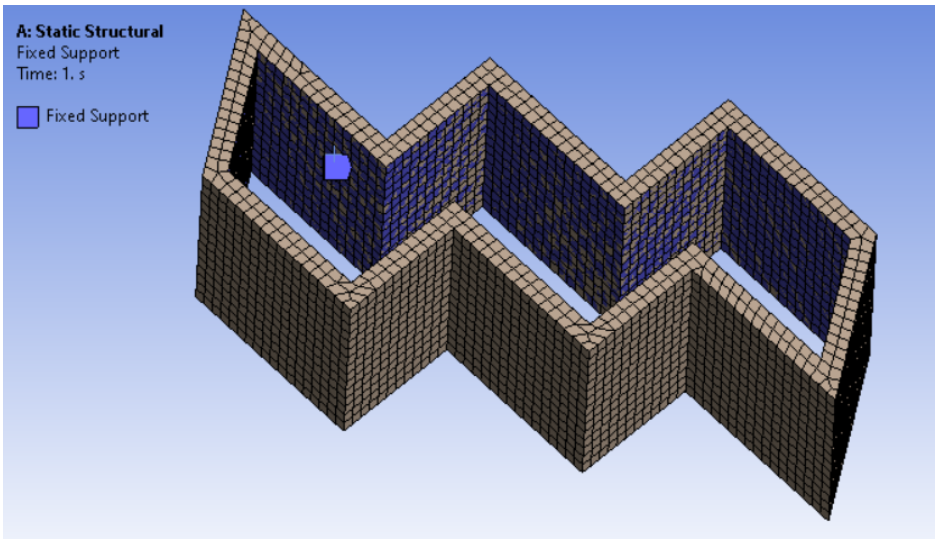

Figure 7.7: Support condition for the FEM model used in structural analysis

7.2.4. Results

The elements were restrained by filling sand inside it, which restrains the element to shrink inwards/ axial. The concrete element will shrink over time due to the moisture loss and self-desiccation process but the inner surface will be restrained from shrinkage. It produces tensile stresses in the inner surface. The shrinkage stresses for element 1 and element 2 for the time of cracking has been shown in figure 7.8. The maximum tensile stresses in both the elements were observed at the inner surface, which is expected. The maximum tensile stress in element 1 is obtained as 4.9 MPa as shown in figure. 7.8 (c) whereas the expected tensile strength at day 3 is 4 MPa. The maximum tensile stress in element 2 is obtained as 6.5 MPa at day 33, restrained after 14 days as shown in figure 7.8 (d). The expected tensile strength is 6 MPa.
Based on the calculated shrinkage strain, element 1 is estimated to crack at 2.7 days whereas it cracked after 5 days. Element 2 is estimated to crack at about 33 days after the printing as compared to the observed cracking after 26 days of printing. As discussed in the calculations of ring test (section 7.1.2), one of the possible reasons could be the overestimation of relaxation effect when calculated according to Eurocode 2. On the contrary, the degree of restraint has been taken as 1 in the modelling although restraining with sand is not expected to be stiff enough to provide 100% restrain. Due to this, the actual stresses should be lower as compared to the calculated stresses. It could be possible that the stress concentrations at the corners could lead to higher stresses.

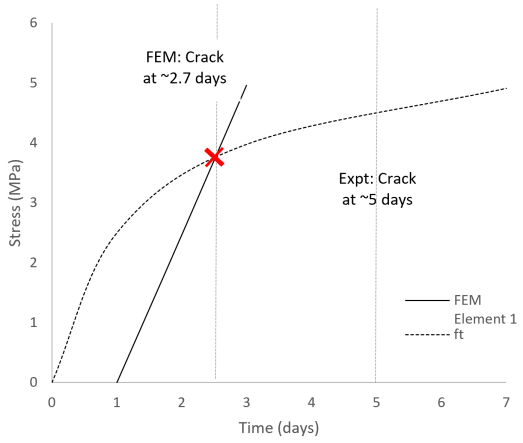

(a) Calculated stress vs time, element 1

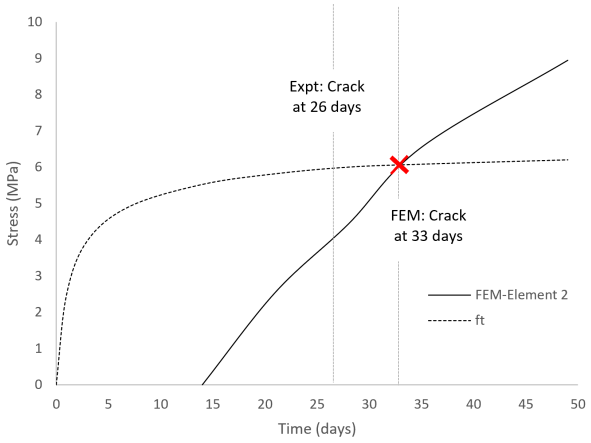

(b) Calculated stress vs time, element 2

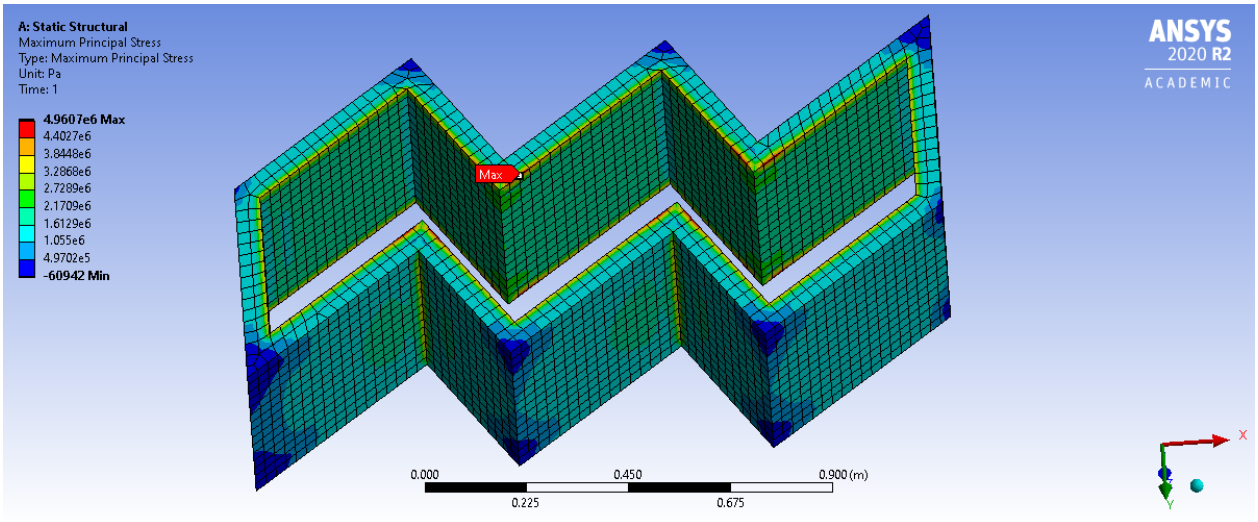

(c) Stress analysis for element 1 at day 3

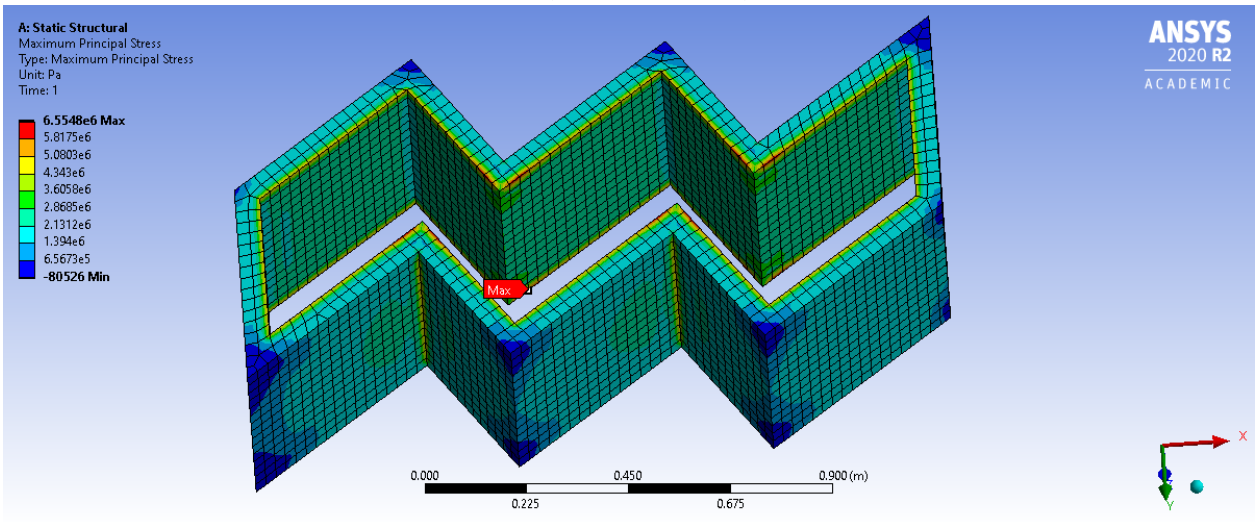

(d) Stress analysis for element 2 at day 35

Figure 7.8: Calculated shrinkage stress for element 1 and element 2

7.3. Parametric Study

A parametric study was designed to test the shrinkage-induced cracking on 3D printed specimens. Specimens of two different shapes: cuboid and cylinder were 3D printed and restrained under four different boundary conditions: (1) No restraint, (2) Axial restrained, (3) Bending restraint and (4) Both axial and bending restrained have been applied to different specimens. First, the shrinkage strain was calculated using the model for each specimen and then the corresponding shrinkage stresses were calculated analytically. The estimated time of cracking was calculated as when the stresses exceed the tensile strength of the material.

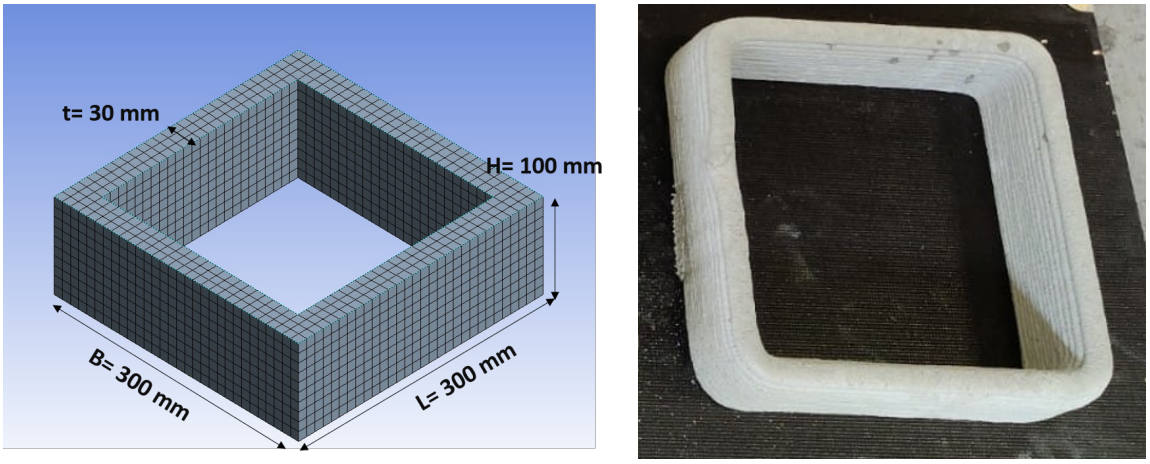

(a) (b)

Figure 7.9: (a) 3D model and (b) 3D printed model of the cuboid specimen

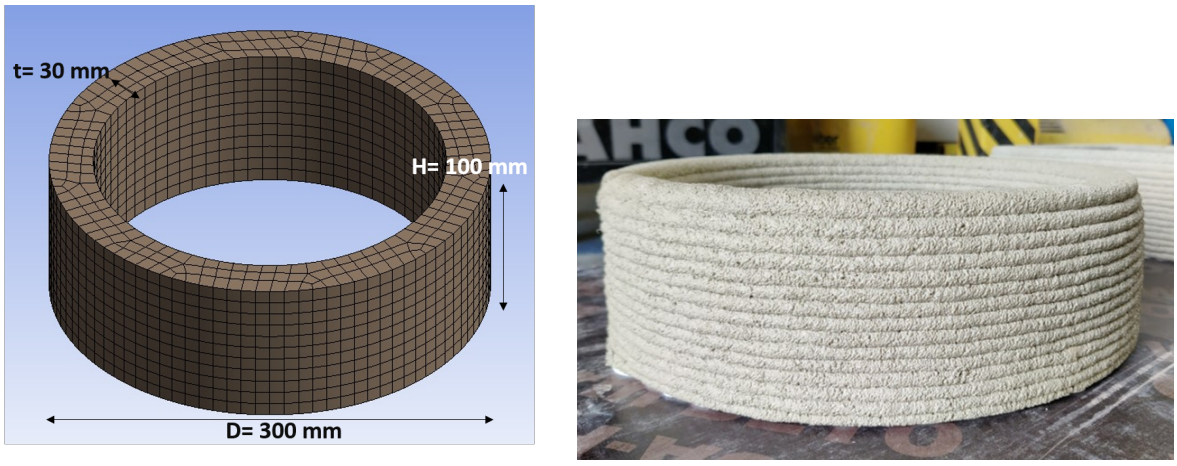

(a) (b)

Figure 7.10: (a) 3D model and (b) 3D printed model of the cylinder specimen

7.3.1. Preparation of samples

The dimensions of the cuboid specimen are taken as L= 300 mm, B= 300 mm and H= 100 mm. The layer thickness has been taken as t= 30 mm. For the cylindrical specimen, the dimensions were taken as D= 300 mm, H= 100 mm and t= 30 mm. A cylindrical shape was selected so that there is no stress concentration due to the corners. The cuboid shape is used to evaluate the additional stresses due to the corners. Slender specimens were designed so that higher shrinkage can lead to cracking within a week due to time constraints.

Four specimen of each shape were 3D printed, one specimen for each boundary condition. All the specimens were cured under plastic sheet for first 24 hours after printing. Then they were restrained according to the boundary condition. The environmental condition inside the print factory is taken

as RH= 65% and T= 20°C. In reality, these conditions can be varying over the day. The specimens restrained axial were filled with sand. The sand was compacted properly so that it can provide maximum restraining for the specimen to shrink inwards. A plastic sheet was applied between the sand and specimen to minimize the effect of friction. The specimen restrained with water were glued tightly to a wooden plank using silicon glue so that there is no water leakage. The specimens restrained with wet sand were first filled with sand and then the sand was saturated with water. The sand was sprayed with water every alternate day. All the specimen after restraining is shown in figure 7.15.

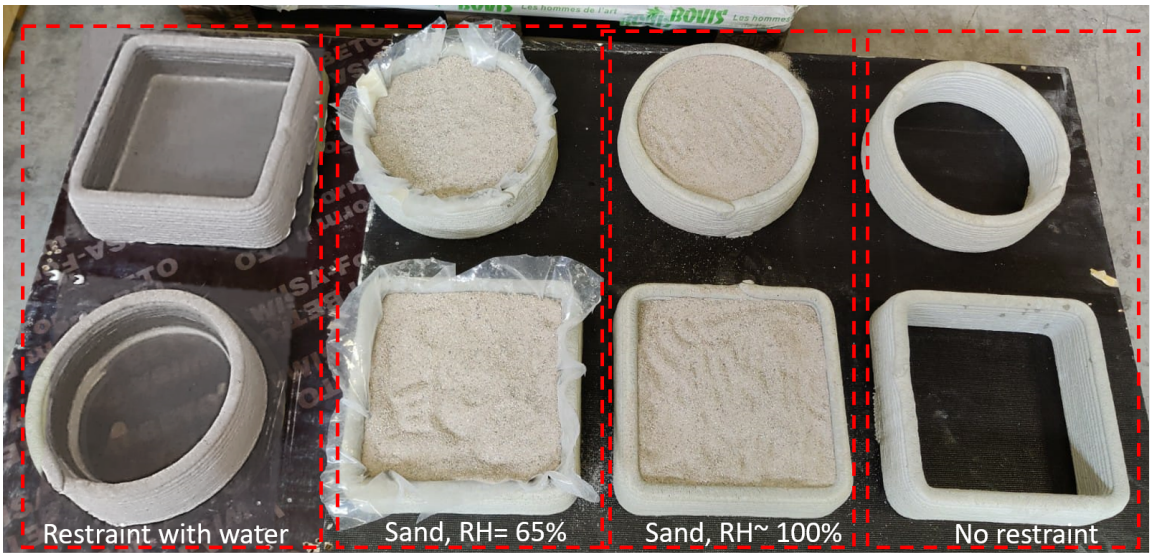

Figure 7.11: The specimens at the beginning of the experiment. From the left= restrained with water, restrained with sand at RH= 65%, restrained with sand at RH= 100% and no restrain

7.3.2. Calculation of shrinkage stresses

The shrinkage strain was calculated using the developed numerical model. First, the strain was calculated assuming a homogeneous, isotropic, elastic linear material. The relative humidity distribution as calculated from the thermal model at a section cut at the mid-point of height is shown in figure 7.12. The models are shown for an RH= 65% at the exposed surface.

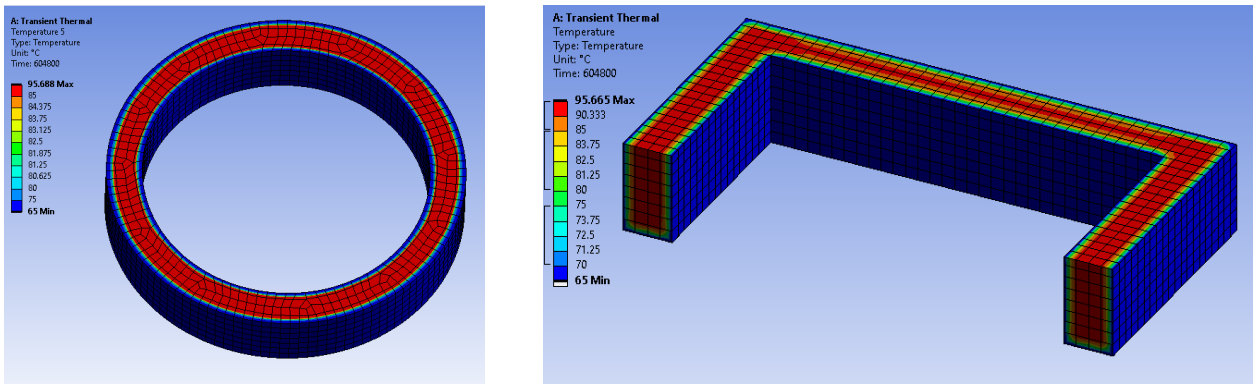

(a) (b)

Figure 7.12: Relative humidity disitribution obtained from the FEM analysis for laterally cut cross-section at mid-point of height (a) cylinder (b) cuboid specimen (half-model) at day 7

The shrinkage stresses have been calculated analytically using the equation 7.2. The shrinkage strain distribution across the cross-section of the structure depending on the environmental condition is made as shown in figure 7.13b. The four boundary conditions are:

No restraint

The specimen is free to deform axially in lateral and vertical direction. For the bending restrain, the cylindrical specimen is restrained in bending deformation due to its shape. However, in this case, there is no differential shrinkage (the relative humidity inside the specimen and outside is the same) so there should be no bending deformations.

Axial restraint

The specimen is restrained from inside by filling sand at the environmental condition (RH= 65%). In this case, as well there is no differential shrinkage as the same relative humidity condition is in the outside and inside of the specimen no bending deformation is expected. A uniform shrinkage strain distribution is expected as shown in figure 7.13b(a).

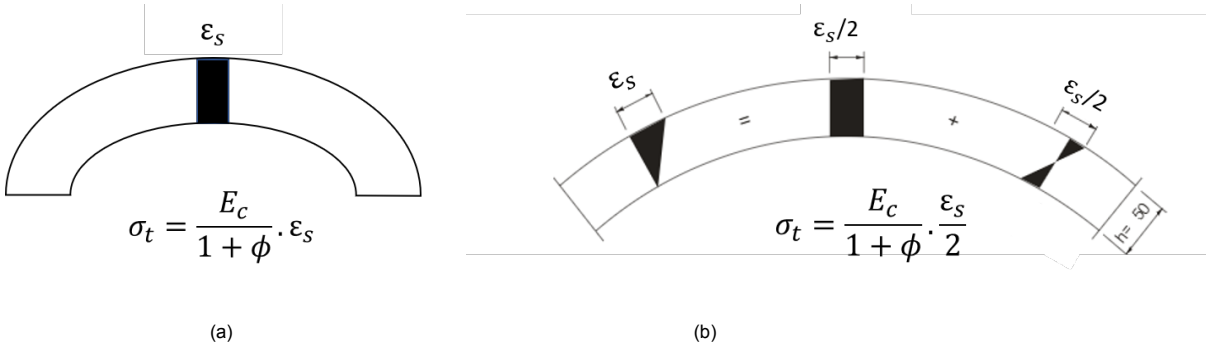

(a) (b)

Figure 7.13: Analytical calculation for (a) only axial restrained, RH= 65% both sides and (b) only bending restraint, RH= 100% one side and RH= 65% other side, adapted from [68]

Bending restraint

The specimen is filled with water so that inside the specimen RH= 100% and outside it is RH=65%. This produces a triangular strain distribution diagram as shown in figure 7.13b (b). The strain distribution can be divided into two components: mean shrinkage and the gradient due to the shrinkage. In this case, the water should allow the specimen to deform freely axial and produce bending deformation due to differential shrinkage. So the shrinkage stresses will only be produced due to the shrinkage gradient.

Axial and bending restraint

The specimen is filled with sand which was saturated with water so that inside the specimen RH= 100% and outside it is RH=65%. The sand will restrain the specimen from shrinking and also the saturated sand should produce bending deformation due to differential shrinkage. In this case, as well a triangular strain diagram will be obtained for one side RH= 100% and other side RH= 65%.

The expected time of cracking has been estimated when the shrinkage-induced stresses increases the tensile strength as shown in figure 7.14.

Result

According to the calculation the specimens restrained axial with dry and wet sand were expected to crack within a week. However, only the cylinder specimen restrained with wet sand cracked after 14 days of restraining it. The specimens after 14 days can be seen in figure 7.15.

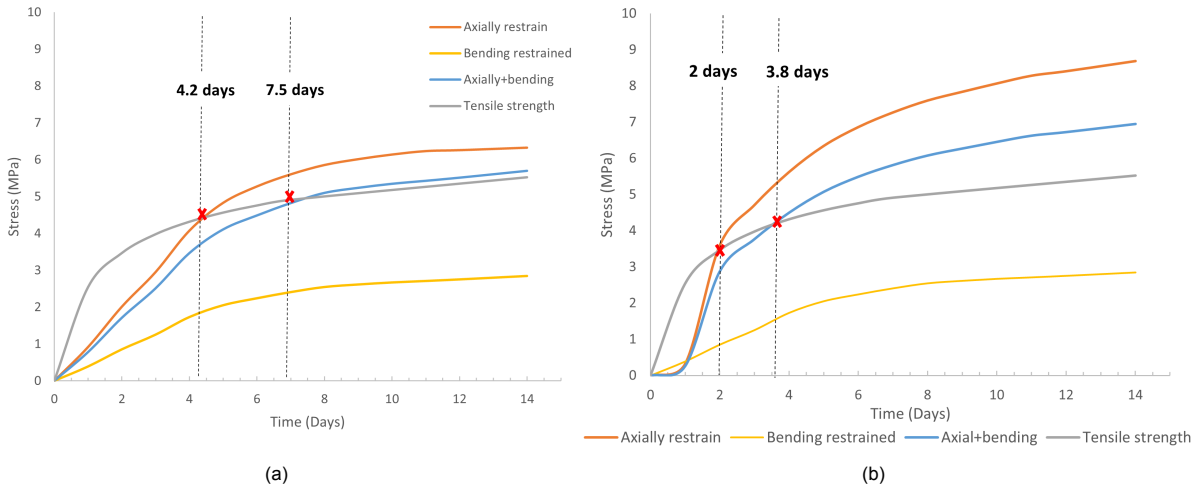

(a) (b)

Figure 7.14: Calculated stress over time for (a) cylindrical specimen and (b) cuboid specimen. Orange= Axial restrained, Yellow= only bending, Blue= both axial and bending, grey= tensile strength. Dotted lines indicate the expected cracking when stresses exceed the tensile strength

Figure 7.15: The specimens after t=14 days. The cracked specimen is highlighted in red

The cuboid specimens were expected to crack faster than the cylindrical specimen due to two reasons: (1) Higher surface to volume ratio indicating more exposed surface area and hence more drying shrinkage, (2) higher stress due to corners. However, the cuboid specimens did not crack. To understand the possible reason, looking at the equation for calculating shrinkage stresses (equation 7.2), the three variables are: effective elastic modulus, shrinkage strain and degree of restraint. In the other two case studies, the relaxation effect was found to be overestimated, lowering the shrinkage stresses. However, in this case, the calculated shrinkage stresses were estimated turn out to be more than the actual stresses. Another variable, the degree of restraint could be a possible reason for the overestimation of stresses. The calculations were made assuming a complete restrained condition, with degree of restraint = 1. However, the sand is not stiff enough to completely restrain it. Especially the sand at RH = 65% could be loosely packed as compared to the saturated sand. The degree of restraint could severely reduce the stresses as it can vary between 0 to 1. The third factor is the shrinkage strain calculated from the developed numerical model. Since the numerical model is based on numerous assumptions and several parameters are taken from the literature, it could be possible that the model deviates from actual scenario.

7.4. Summary

Three case studies were performed to check the applicability of the developed numerical model. The key findings of the chapter are:

- The estimated time of cracking of the experimentally performed ring test has been simulated. The numerical model estimated the cracking of exposed specimen within 1.8 days and no cracking for sealed specimen. However, when compared for different effective modulus more accurate results were obtained estimating cracking at 1.5 days for exposed and 7.5 days for sealed specimen. It showed that to properly estimate the cracking due to shrinkage-induced stresses it is important to study the effect of creep and relaxation as well.
- In the second case study two 3D printed flower pots were analyzed. The model estimated cracking at 2.8 days for element 1 and 33 days for element 2. In the experiment, element 1 cracked after 5 days and element 2 at 26 days. In this case as well, one of the possible reasons could be an overestimation of relaxation effect.
- A parameteric study designed by using the numerical model. Cylindrical and cuboid specimens were placed in four different boundary conditions. The specimens restrained axial and both bending and axial restrained were expected to crack. However, only one specimen restrained with wet sand cracked. The possible reasons could be an overestimation of degree of restraint and/or the shortcoming of the developed numerical model.

8

Discussion

In this chapter, the gained knowledge about the shrinkage behaviour of 3D printing concrete mixture as well as its potential and the limitations of the numerical model is critically reviewed. The outcomes of the experiment are investigated and compared to the literature for reliability.

Experimental study

Concrete mixtures developed for 3D printing processes differ from conventional concrete mixtures. Low w/c ratio, high cement content, absence of coarse aggregate are some of the material composition properties which make the 3D printing concrete mixtures susceptible to autogenous shrinkage. Also, the layer-by-layer printing incorporates higher porosity especially at the interfaces [39]-[40]. Additionally, immediate exposure to the environment due to lack of formwork makes the structure prone to drying shrinkage as well.
To understand the shrinkage behaviour of the concrete mixture, free shrinkage and restrained ring test have been performed under different curing conditions.

Free shrinkage test

The free shrinkage test was performed for two curing conditions, uncovered (where samples were exposed to environment from the time of casting) and covered condition (where the specimens were sealed with plastic after casting). Six samples were 3D printed and six were cast in the laboratory using the concrete mixture from the same batch of production to maintain uniformity. All the samples have dimensions of 160x40x40 mm^3 and were placed in RH= 65% and T= 20°C.
The average shrinkage values for cast sample obtained as 715 microstrains and 860 microstrains in covered and uncovered conditions respectively at 60 days. The results are similar to Zhang et al.[42] who obtained the drying shrinkage of 3DCP cured at RH= 50% and T= 20°C to be 840 microstrains at 70 days. Similarly, Le et al.[41] obtained a drying shrinkage of 730 microstrains at 60 days for specimens cured at T=20°C and RH= 60%.
The samples covered with plastic sheet were expected to have a minimal mass loss to represent solely the autogenous shrinkage present in the specimen. However, the specimen covered in plastic sheet showed a mass loss up to 0.41% at 60 days, suspecting possible moisture loss to the environment as well. So the recorded shrinkage values for specimens in covered condition cannot be attributed as only due to the autogenous shrinkage. The possible reason of the observed mass loss in the covered specimen is that the plastic sheet is not sufficient to prevent moisture loss. Similar results can be seen in the restrained ring test as well for the specimen covered in plastic sheet as compared to one covered with waterproof tape and plastic sheet. It is recommended to use waterproof tape if the autogenous shrinkage has to be measured. However, from a practical point of view, even covering a large 3D printed concrete structure by plastic sheet to minimize drying shrinkage on the site is a stretch. The situation is similar to the conducted experiment.
The shrinkage of the cast specimen is relatively higher than the total shrinkage of high-performance concrete with w/c ratio of 0.25 at 500 microstrains [5]. The concrete mixtures for 3D printing typically have a maximum aggregate size of 2 mm since passing coarse aggregate through the pump and nar-

row nozzle is infeasible. It is logical to compare the shrinkage behaviour of such mixtures to the cement mortars having low water to cement ratio. The coarse aggregates restrain the cement paste limiting the shrinkage. Dueramae et al. [69] found the shrinkage of OPC based mortar having w/b ratio of 0.25 to be 876 microstrains at 180 days kept at temperature of 23±°C and RH= 50±4%. The obtained shrinkage value of the concrete mixture is similar to it. Overall, the shrinkage in concrete mixtures for 3D printing is itself high, even if the structure is conventionally cast.

3D printed compared to cast samples

Despite having the same material for 3D printed and the cast sample in the free shrinkage test, a higher shrinkage is observed in the 3D printed samples. The average shrinkage values in 3D printed samples were obtained as 856 microstrains and 1100 microstrains in covered and uncovered conditions respectively on 60 days. It is higher by almost 22% than the cast specimen. This indicates that 3D printing process can increase shrinkage.

When the shrinkage and mass loss curves are compared together, even though the mass loss in 3D printed and cast sample is same (difference of 1-3%), there is a higher shrinkage observed in the 3D printed sample. This implies that when there is moisture loss from capillary pores of lower radius, higher shrinkage stresses produced (Laplace's Equation 2.2) but the mass loss is not substantial. It is recommended to investigate the pore distribution in both samples for a deeper understanding. Kruger et al. [51] observed a higher increased porosity (7.9%) in 3D printed specimens as compared to the cast samples (6.8%), at 15 microns of CT scanning resolution. It is possible that 3D printed specimens have higher porosity as compared to cast specimens at the interlayer. Other factors such as an increase in temperature of concrete due to friction & heat generation in the machine during extrusion, and lack of compaction are discussed as well. However, a further investigation is required to pinpoint the reason.

Restrained ring test

A restrained ring test was performed to study the shrinkage behaviour of the concrete mixture in completely restrained condition from the time of casting. Three conditions have been studied: uncovered or completely exposed from time of casting, covered with plastic sheet and covered with waterproof tape and plastic sheet. The strain of the inner steel ring is recorded by the strain gauges over time in which a sudden drop indicates the cracking in the specimen.

The specimen in exposed condition cracked after 2.8 days, covered in plastic sheet only cracked after 4 days respectively and covered with tape and plastic sheet cracked after 8 days. In this experiment as well, covering the specimen with plastic sheet showed a possible moisture loss to the environment and a better sealing was provided by waterproof tape. It is not possible to measure the mass loss in the case of ring test due to its setup. Any disturbance in the setup can lead to an error in strain gauge measurements. A possible solution is to keep the setup on a weighing scale during the whole time.

All the specimens cracked at a similar maximum radial stress of 4 MPa. It was expected that since the specimen sealed with waterproof tape cracked at 8 days, the tensile strength should be higher than 3 days. However, a better argument could have been made if the tensile strength of the concrete at 3 days and 8 days have been known for the comparison. Presently only the flexural strength of 10.1 MPa is known at 28 days, which can only be used as an indicator. The curing conditions of the specimen are different which impacts the strength development. Also, another possible reason according to Zhutovsky [53] is that the sealed specimens only have autogenous shrinkage which is uniform across the cross-section, the mode of failure is tensile in nature. Whereas the drying shrinkage produces a stress gradient across the cross-section which resembles flexural mode of failure. Also, the relaxation of the stress reduces the stresses in the sealed specimen, delaying the occurrence of cracking.

The specimen in exposed condition has the highest average crack width of 0.9 mm, followed by the specimen covered in plastic sheet having 0.8 mm and the least average crack width of 0.1 mm was observed in the specimen sealed with waterproof tape and plastic sheet. It should be noted that the average crack-width was not measured exactly at the time of the cracking and thus could be an overestimation as crack-width increases over time.

The experiment indicates that the autogenous shrinkage is high enough in the 3DCP mixtures to cause shrinkage-induced cracking in a specimen tightly sealed with waterproof tape and plastic sheet.

Finite Element Model Development

To predict the shrinkage behaviour of the concrete mixture, a finite element model is developed. The capillary tension approach has been used which uses the Kelvin-Laplace equation and Bentz deformation equation to calculate the shrinkage strain. It is the governing mechanism when RH $\geq 40\%$ and has been used to model autogenous and drying shrinkage by numerous researchers [14]. The required input parameters for the calculation of shrinkage strain (equation 5.11) are degree of saturation, relative humidity distribution over time and the elastic properties of the concrete. Since obtaining the exact values of these parameters for the particular concrete mixture requires numerous experiments, the values are taken to the best estimation from the literature.
The degree of saturation is calculated based on Power's volumetric model for the Portland cement paste which requires degree of Hydration over time as input. The present model approximates the degree of hydration using OPC cement mortar having a W/C ratio of 0.3, using the HYMOSTRUC software. 3D printing concrete mixtures have different admixtures such as accelerators, thixotropic chemicals, retarders to obtain the required rheological properties. The degree of hydration will be different from the normal concrete. It is recommended to perform the isothermal calorimetry test to obtain the evolution of degree of hydration over time for the specific concrete mixture.
The mechanical properties such as the development of elastic modulus over time have been calculated using Eurocode 2. The NEN-EN 12390-13:2012 test performed on the concrete mixture reported the elastic modulus as 30 GPa at 28 days. However, due to the lack of values at the discrete-time point, the development of elastic modulus over time has been calculated using Eurocode 2 approximating as C30/37 which has an elastic modulus of 30 GPa at 28 days. It should be noted that the Eurocode 2 is developed for OPC concrete having coarse aggregates, which may increase the elastic-modulus.
Another influencing parameter is the effect of creep over time on the shrinkage strain. Since the creep behaviour of the 3D concrete mixture is not known in depth, the effective elastic of modulus is taken while calculating the shrinkage strain. Lura (2003) [23] and Song et al. [54] suggest a factor of 3 for high strength concrete.

The parameters have been estimated from literature and their influence on the calculated shrinkage strain has been studied by sensitivity analysis. Since the numerical model is developed from inverse analysis, it is important to first study the influence of the other assumptions of calculations to ensure reliability of the calibrated values. Each parameter is varied between ±30% to study the influence on the calculated shrinkage strain, keeping the relative humidity distribution as a constant. The sensitivity analysis showed that the influence of the parameters increases over time but remains under the maximum value of 10% at 28 days if varied by ±30%.

Relative humidity distribution

The shrinkage strain is dependent on the relative humidity distribution due to the autogenous and drying shrinkage. The moisture diffusion process has been modelled for which the input parameters are calibrated using the inverse analysis of the free shrinkage test. The shrinkage strain of the cast samples in covered and uncovered condition have been modelled. Modelling the 3D printed structures requires an extensive study focused on the influence of 3D printing processes such as interlayer adhesion at layers, layer thickness etc which is out of the scope of the present study.

The main input requirements to model the diffusion process are: non-linear diffusion coefficient, RH reduction due to autogenous shrinkage and the convective surface factor. From the inverse analysis, the calibrated value of the non-linear diffusion coefficient is obtained as D_1= 2.48x10^{-11} m^2/s, n= 15 and α=0.005 for the particular concrete mixture. The range of the parameters lies is similar as suggested in literature (table 5.1). Ideally, the data required to calibrate the diffusion coefficient for the particular concrete mixture should be the evolution of RH in the pores over time and the humidity profiles throughout the cross-section for different specimen sizes, environmental conditions and exposure time to the drying atmosphere. However, due to the lack of the data and experiment at such large scale, the parameters in the equations are judiciously assumed and are empirically calibrated.
To improve the accuracy of the diffusion model, it is important to consider the relative humidity reduction due to self-desiccation process especially for concrete mixture having low w/c ratio. Also, it plays a crucial role in early age concrete when autogenous shrinkage is dominant. The analytical model

provided by Rahimi et al. [55] has been used to calculate the reduction in relative humidity due to self-desiccation. The model showed a good agreement with the experimental results with an error of 5-6%.
Since the diffusion parameters are calibrated using inverse analysis, to minimize the number of unknowns, the relative humidity at the surface is assumed to be constant as suggested by Zhao et al.**li** as the experiment showed that the moisture gradient at the surface gradually diminishes, forming an equilibrium with the environment. In reality, a convective boundary condition should be applied to account for the moisture loss from the surface to the environment as well. When compared to the shrinkage strain of the uncovered cast specimen, the simulated values have an error of up to 7-8%, which seems reasonable.

Verification of moisture profile
The moisture profile of the finite element model has been verified using the analytical model suggested by Li et al. [64]. The main assumptions of the analytical model to calculate the relative humidity distribution across the cross-section of the specimen are: (1) constant diffusion constant and (2) the effect of autogenous shrinkage is neglected. The numerical model showed good agreement with the analytical model.

A mesh size of 0.0025 mm has been used. The mesh sensitivity analysis showed that the model requires a finer mesh, especially at the surface nodes to properly model the transition or diffusion between the surface and inside the specimen. A coarse mesh can overestimate the RH for surface nodes whereas mesh size has minimal influence on the RH of nodes at the center.

It should be understood that the model has been developed based on the shrinkage behaviour of a particular specimen of a relatively small size (160x 40x 40 mm ^{3}) studied in a particular ambient RH condition. To enhance the reliability of the model over different geometrical and environmental condition, it is important to measure the shrinkage strain on various specimens.

Case studies

Three case studies were taken to assess the numerical model to predict the shrinkage strain and the corresponding shrinkage-induced stresses. First the model was used to predict the shrinkage-induced stresses in the case of the ring test performed during the experiment. The numerical model estimated the cracking of exposed specimen within 1.8 days and no cracking for sealed specimen when the relaxation effects are calculated according to Eurocode 2. However, when compared for different effective modulus, more accurate results were obtained estimating cracking at 1.5 days and 7.5 days for sealed specimen as compared to 3 days and 8 days observed in the experiment. It showed that to properly estimate the cracking due to shrinkage-induced stresses, it is important to investigate the effect of creep for the particular concrete mixture.

Second, the case study two 3D printed flower pots were analyzed. The model estimated cracking at 2.8 days for element 1 and 33 days for element 2. In the experiment, element 1 cracked after 5 days and element 2 at 26 days. In this case as well, one of the possible reasons could be an overestimation of relaxation effect as seen in the ring test. Even though the calculations were made assuming degree of restraint to be 1, in reality, the sand is not stiff enough to completely restrain the element from inside. So the calculated stresses could be higher than the actual stresses. Also, the stress concentration due to the corner could increase the stresses.

Third, a parametric study is designed by using the numerical model. Cylindrical and cuboid specimens were 3D printed and placed in four different boundary conditions. The specimens restrained axially and both bending and axial restrained were expected to crack within a week. However, only one specimen (cylindrical restrained with wet sand) cracked after 14 days. To understand the possible reason, three variables are considered: effective elastic modulus, degree of restraint and shrinkage strain calculated from the model. In the previous two case studies, an overestimation of relaxation was observed. However, in this case, the actual stresses are supposedly lower than the calculated stresses. The degree of restraint could be highly affecting the stresses, especially sand at RH= 65% could be loosely packed compared to saturated sand. The shrinkage strain calculated from the model

could be deviating from the actual scenario. However, given that reasonable results were obtained from the other two case studies, the error from the model was not expected to be huge.

Overall, the case studies showed that to accurately estimate the shrinkage-induced stresses it is important to study the creep and relaxation process in the 3D printing concrete mixture as well. Since the concrete mixture does not contain coarse aggregate, it is expected to have higher creep.

9

Conclusions and Recommendations

Shrinkage is an important factor for the concrete structures which may influence the durability and mechanical properties. 3D printed concrete structures pose higher risks of shrinkage as compared to traditional concrete structures due to their material composition and execution process. This research investigates the shrinkage behavior of 3D printing concrete mix under different curing conditions to understand if the shrinkage is an issue for 3D printable concrete mixtures? Based on the experimental results, a finite element model was developed to predict the shrinkage strain of the concrete structures. The main conclusions of the study are:

How is the free shrinkage behavior of cast and 3D printed samples? Two curing conditions are investigated: samples being covered and uncovered

It was observed that the shrinkage of 3D printing concrete mixtures is high even for conventionally cast specimens. The free shrinkage test was conducted on cast and 3D printed samples under covered and uncovered conditions. The average shrinkage value for the cast samples at 60 days were obtained as 715 microstrains and 860 microstrains respectively in covered and uncovered conditions. Compared to the total shrinkage of High-Performance concrete with w/c ratio of 0.25 at around 500 microstrains [5], the shrinkage is relatively high. The shrinkage is comparable to low w/c ratio mortar having 876 microstrain shrinkage at 180 days [69]. Based on the results, it can be said that compared to normal concrete, 3D printing concrete mixture has a higher shrinkage.

Even though the cast sample and 3D printed samples have the same material, a higher shrinkage was observed in the 3D printed samples attributed to the 3D printing processes. The average shrinkage value for the 3D printed samples at 60 days were obtained as 856 microstrains and 1100 microstrains respectively in covered and uncovered conditions. Compared to the cast samples, 3D printed samples showed a higher shrinkage of 18-20%. The mass loss in the 3D printed and cast sample only a difference of 1-3% .

In conclusion, 3D printed concrete structures have a higher shrinkage both due to their material properties and printing process. A proper curing condition can reduce the shrinkage. As seen in the free shrinkage test, the samples covered with the plastic sheet showed a lower shrinkage by 16% as compared to samples in exposed condition. Although the 3D printed samples covered with plastic sheet showed a shrinkage for up to 856 microstrains which is comparable to the uncovered cast sample.

The experiment showed that in the first 14 days, the shrinkage was up to 400 microstrains for the covered samples, indicating high autogenous shrinkage. It implies that there is a need for improvement in the material properties of the concrete to reduce the autogenous shrinkage, especially at the early age.

Research question 2: How is the shrinkage strain development when restrained? Two curing conditions are investigated: samples being covered and uncovered

The restrained ring test showed that the samples in exposed condition cracked after 2.8 days, those covered with plastic sheet after 4 days and the ones sealed with waterproof tape after 8 days. The specimen tightly sealed cracked within 8 days indicates that the autogenous shrinkage in the concrete

mixture is enough to cause shrinkage-induced cracking if restrained immediately after casting. Practically the feasible solution is covering the 3D printed structures with plastic sheets to minimize the risk of autogenous and drying shrinkage. Samples having similar curing conditions cracked within 4 days. It can be concluded that the 3D printed structures should be designed such that the degree of restrain due to internal or external restrain is minimum. From the free shrinkage test it can be seen that the rate of shrinkage is high for first 28 days after which it stabilizes. This can be utilized when restraining the structure. The 3D printed structures can be let to shrink freely for the first few days and then assembled so that the shrinkage strain is not high enough to induce cracking. Restraining due to structural components such as windows, door frames, etc. should be applied by properly optimizing the time of restrain.

Research question 3: How can a finite element model be developed to predict the shrinkage behavior of 3D printed concrete structures over time under different environmental conditions?
A finite element model has been developed based on the capillary tension approach to predict the shrinkage behaviour for the particular concrete mixture. Several assumptions have been made to calculate the shrinkage strain combining the Kelvin-Laplace equation and Bentz Deformation model. The main input parameters for the model are: degree of hydration, mechanical properties such as elastic modulus, creep factor, diffusion coefficient and relative humidity due to the drying and autogenous shrinkage.
The analogy between the heat diffusion to model the moisture diffusion in the concrete can be used to model the relative humidity distribution over time. The non-linear diffusion coefficient suggested by CEB FIB Model 2010 [8] is used. The standard guidelines such as Eurocode provides models to calculate shrinkage for concrete mixtures with coarse aggregates. It can highly underestimate the shrinkage of 3D printing concrete mixtures. The developed finite element model can be used as a tool to estimate the shrinkage strain over time for the cast samples for the particular concrete mixture kept over a relative humidity of 40%. Presently, 3D printed structures are printed in an environmental-controlled laboratory. The model can be used to optimize the dimensions of the structure and the relative humidity conditions to minimize the shrinkage.
The case studies showed that there is further room for improvement in the developed finite element model to determine the cracking due to shrinkage-induced stresses, especially on the creep and relaxation effects.

Recommendations

The research is a first step towards the investigation of the shrinkage behaviour of the 3D printed concrete mixtures. The results of the study have shown that the shrinkage is higher than the normal and high strength concrete. A numerical model has been developed as well to predict the shrinkage strain assuming the concrete to be a homogeneous, elastic matrix. However, there are some missing links in the model and unanswered questions of the shrinkage behaviour which are required to improve and reinforce the conclusions of the study. Next, the recommendations are suggested for future research.

- The model has been developed based on the shrinkage behaviour of a particular specimen studied in a specific environmental condition. The validation has been performed based on the moisture profile and the occurrence of cracking using different case studies. However, to check the accuracy of the model, the model should be tested specifically for the shrinkage strains of specimens with different geometries and environmental conditions.
- From the experiments it is evident that the autogenous shrinkage is quite high in the concrete mixture. Although the exact autogenous shrinkage was not captured properly in this research. Methods such as shrinkage-reducing admixtures or internal curing techniques should be explored to reduce the risk of cracking due to the autogenous shrinkage.
- The present study captures the shrinkage behaviour for up to 60 days. In reality, the drying shrinkage continues for years so it is advised to measure the long-term shrinkage as well.
- In the present study a higher shrinkage in a 3D printed specimen is observed as compared to the cast specimen for both covered and uncovered samples. The exact reason behind is still unknown

and should be studied in depth. The possible causes could be due to the role of interfaces in the case of 3D printed structures. It should be noted that the 3D printed sample in this case was only 4 layers. It will be interesting to study the role of 3D printing process parameters such as the number of layers, layer thickness and height, printing speed on the shrinkage of the specimen. For example, more number of layers could have more shrinkage due to higher interfacial pores, thicker layers could dry at a slower rate, faster printing speed could lead to poor layer adhesion increasing the interfacial pores.

- From the case studies, it has been observed that the creep and the relaxation behaviour play an important role while predicting the occurrence of the shrinkage-induced cracking. It is advisable to have a separate study of both the early age and long term creep in case of such concrete mixtures.
- Several assumptions of the mechanical properties have been made during the development of the numerical model. The sensitivity analysis of the variables showed that the elastic modulus and the creep behaviour have the highest influence on the calculated shrinkage behaviour. It is advisable to study the tensile strength of the concrete mixtures at least 7, 14 and 28 days.

Bibliography

[1] R. Buswell, W. Silva, S. Jones, and J. Dirrenberger, "3d printing using concrete extrusion: A roadmap for research," *Cement and Concrete Research*, vol. 112, 2018. DOI: 10.1016/j.cemconres.2018.05.006.

[2] Z. Li, M. Hojati, Z. Wu, J. Piasente, N. Ashrafi, J. P. Duarte, S. Nazarian, S. G. Bilén, A. M. Memari, and A. Radlińska, "Fresh and hardened properties of extrusion-based 3d-printed cementitious materials: A review," *Sustainability*, vol. 12, no. 14, p. 5628, 2020.

[3] G. M. Moelich, J. Kruger, and R. Combrinck, "Plastic shrinkage cracking in 3d printed concrete," *Composites Part B: Engineering*, vol. 200, p. 108 313, 2020.

[4] G. Slavcheva, "Drying and shrinkage of cement paste for 3d printable concrete," in *IOP Conference Series: Materials Science and Engineering*, IOP Publishing, vol. 481, 2019, p. 012 043.

[5] W. Piasta and B. Zarzycki, "The effect of cement paste volume and w/c ratio on shrinkage strain, water absorption and compressive strength of high performance concrete," *Construction and Building Materials*, vol. 140, pp. 395–402, 2017. DOI: 10.1016/j.conbuildmat.2017.02.033.

[6] ACI, "Aci 209.2r-08: Guide for modeling and calculating shrinkage and creep in hardened concrete," *American Concrete Institute, Farmington Hills*, 2008.

[7] *EN 1992-1-1 Eurocode 2: Design of concrete structures - Part 1-1: General rules and rules for buildings*, CEN, 2004.

[8] *CEB-FIP Model Code 1990*. Thomas Telford Publishing, 1993. DOI: 10.1680/ceb-fipmc1990.35430.

[9] J. S. of Civil Engineering (JSCE), "Standard specifications for concrete structure," *JSCE Guidelines for concrete*, 2007.

[10] H. Huang, R. Garcia, M. Guadagnini, and K. Pilakoutas, "Effect of section geometry on development of shrinkage-induced deformations in box girder bridges," *Materials and Structures*, vol. 50, no. 5, pp. 1–14, 2017.

[11] J. Zhang, J. Wang, and Y. Gao, "Moisture movement in early-age concrete under cement hydration and environmental drying," *Magazine of Concrete Research*, vol. 68, pp. 391–408, 2016.

[12] J. Zhang, D. Hou, and Y. Han, "Micromechanical modeling on autogenous and drying shrinkages of concrete," *Construction and Building Materials*, vol. 29, pp. 230–240, 2012.

[13] *Klimaat viewer,koninklijk nederlands meteorologisch instituut*. [Online]. Available: https://www.knmi.nl/klimaat-viewer/kaarten/vocht/gemiddelde-relatieve-vochtigheid/jaar.

[14] F. Wittmann, "Surface tension. shrinkage. and strength of hardened cement paste," *Matériaux et Constructions*, vol. 1, pp. 547–552, 1968.

[15] V. Baroghel-Bouny, M. Mainguy, T. Lassabatere, and O. Coussy, "Characterization and identification of equilibrium and transfer moisture properties for ordinary and high-performance cementitious materials," *Cement and concrete research*, vol. 29, no. 8, pp. 1225–1238, 1999.

[16] N. F. Tanue, T. Fabian, F. Didier, and T. Gilbert, "Characterisation of early age deformations in cement paste: Case of chemical and autogenous shrinkage," *Journal of Minerals and Materials Characterization and Engineering*, vol. 8, no. 4, pp. 223–239, 2020.

[17] R. Mors, "Autogenous shrinkage of cementitious materials containing bfs," 2011.

[18] D. P. Bentz and O. M. Jensen, "Mitigation strategies for autogenous shrinkage cracking," *Cement and Concrete Composites*, vol. 26, no. 6, pp. 677–685, 2004.

[19] J. K. Kim and C. S. Lee, “Moisture diffusion of concrete considering self-desiccation at early ages,” *Cement and Concrete Research*, vol. 29, pp. 1921–1927, Dec. 1999. DOI: 10.1016/S0008-8846(99)00192-1.

[20] Z. Jiang, Z. Sun, and P. Wang, “Internal relative humidity distribution in high-performance cement paste due to moisture diffusion and self-desiccation,” *Cement and concrete research*, vol. 36, no. 2, pp. 320–325, 2006.

[21] T. Lu, “Autogenous shrinkage of early age cement paste and mortar,” Ph.D. dissertation, Delft University of Technology, 2019. DOI: 10.4233/uuid:e06bd615-7fc4-481b-a334-37627f142e3d.

[22] X. Zhang and H. Zhao, “Characterization of moisture diffusion in cured concrete slabs at early ages,” *Advances in Materials Science and Engineering*, vol. 2015, pp. 1–10, May 2015. DOI: 10.1155/2015/154394.

[23] P. Lura, “Autogenous deformation and internal curing of concrete,” Ph.D. dissertation, Delft University of Technology, 2003.

[24] E. E. Holt, “Early age autogenous shrinkage of concrete,” Ph.D. dissertation, University of Washington, 2001.

[25] J. W. Bullard, H. M. Jennings, R. A. Livingston, A. Nonat, G. W. Scherer, J. S. Schweitzer, K. L. Scrivener, and J. J. Thomas, “Mechanisms of cement hydration,” *Cement and concrete research*, vol. 41, no. 12, pp. 1208–1223, 2011.

[26] A. Bentur, R. L. Berger, J. H. Kung, N. B. Milestone, and J. F. Young, “Structural properties of calcium silicate pastes: Ii, effect of curing temperature,” *Journal of the American Ceramic Society*, vol. 62, no. 7□8, pp. 362–366, 1979. DOI: https://doi.org/10.1111/j.1151-2916.1979.tb19079.x.

[27] L. Liu, X. Wang, H. Chen, and C. Wan, “Microstructure-based modelling of drying shrinkage and microcracking of cement paste at high relative humidity,” *Construction and Building Materials*, vol. 126, 2016. DOI: 10.1016/j.conbuildmat.2016.09.066.

[28] A. Garrabrants and D. Kosson, “Modeling moisture transport from a portland cement-based material during storage in reactive and inert atmospheres,” *Drying Technology*, vol. 21, pp. 775–805, 2003. DOI: 10.1081/DRT-120021686.

[29] A. E. Idiart, *Coupled analysis of degradation processes in concrete specimens at the meso-level*. Universitat Politècnica de Catalunya, 2009.

[30] H. Jennings, “Colloid model of c–s–h and implications to the problem of creep and shrinkage,” *Materials and Structures*, vol. 37, pp. 59–70, 2004. DOI: 10.1007/BF02481627.

[31] R. Alberty and F. Daniels, *Physical Chemistry*. 1975.

[32] D. P. Bentz, E. J. Garboczi, and D. A. Quenard, “Modelling drying shrinkage in reconstructed porous materials: Application to porous vycor glass,” *Modelling and Simulation in Materials Science and Engineering*, vol. 6, no. 3, pp. 211–236, 1998. DOI: 10.1088/0965-0393/6/3/002.

[33] D. Bentz, “Curing with shrinkage-reducing admixtures: Beyond drying shrinkage reduction,” *Concrete International*, vol. 27, pp. 55–60, 2005.

[34] H. Ceylan, K. Gopalakrishnan, S. Kim, P. Taylor, A. A. Alhasan, and S. Yang, “Impact of curling and warping on concrete pavement,” 2016.

[35] T. Salet, F. Bos, R. Wolfs, and Z. Ahmed, “3d concrete printing–a structural engineering perspective,” in *2017 fib Symposium-High Tech Concrete: Where Technology and Engineering Meet*, Springer, 2017, pp. xliii–lvii.

[36] A. Kazemian, X. Yuan, E. Cochran, and B. Khoshnevis, “Cementitious materials for construction-scale 3d printing: Laboratory testing of fresh printing mixture,” *Construction and Building Materials*, vol. 145, pp. 639–647, 2017.

[37] R. Lediga and D. Kruger, “Optimizing concrete mix design for application in 3d printing technology for the construction industry,” *Solid State Phenomena*, vol. 263, pp. 24–29, 2017. DOI: 10.4028/www.scientific.net/SSP.263.24.

[38] B. Panda, S. Paul, and M. Tan, “Anisotropic mechanical performance of 3d printed fiber reinforced sustainable construction material,” *Materials Letters*, vol. 209, Jul. 2017. DOI: 10.1016/j.matlet.2017.07.123.

[39] V. N. Nerella, S. Hempel, and V. Mechtcherine, “Effects of layer-interface properties on mechanical performance of concrete elements produced by extrusion-based 3d-printing,” *Construction and Building Materials*, vol. 205, pp. 586–601, 2019. DOI: 10.1016/j.conbuildmat.2019.01.235.

[40] J. V. D. Putten, M. D. Volder, P. V. D. Heede, G. Schutter, and K. V. Tittelboom, “3d printing of concrete: The influence on chloride penetration,” in *Second RILEM International Conference on Concrete and Digital Fabrication (DC 2020)*, 2020.

[41] T. T. Le, S. A. Austin, S. Lim, R. A. Buswell, R. Law, A. G. Gibb, and T. Thorpe, “Hardened properties of high-performance printing concrete,” *Cement and Concrete Research*, vol. 42, no. 3, pp. 558–566, 2012.

[42] Y. Zhang, Y. Zhang, W. She, L. Yang, G. Liu, and Y. Yang, “Rheological and harden properties of the high-thixotropy 3d printing concrete,” *Construction and Building Materials*, vol. 201, pp. 278–285, 2019.

[43] H. Lee, W.-W. Kim, and J.-H. Moon, “Study on rheological properties of mortar for the application of 3d printing method,” *Journal of the Korean Recycled Construction Resources Institute*, vol. 6, no. 1, pp. 16–24, 2018.

[44] R. J. M. Wolfs, “Experimental characterization and numerical modelling of 3d printed concrete: Controlling structural behaviour in the fresh and hardened state,” 2019.

[45] R. J. Wolfs, F. Bos, and T. Salet, “Early age mechanical behaviour of 3d printed concrete: Numerical modelling and experimental testing,” *Cement and Concrete Research*, vol. 106, pp. 103–116, 2018.

[46] K. Wang, “Feasibility study of 3d printing of concrete for transportation infrastructure,” 2020.

[47] P. G. Shakor Pshtiwan Nejadi Shami, “Review of emerging additive manufacturing technologies in 3d printing of cementitious materials in the construction industry,” *Frontiers in Built Environment*, vol. 4, p. 85, 2019. DOI: 10.3389/fbuil.2018.00085.

[48] M. Hoffmann, S. Skibicki, P. Pankratow, A. Zielinski, M. Pajor, and M. Techman, “Automation in the construction of a 3d-printed concrete wall with the use of a lintel gripper,” *Materials*, vol. 13, p. 1800, 2020. DOI: 10.3390/ma13081800.

[49] A. Hossain, B. Pease, and W. Weiss, “Quantifying early-age stress development and cracking in low water-to-cement concrete: Restrained-ring test with acoustic emission,” *Transportation Research Record*, vol. 1834, pp. 24–32, Jan. 2003. DOI: 10.3141/1834-04.

[50] Z. Li, S. Zhang, X. Liang, J. Granja, M. Azenha, and G. Ye, “Internal curing of alkali-activated slag-fly ash paste with superabsorbent polymers,” *Construction and Building Materials*, vol. 263, p. 120 985, 2020.

[51] J. Kruger, A. du Plessis, and G. van Zijl, “An investigation into the porosity of extrusion-based 3d printed concrete,” *Additive Manufacturing*, vol. 37, p. 101 740, 2021.

[52] J. G. Sanjayan, B. Nematollahi, M. Xia, and T. Marchment, “Effect of surface moisture on interlayer strength of 3d printed concrete,” *Construction and Building Materials*, vol. 172, pp. 468–475, 2018.

[53] S. Zhutovsky, “Stress distribution in restrained ring test due to drying and autogenous shrinkage,” *International Conference on Interdisciplinary Approaches for Cement-based Materials and Structural Concrete*,

[54] S. Han, Y. Liu, D. Liu, M. An, and Z. Yu, “The modeling research on the early-age shrinkage of uhpfrc in different curing conditions,” *Advances in Civil Engineering*, vol. 2018, pp. 1–8, 2018. DOI: 10.1155/2018/9291725.

[55] S. Rahimi-Aghdam, M. Rasoolinejad, and Z. P. Bažant, “Moisture diffusion in unsaturated self-desiccating concrete with humidity-dependent permeability and nonlinear sorption isotherm,” *Journal of Engineering Mechanics*, vol. 145, no. 5, p. 04 019 032, 2019.

[56] Q. Peng and W. Liu, “Inverse analysis of related parameters in calculation of concrete drying shrinkage based on ansys design optimization,” *Journal of materials in civil engineering*, vol. 25, no. 6, pp. 683–692, 2013.

[57] Z. Bažant and L. Najjar, “Nonlinear water diffusion in nonsaturated concrete,” *Matériaux et Construction*, vol. 5, no. 1, pp. 3–20, 1972.

[58] W. Ali and G. Urgessa, “Computational model for internal relative humidity distributions in concrete,” *Journal of Computational Engineering*, vol. 2014, 2014.

[59] R. P. West and N. Holmes, “Predicting moisture movement during the drying of concrete floors using finite elements,” *Construction and building materials*, vol. 19, no. 9, pp. 674–681, 2005.

[60] C. Li, “Study on water and ionic transport processes in cover concrete under drying-wetting cycles,” *Tsinghua University, Beijing, China*, 2009.

[61] R. H. Mills, “Factors influencing cessation of hydration in water cured cement pastes,” *Highway Research Board Special Report*, 1966.

[62] N. Jafarifar, K. Pilakoutas, and T. Bennett, “Moisture transport and drying shrinkage properties of steel–fibre-reinforced-concrete,” *Construction and building materials*, vol. 73, pp. 41–50, 2014.

[63] J. Crank, *The mathematics of diffusion*. Oxford university press, 1979.

[64] Z. Li, M. A. P. Lara, and J. Bolander, “Restraining effects of fibers during non-uniform drying of cement composites,” *Cement and Concrete Research*, vol. 36, no. 9, pp. 1643–1652, 2006.

[65] J.-H. Moon, F. Rajabipour, B. Pease, and J. Weiss, “Quantifying the influence of specimen geometry on the results of the restrained ring test,” *Journal of ASTM international*, vol. 3, no. 8, pp. 1–14, 2006.

[66] J. H. Moon, F. Rajabipour, and W. Weiss, “Incorporating moisture diffusion in the analysis of the restrained ring test,” in *Proc. 4th Int. Conf. Concrete Under Severe Conditions: Environment & Loading*, vol. 2, 2004, pp. 1973–1980.

[67] X. Zhou, W. Dong, and O. Oladiran, “Experimental and numerical assessment of restrained shrinkage cracking of concrete using elliptical ring specimens,” *Journal of Materials in Civil Engineering*, vol. 26, no. 11, 2014.

[68] K. V. Breugel, C. Braam, C. Van der Veen, and E. Koenders, *Concrete structures under imposed thermal and shrinkage deformations: Theory and practice*. 2016.

[69] S. Dueramae, W. Tangchirapat, P. Chindaprasirt, C. Jaturapitakkul, and P. Sukontasukkul, “Autogenous and drying shrinkages of mortars and pore structure of pastes made with activated binder of calcium carbide residue and fly ash,” *Construction and Building Materials*, vol. 230, p. 116 962, 2020.

List of Figures

A

Analytical caluclation of flower pot

Different standard model codes such as Eurocode 2 and JSCE (Standard Specification of Japanese Society of Civil Engineers) are used to analytically calculate the autogenous and drying shrinkage over time for the two elements. Since the exact properties are not known assumptions have been made regarding the environmental conditions and material composition. Several assumptions such as rapid hardening cement (Class R), lower w/c ratio, lower time until curing etc. have been made so that the behaviour is similar to 3D printed concrete mixture. The detailed assumptions in the material properties used for the calculations are shown in table below.

Concrete strength class	C30/37
Cement type	Rapid hardening cement (Class R)
RH (inside condition)	50%
Ambient temperature	20°C
Time until curing	1 day
w/c ratio	0.3
water content	200 kg/m^3

A.1. Calculations according to JSCE

Typically the range of w/c ratio of 3D printed concrete is 0.25-0.35. For such lower w/c ratio, the autogenous shrinkage can have a significant influence on the deformation. Since Eurocode only calculates the autogenous shrinkage based on the compressive strength, JSCE has been used which also incorporate the effect of w/c ratio in the calculations for a more realistic values.

Autogenous shrinkage

$$\varepsilon_{as}(t, t_0) = \varepsilon_{as}(t) - \varepsilon_{as}(t_0)$$
$$\varepsilon_{as}(t) = \gamma \varepsilon_{as,\infty}[1 - exp(-a(t - t_s)^b)]$$

where $\varepsilon'_{as}(t)$ is the autogenous shrinkage strain from the beginning of setting.
γ is the coefficient representing the influence of the cement and admixture type (1 if Ordinary Portland cement is used).
t_0 is the beginning of drying between 1 and 98 days.
t is the time during drying.

$$a = 3.27 \exp\left(-6.83\left(\frac{w}{c}\right)\right) = 0.421$$
$$b = 0.251 \exp\left(2.49\left(\frac{w}{c}\right)\right) = 0.528$$
$$\varepsilon'_{a\infty} = \mathbf{354.048 \times 10^{-6}}$$

Drying shrinkage

$$\varepsilon'_{ds}(t,t_0) = \frac{\varepsilon'_{ds\infty} \times (t-t_0)}{\beta + (t-t_0)}$$

$$\varepsilon_{ds\infty} = \frac{\varepsilon_{ds\rho}}{1+\eta t_0} = \mathbf{1489.205 \times 10^{-6}}$$

The shrinkage strain of concrete calculated according to the equation C5.2.6 JSCE is:

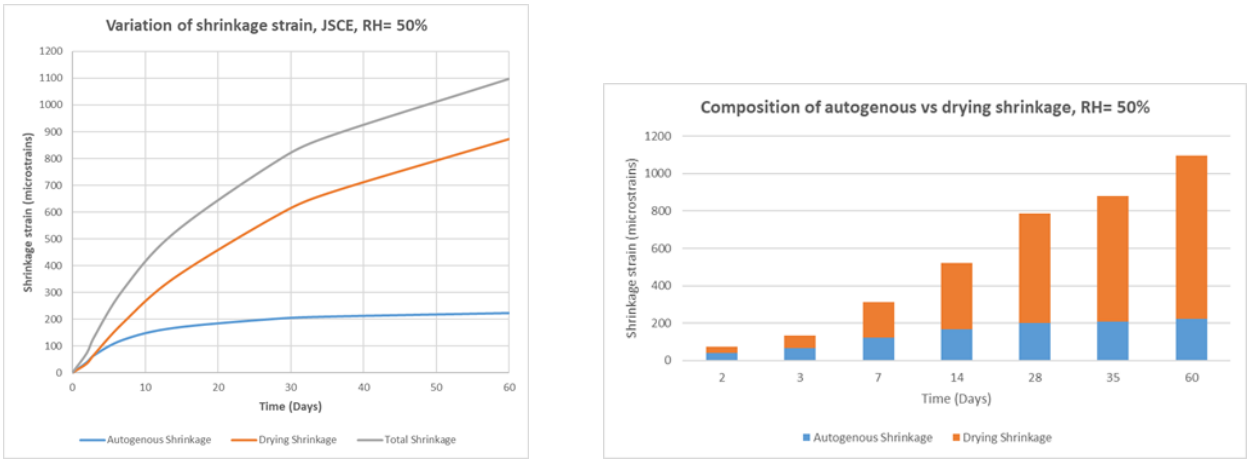

Figure A.1: Variation of shrinkage strain with time according to JSCE (a)Total shrinkage (b)Composition of autogenous and drying shrinkage

Calculation of shrinkage stress for element 1 and 2

Considering the relaxation effect, the stresses produced due to the total shrinkage strains can be calculated for an element under a fully restrained condition $\sigma_{sh}(t)$ can be calculated by following equation, based on Effective Modulus Method (EMM). The total shrinkage upto the time sand is poured has been deducted so that the stresses generated to restrain the additional shrinkage after time of pouring sand are calculated. However, in this case the drying profile is also assumed to be uniform which is not the case in reality.

$$\sigma_{sh}\left(t, t_{loading}\right) = \frac{E(t)}{1+\phi(t,t_0)} * \left(\varepsilon_{sh}(t) - \varepsilon_{sh}(t_r)\right)$$

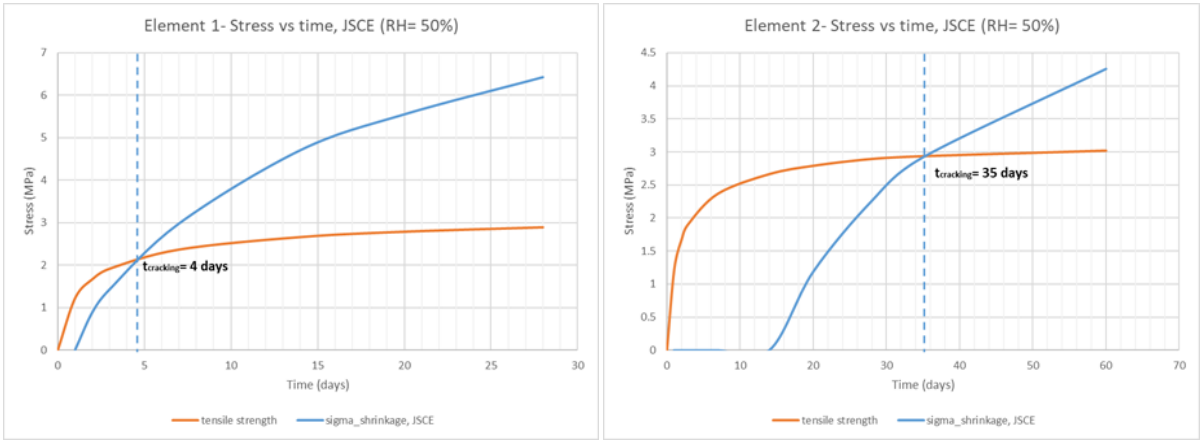

Figure A.2: Variation of shrinkage stress with time according to JSCE (a) Element 1 (b) Element 2

A.2. Calculations according to Eurocode 2

Autogenous shrinkage

Eurocode 2 calculates the autogenous shrinkage using the compressive strength of the concrete and assumes it to be a linear function of the strength. However, since the 3D printed mix has lower w/c ratio, the strains due to autogenous shrinkage may be highly underestimated. The autogenous shrinkage is calculated as follows based on clause 3.1.5 (6), EN 1992-1-1:2004 [7].

$$\varepsilon_{ca}(t) = \beta_{as}(t)\,\varepsilon_{ca}(\infty)$$
$$\varepsilon_{ca}(\infty) = 2.5\,(f_{ck} - 10)\,10^{-6} = \mathbf{50 \times 10^{-6}}$$
$$\beta_{as}(t) = 1 - \exp\left(-0.2t^{0.5}\right),$$

Drying shrinkage

The development of the drying shrinkage is determined based on the ambient relative humidity (RH), the size of the structure (k_h), time of the end of curing (t_s). According to Annex B.2 EN 1992-1-1:2004 [7], the drying shrinkage can be calculated as:

$$\varepsilon_{cd,0} = 0.85 * \left[(220 + 110.\alpha_{ds1}).\exp\left(-\alpha_{ds2}.\frac{f_{cm}}{f_{cmo}}\right)\right].10^{-6}.\beta_{RH}$$
$$\beta_{RH} = 1.55\left[1 - \left(\frac{RH}{RH_0}\right)^3\right] = 1.55\left[1 - \left(\frac{50}{100}\right)^3\right] = 1.356$$

The calculated shrinkage is:

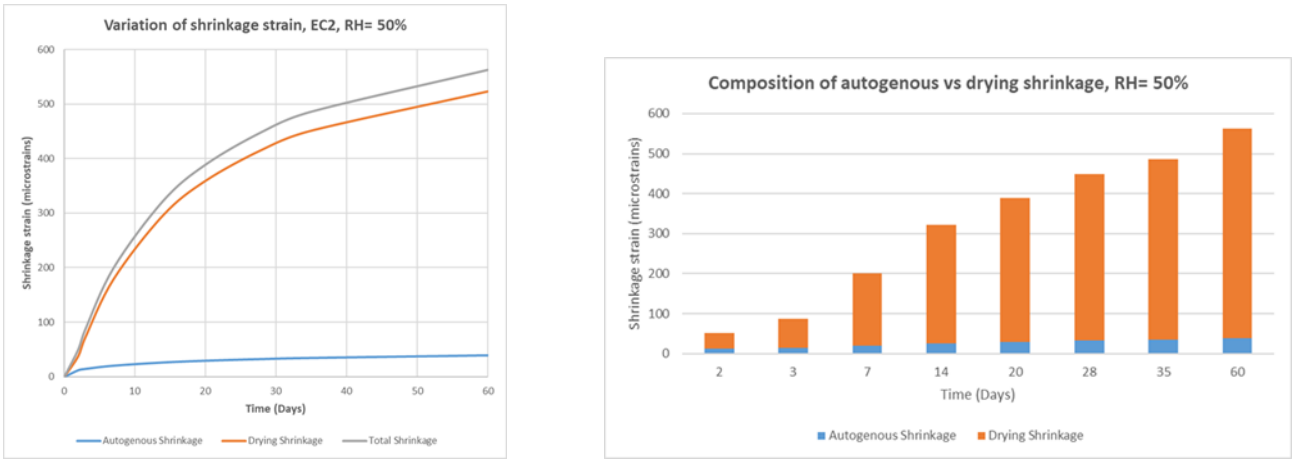

Figure A.3: Variation of shrinkage strain with time according to JSCE (a)Total shrinkage (b)Composition of autogenous and drying shrinkage

Calculation of shrinkage stress for element 1 and 2

Similar calculations of shrinkage stresses has been made as done for JSCE in the previous section. The results are:

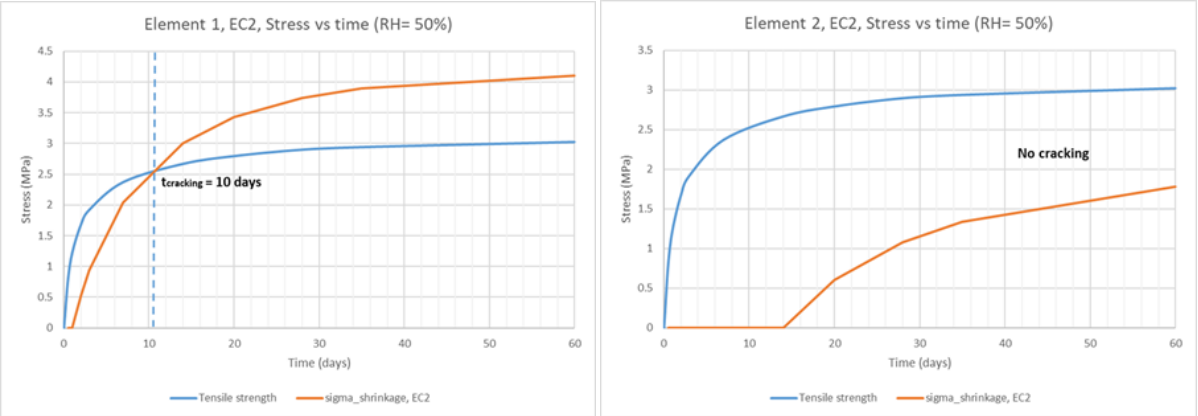

Figure A.4: Variation of shrinkage stress with time according to JSCE (a) Element 1 (b) Element 2

B

Additional results of ring test

The recorded shrinkage strain of the steel ring by individual strain gauge applied diametrically opposite on the ring has been shown for each specimen.

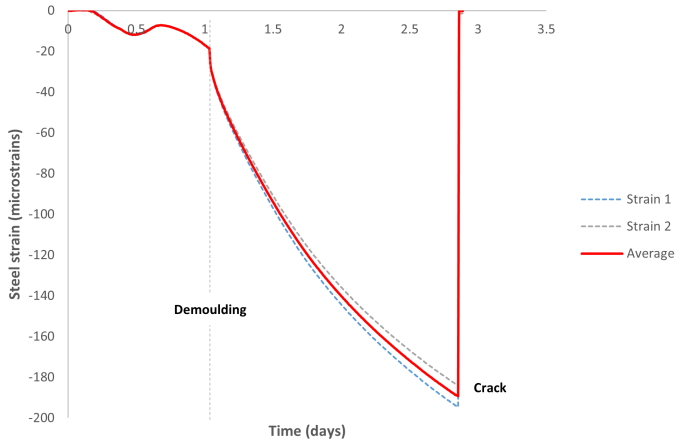

Figure B.1: Strain of steel ring for specimen in exposed condition (SE)

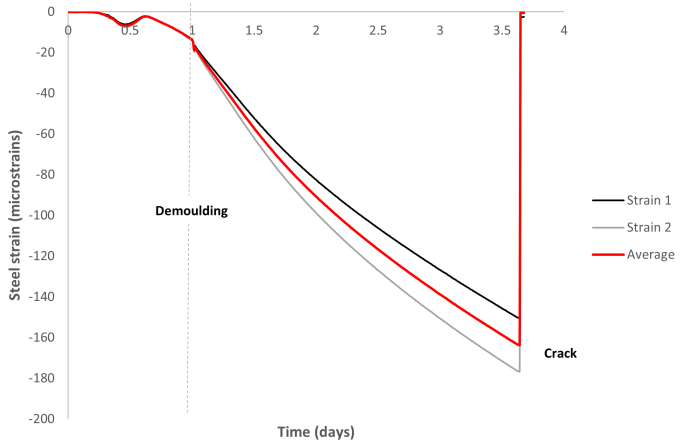

Figure B.2: Strain of steel ring for specimen covered with plastic (SP-1)

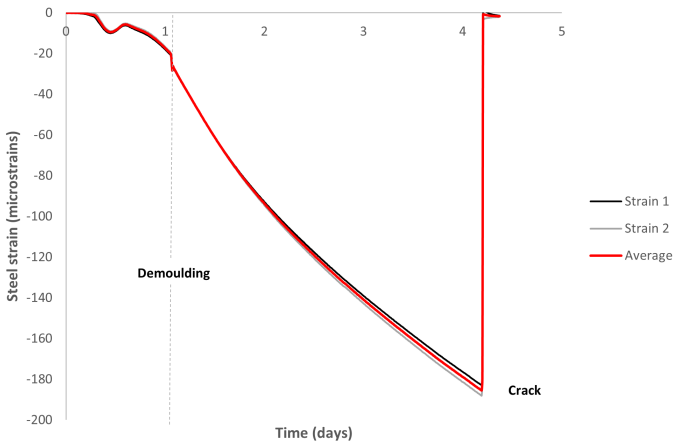

Figure B.3: Strain of steel ring for specimen covered with plastic (SP-2)

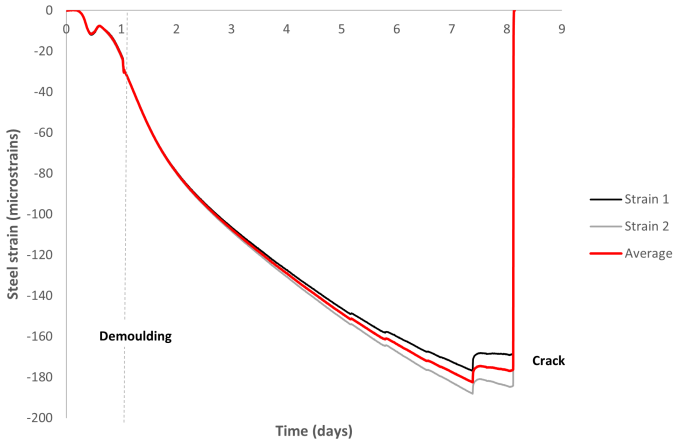

Figure B.4: Strain of steel ring for specimen covered with plastic and tape (S-TP)

C

Influence of input parameters

C.1. Variation of D_1

It determines the diffusion at the saturation (h=100%) and is determined as a function of the pore size distribution. Higher the diffusion coefficient value, faster the rate of diffusion leading to lower relative humidity.

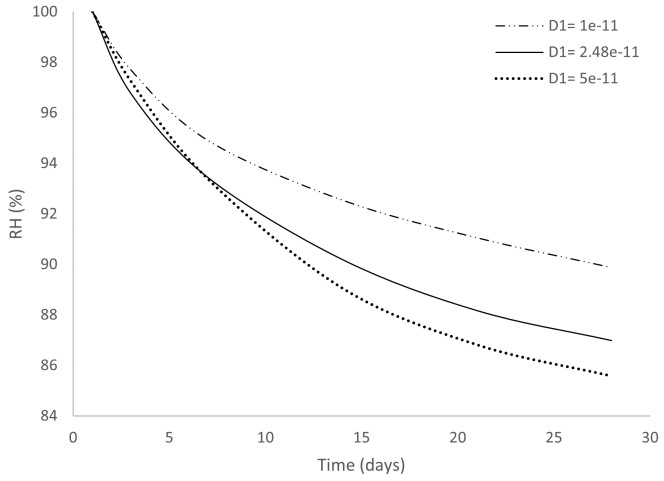

Figure C.1: Variation of D_1

C.2. Variation of n

The influence of change of n on the relative humidity distribution for upto 28 days is shown in figure C.2 . The higher the value of n, lower the relative humidity, especially at the later stage. The parameters determines the steepness of the permeability decrease with the humidity. The lower the value, smoother the permeability decrease.

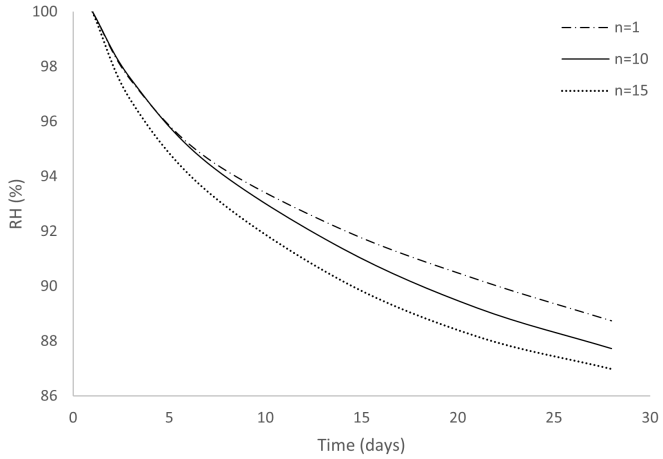

Figure C.2: Variation of n

C.3. Variation of alpha

The influence of change of α on the relative humidity distribution for upto 28 days is shown in figure C.3 .It indicates as the value of α increases, the relative humidity increases as well.

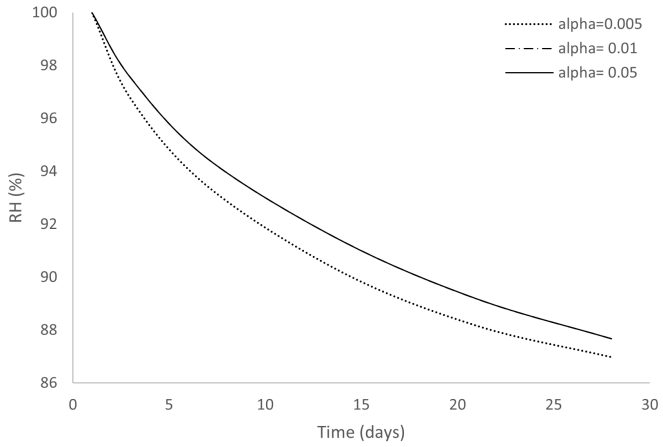

Figure C.3: Variation of alpha values

h_c- The transitional humidity indicates the RH at which the transition point of the steep permeability exist. A concrete with high w/c ratio constitutes more number of large pores due to which permeability starts to decrease at a higher RH.

D

Mesh Sensitivity Analysis

The result of the relative humidity distribution at t=28 days for coarser to finer mesh is shown.

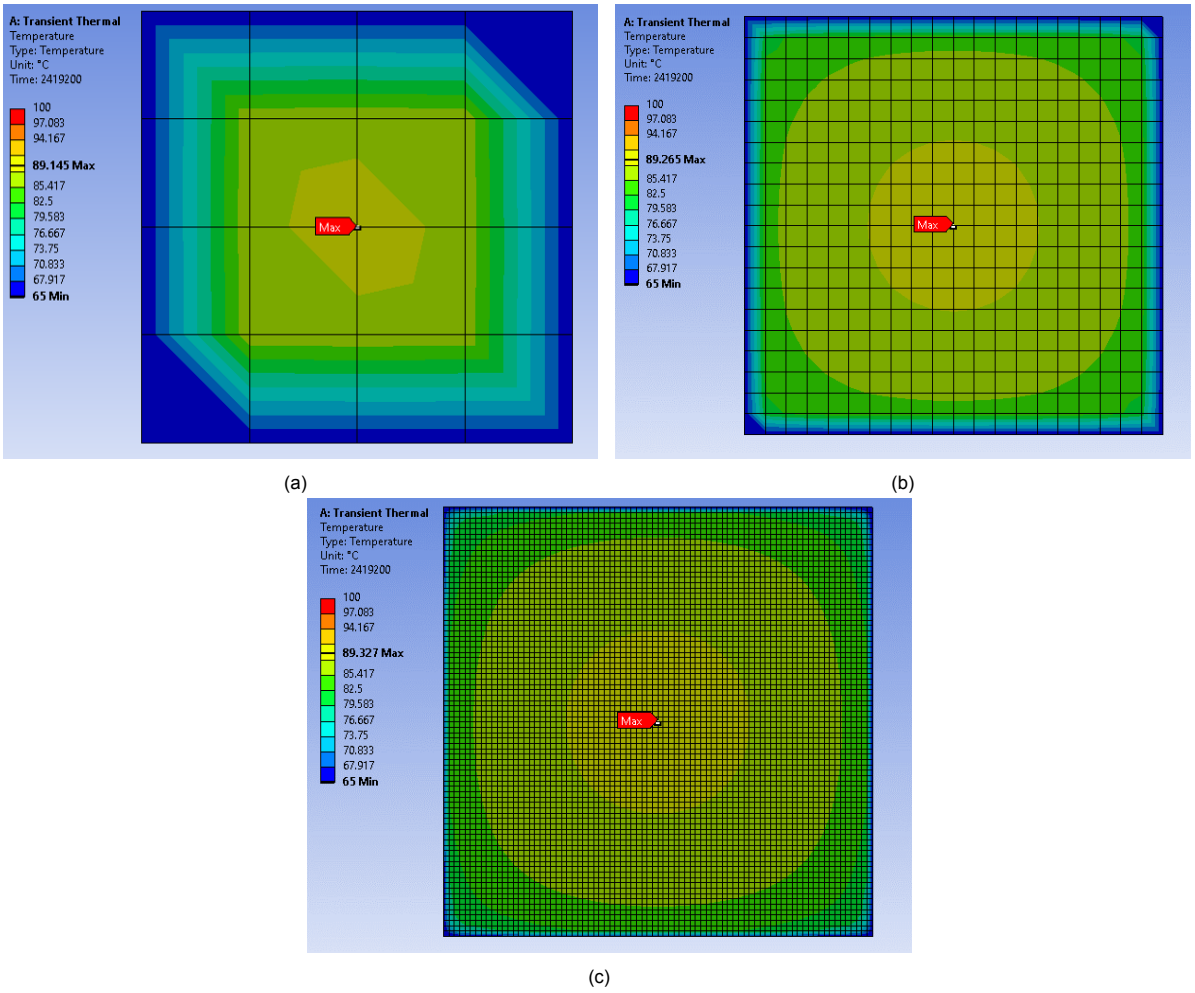

Figure D.1: RH distribution across the cross-section at t= 28 days for mesh size (a) 0.01 m (b) 0.0025 m (c) 0.0005 m